Master's thesis

NTNU
Norwegian University of Science and Technology
Faculty of Natural Sciences
Department of Physics

Andreas Norum

^{31}P MRS protocol optimization and repeatability testing in calf muscle of healthy volunteers on a clinical 7 Tesla MR scanner

Master's thesis in Applied Physics and Mathematics
Supervisor: Pål Erik Goa
Co-supervisor: Maria Tunset Grinde
June 2021

NTNU
Norwegian University of
Science and Technology

Andreas Norum

^{31}P MRS protocol optimization and repeatability testing in calf muscle of healthy volunteers on a clinical 7 Tesla MR scanner

Master's thesis in Applied Physics and Mathematics
Supervisor: Pål Erik Goa
Co-supervisor: Maria Tunset Grinde
June 2021

Norwegian University of Science and Technology
Faculty of Natural Sciences
Department of Physics

NTNU
Norwegian University of
Science and Technology

Preface

This master's thesis concludes a five-year master's degree program in Applied Physics and Mathematics at the Norwegian University of Science and Technology. This work is a continuation of the specialization project written during the fall semester of 2020. Portions of chapter 2 and 3 was written to the specialization project, with some improvements and structural changes. My specialization for the last three year has been Biophysics and medical technology. This gave me the opportunity to learn and take part of the rapid development in medical technology.

I would like to express my gratitude to my supervisors Maria T. Grinde, at St. Olavs Hospital, and Pål Erik Goa, at NTNU, for giving me the opportunity to work on this project, and for all the guidance and support throughout this time. I would also like to thank my volunteers for their time used to participate in this thesis. At last, I would also like to thank my family and my fellow students at Biophysics and medical technology.

Andreas Norum
Trondheim, June 2021

Abstract

The main objective for this master's thesis was to establish a scan protocol and evaluate the repeatability in ^{31}P MRS in calf muscles of healthy volunteers at the clinical 7T MR scanner at St. Olavs Hospital. The protocol optimization was based on the protocol found optimal for the '^{31}P metabolites phantom' made during the specialization project during the fall semester of 2020. To confirm the content of ^{31}P metabolites in the phantom, a small sample from the phantom was analyzed using high resolution magic angle spinning magnetic resonance spectroscopy (HR MAS MRS). The metabolites were identified using the softwares Chenomx and TopSpin. The metabolites found were PC, PE, Pi, GPC, α-ATP, β-ATP, γ-ATP and NAD.

A protocol with shorter repetition time (800 ms) and changed pulse type (rectangular) was found optimal in a calf muscle of a healthy volunteer compared to the optimal protocol found for the '^{31}P metabolites phantom'. These results suggests that optimal acquisition parameters are quite different in a phantom compared to in a muscle in a volunteer. Using a phantom can be very useful when, for example, testing ^{31}P MRS protocols in an initial phase.

The scan setup used for repeatability testing consisted of segments with three scans separated by repositioning of the ^{31}P loop coil. After three such segments the volunteer flexed the calf muscle, without repositioning the coil, for a fourth segment. At the end a final segment of five scans was performed with relaxed muscle.

The key results showed that the repeatability was sublime for scans performed right after each other without repositioning the ^{31}P loop coil. When comparing scans before and after repositioning of the coil the differences were larger. The metabolic changes before, during and after flexing of the calf muscle was also analyzed by looking at the peak area of PCr measured with the use of the analysis software FID-A, and the intracellular pH calculated from the chemical shift difference between Pi and PCr. Measured pH in the volunteers for a relaxed calf muscle was around 7.04 $\pm$ 0.1. A pH of 6.98 $\pm$ 0.1 was found when the muscle was flexed. The amount of PCr decreased during muscle flexion for five out of six scans. Overall, these data are in line with earlier findings made by others.

The repeatability for the ^{31}P loop coil at the 7T MR scanner was in general very good, even though some intra-individual differences were found. The main source leading to less adequate repeatability was the repositioning of the ^{31}P loop coil between the scans of the healthy volunteers. The coil was also able to detect and repeat good results considering the chemical shift difference used to calculate the pH in the muscle of the volunteers.

Sammendrag

Hovedmålet for denne masteroppgaven var å etablere en skannprotokoll og evaluere repeterbarheten i ^{31}P MRS i leggmuskelen hos friske frivillige på den kliniske 7T MR-skanneren ved St. Olavs Hospital. Startpunktet for protokolloptimaliseringen var basert på protokollen som ble funnet optimal for et ^{31}P metabolittfantom laget i forbindelse med fordypningsprosjektet høstsemesteret 2020. For å bekrefte innholdet av ^{31}P metabolitter i fantomet ble en liten prøve fra fantomet analysert ved bruk av high resolution magic angle spinning magnetic resonance spectroscopy (HR MAS MRS). Metabolittene ble identifisert ved brukt av analyseprogrammene Chenomx og TopSpin. De identifiserte metabolittene var: PC, PE, Pi, α-ATP, β-ATP, γ-ATP og NAD.

En protokoll med kortere repetisjonstid (800 ms) og endret pulstype (rektangulær) ble funnet optimal i en leggmuskel hos en frisk frivillig sammenlignet med den optimale protokollen som ble funnet for fantomet i fordypningsprosjektet. Disse resultatene antyder at optimale opptaksparametere er vesentlig forskjellig i et fantom sammenlignet med en muskel hos en frivillig. Bruken av fantomer kan være veldig nyttig til for eksempel testing av ^{31}P MRS-protokoller i en tidlig fase.

Oppsettet til repeterbarhetstestingen bestod av segmenter med tre skanninger, hvor hvert segment ble skilt ved reposisjonering av ^{31}P -overflatespolen. Etter tre slike segmenter strammet den frivillige leggmuskelen, uten at spolen ble reposisjonert, for et fjerde segment. Til slutt ble et siste segment bestående av fem skanninger gjennomført med avslappet muskel.

Hovedresultatene viste at repeterbarheten var sublim for skanninger som ble gjennomført rett etter hverandre uten at ^{31}P -spolen ble reposisjonert. Sammenligningen av skanninger før og etter reposisjonering ga større differanser. De metabolske forandringene før, under og etter stramming av muskelen ble også analysert ved å se på arealet under toppen i spekteret for metabolitten PCr, målt ved bruk av analyseverktøyet FID-A. Intracellulær pH ble beregnet fra den kjemiske skift-differansen mellom Pi og PCr. Beregnet pH i de frivillige da muskelen var avslappet var rundt 7.04 ± 0.01. pH lik 6.98 ± 0.01 ble beregnet da muskelen var strammet. Målingen av signalet fra PCr avtok ved stramming av muskel for fem av seks skanninger. Samlet sett er disse dataene i samsvar med det andre har funnet tidligere.

Repeterbarheten for ^{31}P -overflatespolen på 7T MR-skanneren var generelt god, selv om noen intra-individuelle forskjeller ble funnet. Hovedkilden som førte til mindre optimal repeterbarhet var reposisjoneringen av ^{31}P -spolen mellom skanninger av de friske frivillige. Spolen var kapabel til å detektere og repetere gode resultater med tanke på den kjemiske skift-differansen som ble brukt til å beregne pH i de frivilliges muskel.

Table of Contents

List of Figures

List of Tables

Chapter 1

Introduction

Phosphorus-31 magnetic resonance spectroscopy (^{31}P MRS) was first used for metabolic investigations in the 1960's. The first persons to acquire a high-resolution ^{31}P spectrum of a solution of ATP were Cohn and Hughes [3]. They also observed that the phosphorus nuclei of ATP had a dependence of the chemical shift on the pH of the solution under investigation. In parallel with the development of MRI, the field of ^{31}P MRS for metabolic investigations developed during the decade of 1970. The first *in vivo* ^{31}P MRS study was performed on a mouse brain. Many other organs were also studied during this decade, but most of them were performed on excised organs to avoid the need for spatial localization.

The 1980s started with two important publications that aimed at acquiring ^{31}P spectra from spatially defined regions *in vivo*. The paper from Ackerman *et al.* [4] were the first that detected ^{31}P signal in localized regions using a surface coil. By using the surface coil, it was now possible to acquire ^{31}P spectra *in vivo* without the use of spatial localization sequences. Studies using surface coils are still used today due to the simplicity of such an approach. At the same time as the study from Ackerman *et al.*, Bendel *et al.* [5] demonstrated for the first time the feasibility of spatial mapping of phosphate metabolites in a phantom, containing ATP, phosphocreatine (PCr) and inorganic phosphate (Pi). During late 1980s and early 1990s, several different single-voxel spectroscopy techniques from multiple voxels in a human brain was done. These studies opened the doors for unprecedented dimensions of spatial and spectral information in metabolic studies of ^{31}P MRS and ^{31}P MRS imaging (^{31}P MRSI) [6].

More than 60 years ago Bloch [7] identified that by introducing a spinning motion to the sample during a NMR experiment would improve the effective homogeneity of the magnetic field. The improved effect was demonstrated by Anderson and Arnold [8], and an analysis of the effect was given by Williams and Gutowsky [9]. A few years later, both Lowe [10] and Andrew *et al.* [11] independently documented that by using this technique in solid state NMR, it was possible to achieve narrowing of line widths. The crucial point in both their methods was to use an angle of 54.74°to spin the sample around axis relative to the direction of the static magnetic field. This technique has today become known as magic angle spinning (MAS) [12].

The first demonstration of high resolution MAS (HR MAS) was done in 1996 [13]. HR MAS permits the analysis of solid samples with a high spectral resolution. The probes used in HR MAS combines the magic angle spinning found in solid-state MAS probes with low power RF handling, a pulsed field gradient that are characteristic of solution-state NMR, and a lock channel [14]. The main use of the MAS technique has been to

perform solid-state MRS experiments [15]. Analysis of different kinds of tissues with HR MAS gives quantitative metabolite measurements with minimum of sample preparation [16].

In vivo ^{31}P MRS experiments and studies of skeletal muscles and other organs is a method that is preferred when investigating cellular energetics. This is because it is much more functional, in the ways that it can be used for studies in various functional states. This method also avoids the many limitations of the more classical method biopsy. *In vivo* ^{31}P MRS has been used in studies of skeletal muscles over 500 times the last four decade, which is more than any other studied organ [17]. This method using *in vivo* ^{31}P MRS can only detect metabolites containing phosphorus with concentrations of around 100 μM and above, but this limit is low enough to be able to detect the key metabolites in ATP metabolism, PCr, Pi, and cellular functions phosphorus metabolites contributes to e.g. force production [2]. These types of studies provide a unique non-invasive way to learn more about the metabolism in skeletal muscle. One type of study is measurement of PCr or other metabolites before, during and after exercise. Measuring multiple metabolites during the experiment/study is one of the advantages with *in vivo* ^{31}P MRS, and MRS techniques in general. A major drawback is that these experiments often uses a surface coil in the data collection which has a limited depth sensitivity [18].

The first proposals of measuring intracellular pH by the use of ^{31}P MRS came about 40 years ago. The earliest human applications studies included muscle exercise [19] and detection of some types of muscle pathologies. Chemical shift difference between a pH-independent reference peak and the pH-dependent metabolite inorganic phosphate (Pi) is measured with ^{31}P MRS to be able to determine the pH [20, 21]. A key advantage by using *in vivo* ^{31}P MRS is that it is a noninvasive and nonpertubing technique [22]. Measuring intracellular pH is of great interest because it is a parameter that controls cell activity, functionalities, and cellular events. Changes or abnormalities measured in the intracellular pH could tell something about the healthy status of a cell, which could further tell something about pathological changes in a macro perspective for the patient in question [23].

The ability to repeat data in an experiment within the same or in different volunteers/patients is important in order to know that change in results can be trusted. Some studies have shown that the repeatability in ^{31}P MRS is generally very good [24, 25]. Even though some intra-individual differences have been found, there are no testing in these studies that has shown a systematic bias or a population dependent variability (inter-individual) [26, 27, 28]. These types of studies have not been done at the 7T MR at St. Olavs Hospital, and they are important to figure out any systematic bias or other errors for the ^{31}P MRS at this MR scanner. Although the ^{31}P is generally very reproducible, it has been shown that the results from mitochondrial functions are less reproducible compared to, for example, measurements of phosphocreatine concentration [24, 29].

The overall research objective for this master's thesis is to test the repeatability in ^{31}P MRS experiments at the 7T MR at St. Olavs Hospital. This will be done using a protocol which is found optimal for a healthy volunteer. The protocol optimization will be based on the parameters found optimal for the ^{31}P MRS metabolite phantom at the 7T MR in the specialization project last fall to see if the settings are directly transferable to a healthy volunteer. We will also take a short look at the metabolic changes before, during and after flexing the calf muscle during scanning.

Chapter 2

Theory

2.1 Magnetic resonance

The technique of magnetic resonance spectroscopy (MRS) allows tissue to be interrogated for the presence and concentrations of various metabolites. While magnetic resonance imaging (MRI) identifies the anatomical location of for example a tumor in the brain, MRS compares the chemical composition of normal brain tissue with the abnormal tumor tissue [30]. MR spectra can be acquired from any 'NMR-active' nucleus, which means a nucleus possessing non-zero spin, e.g., proton, carbon-13 and phosphorus-31 [31].

A nucleus with an odd number of protons spins along its axis, as for example ^{1}H, ^{13}C and ^{31}P. ^{31}P has two possible spin states: $+1/2$ or $-1/2$. These spins aligns randomly in the absence of a magnetic field, but in the presence of an external magnetic field, the nuclei align with or against the magnetic field. Depending on if the nuclei aligns with or against the magnetic field, the spins have either a lower or a higher energy state, respectively [32]. This is shown in Figure 2.1. The distribution of spins aligned with or against can be described by a Boltzmann distribution

$$\frac{N^-}{N^+} = e^{-E/kT}, \tag{2.1}$$

where N^- represents the spins aligned against the magnetic field and N^+ represents the spins aligned with the magnetic field. T is the temperature in Kelvin, k is the Boltzmann's constant equal to $1.38 \cdot 10^{-23}$ J/Kelvin, and E is the difference in energy between the spin states. N^+ is slightly larger than N^- at room temperature. From equation (2.1) the ratio of N^-/N^+ decreases with decreasing room temperature, and approaches one with increasing temperature. The MRS signal is proportional to the population difference between the spin states because the signal results from the net difference between absorbed energy and emitted energy. Absorbed energy comes from transition of spins from lower to higher energy state while the emitted energy comes from transition of spins from higher to lower energy states simultaneously [33].

Precession
Precession is a motion that occurs when an external force affects a spinning object. In MRS this motion occurs when the nuclei of interest (^{1}H, ^{31}P etc.) generates a magnetic field from its own spin and from that gets a magnetic dipole moment. The magnetic dipole moment is parallel to the axis of rotation and when placed in a magnetic field this dipole moment will start its precession with an angular frequency, Larmor frequency,

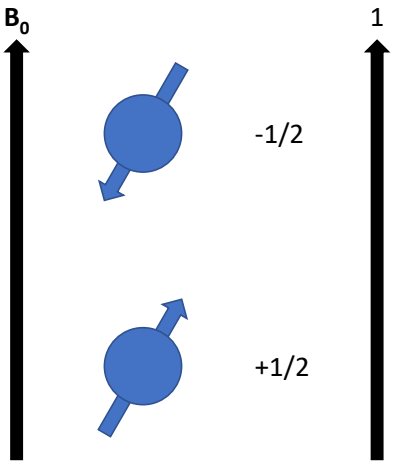

Figure 2.1: Nuclear spin state energy for spin either aligned with or against the magnetic field. 1) Direction of the nuclear spin state energy.

around the direction of the magnetic field [34]. The connection between the frequency of the precession and the magnetic field strength is described in the Larmor equation

$$\nu_0 = \frac{\gamma}{2\pi} \mathrm{B}_0, \tag{2.2}$$

where γ is the gyromagnetic ratio and B_0 is the magnetic field strength.

Chemical shift

The effect referred to as the chemical shift is caused by shielding of the nuclei from the external magnetic field by the electrons surrounding them. Without this effect, spectroscopy would not be possible because all nuclei of the same element would resonate with equal frequency. This can understood from equation (2.2) where the gyromagnetic ratio is the only factor depending on the nuclei, which is identical for the same nuclei in different molecules. When the molecule is placed in an external magnetic field, the electrons surrounding the nucleus will rotate about B_0 in an opposite sense to the nuclei spin precession, as shown to the left in Figure 2.2. This give rise to a magnetic moment μ_e at the nucleus since the electrons surrounding the nucleus can be regarded as small currents since the precession of electrons involves motion of charges. This electron induced magnetic moment will oppose the primary applied magnetic field B_0, and this leads to a reduction of the magnetic field sensed by the nucleus, which is shown to the right in Figure 2.2. The effect caused by this can be expressed in terms of an effective magnetic field B sensed at the nucleus:

$$\mathrm{B} = \mathrm{B}_0(1 - \sigma), \tag{2.3}$$

where σ is a dimensionless shielding constant, often expressed in parts per million (ppm), which depends on the chemical environment around the nucleus. By combining equation (2.2) and (2.3), the condition of calculating the resonance frequency can be altered to:

$$\nu = \frac{\gamma}{2\pi} \mathrm{B}_0(1 - \sigma). \tag{2.4}$$

The result of equation (2.4) is expressed in units of Hertz. This unit is not usually used for representation of chemical shifts, since it would make chemical shifts dependent on the magnetic field strength. The chemical shift is instead expressed in terms of ppm:

$$\delta = \frac{\nu - \nu_{\mathrm{ref}}}{\nu_{\mathrm{ref}}} \cdot 10^6, \tag{2.5}$$

where ν is the frequency of the nuclei under investigation and ν_{ref} is the frequency of a reference nuclei. Choosing a stable reference nuclei is important to get good and reliable results. The reference nuclei should be chemically inert and the chemical shift should be independent of external variables like, for example, temperature, ionic strength, and shift reagents. It should also produce a strong resonance signal that is well separated from other smaller and larger resonances. The accepted reference nuclei varies for different types of spectroscopy, and for ^{31}P MRS the chosen reference is often PCr [35].

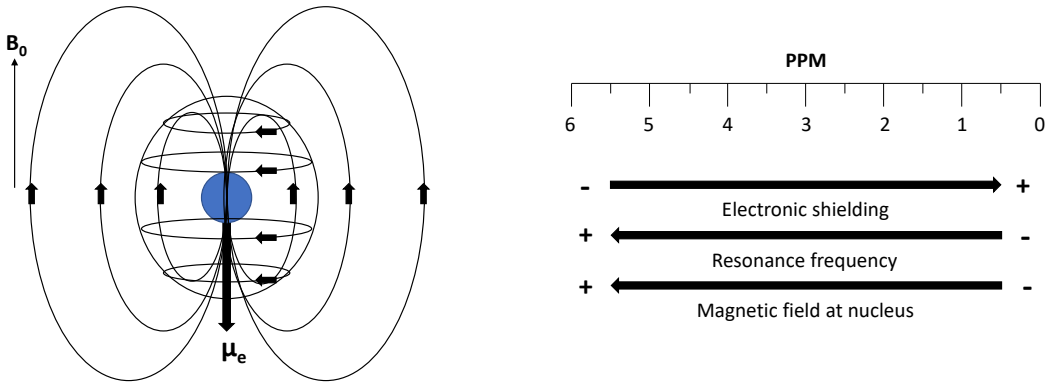

Figure 2.2: *Left:* Electrons surrounding a nucleus can be regarded as small currents. These will then give rise to a magnetic moment μ_e at the nucleus which reduces the effective magnetic field at the nucleus since the magnetic moment from the electrons opposes the external magnetic field. *Right:* The Figure shows how the different effects affect the chemical shift.

Spin-spin coupling

MRS can be seen as a quantitative technique because of different features like chemical shifts, which gives information about the chemical environment of a nuclei, and measuring the integrated resonance area, which is directly proportional to the concentration of the compound in question. But in order for it to be used as a quantitative technique, it is required that a quantitative MRS sequence is used, or that it is corrected, for example, for T_1 relaxation.

In addition to these features is the splitting of resonances into several smaller lines observed in high-resolution MRS, a phenomenon often referred to as spin-spin coupling or scalar coupling J [35]. Spin-spin coupling is known as the interactions between different types of nuclei present in a molecule that causes a single peak to split into a doublet, triplet, or multiplet. The core of spin-spin coupling involves spinning nuclei. The orientation of the spin will then either increase or decrease the effective magnetic field on the nuclei with a small amount. These spinning nuclei gives rise to the coupling phenomenon in MRS. The precession frequencies of the nuclei are affected by the interactions of the magnetic spins of these resonating nuclei. The experienced effective magnetic field from the neighboring nuclei as a result of magnetic spins affect the chemical shift values, and in addition the nature of the MRS spectrum [32].

T_1 relaxation

T_1 recovery is the process by which the longitudinal magnetization recovers to it's initial value parallel to the main magnetic field. This type of relaxation is called spin-lattice

energy transfer, and that is because the T_1 relaxation time quantifies the rate of energy transfer to the neighboring molecules from the nuclear spin system [36]. The rate of T_1 recovery is an exponential process and occurs at different rates for different molecules and nuclei. There is a time constant associated with this exponential relationship, and it is called the T_1 recovery time and is the time it takes for 63% of the longitudinal magnetization to recover in a tissue. The value of the T_1 recovery time can be calculated by using the equation

$$\mathrm{SI} = 1 - e^{-t/\mathrm{T}_1} \tag{2.6}$$

where SI is the signal intensity in a tissue, T_1 is the recovery time (ms) and t is the time (ms). The signal intensity in equation (2.6) can also be described by the fraction $\frac{\mathrm{Mz}_t}{\mathrm{Mz}}$ where Mz_t is the amount of longitudinal magnetization at time t after the removal of the excitation pulse and Mz is the full longitudinal magnetization [37]. The T_1 relaxation time for different phosphorus metabolites decreases significantly when analyzed at a higher field strength [6].

T_2 decay

T_2 decay is the process by which the transverse components of magnetization decay or dephase, and T_2 refers to that the decay is the secondary relaxation process. This relaxation is also called spin-spin relaxation caused by dephasing of magnetic moments of the spins. The rate of the T_2 process is a exponential decay with a time constant associated with the exponential relationship called T_2 decay time. The T_2 decay time is the time it takes for 63% of the transverse magnetization to dephase in a tissue. This connection can be described by the equation

$$\mathrm{SI} = e^{-t/\mathrm{T}_2}, \tag{2.7}$$

where SI is the signal intensity in a tissue, t is the time in milliseconds and T_2 is the decay time for a specific tissue. The signal intensity can also be expressed as $\frac{\mathrm{Mxy}_t}{\mathrm{Mxy}}$ where Mxy_t is the is the transverse magnetization at time t after the removal of the excitation pulse and Mxy is the full transverse magnetization [37]. Figure 2.3 shows how the T_1 recovery and T_2 decay processes can be represented.

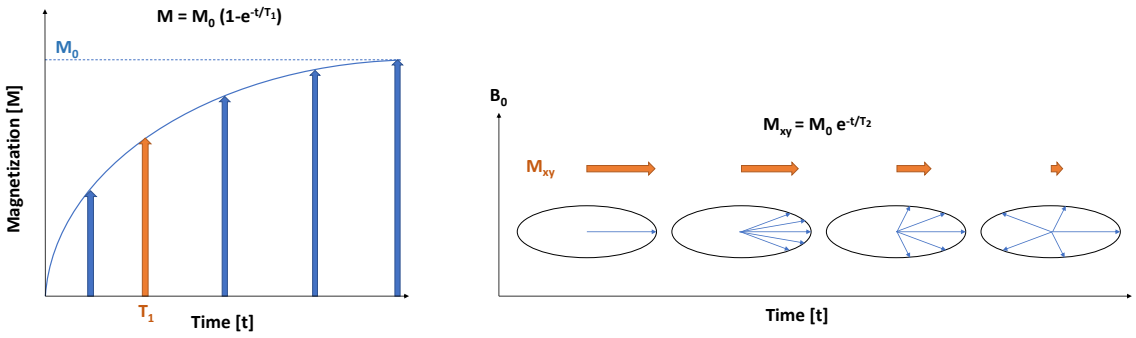

Figure 2.3: *Left:* T_1 relaxation where the longitudinal magnetization recovers back to it's initial magnitude. *Right:* Dephasing (T_2 relaxation) of the transverse magnetization in the Mxy plane.

Tuning and matching

Tuning and matching of the radio frequency (RF) coils is necessary to do each time a new patient or sample is placed in a scanner in order to reach the wanted Larmor frequency and characteristic impedance for the scanners RF system. This is necessary for optimal

power transfer efficiency because susceptibility effects distorts the magnetic field produces small changes in the Larmor frequency of the patient or sample. The tuning is used get a precise resonance frequency of the patient or sample. Tuning is performed by using variable capacitors together with the fixed capacitance and inductance of the RF coils. Matching is used to maximize the energy transfer between coil and patient or sample. It is done by changing the coil impedance of the system to match the impedance of the patient or sample. Tuning and matching is normally done automatically in clinical MR scanners, but it can also be done manually in NMR scanners or HR MAS MRS [38, 39].

2.2 Phosphorus-31 MR spectroscopy

Phosphorus-31 is used in MR spectroscopy du of the relatively high sensitivity of phosphorus MR, which is about 7% of protons sensitivity, together with a 100% natural abundance allows the acquisition of high-quality spectra within minutes. Also, the chemical shift dispersion of the phosphate metabolites found *in vivo* is relatively large (ca 30 ppm), which even at low clinical magnetic field strengths can result in excellent spectral resolution. The main product of MRS is a spectrum with a frequency axis in parts per million (ppm) and a signal amplitude axis. The signal amplitude on the y-axis is a measure of the concentration of a specific metabolite. Each metabolite detected in a spectroscopy give rise to either a single peak or multiple peaks that are uniquely positioned along the frequency axis known as the chemical shift. The dispersion of the chemical shift along the x-axis is directly proportional with the magnetic field strength, and the peak amplitude is directly related to the concentration of the specific metabolite which is displayed along the y-axis [40].

^{31}P MRS also has the property that no techniques involving suppression is necessary due to the absence of a dominant fat signal or water signal. The T_1 relaxation time for different phosphorus metabolites is reduced significantly at higher field strengths, which therefore allows for data acquisition with a relatively short repetition time [6].

Phosphorus MR is capable of detecting metabolites that play key roles in tissue energy metabolism, and it is very useful because these metabolites can be detected with simple MR methods. Other relevant parameters such as intracellular pH may be indirectly deduced from a ^{31}P MR spectrum [35]. Some of the major metabolites detected by ^{31}P MR spectroscopy are:

- Adenosine triphosphate (ATP) is together with phosphocreatine the principal donor of free energy in biological systems. ATP is normally detected with three well-separated resonances, α, β and γ [35]. Combining the concentrations from these three peaks in a MRS spectra can be used to calculate the concentration of ATP.
- Phosphocreatines (PCr) main role is suggested to be an energy buffer, retaining constant ATP levels through the creatine kinase reaction and as an energy shuttle, diffusing from energy producing to energy utilizing sites [35].
- Phosphocholine (PC) is a precursor as well as a degradation product of phosphatidylcholine, a major phospholibid of eukaryotic bio-membranes. PC-modified macromolecules are also known to provoke strong anti-inflammatory effects and contribute to immune evasion of parasites [41].
- Phosphorylethanolamine (PE) has four MRS-observable protons in two methylene groups which give rise to two multiplet resonances [35]. Increased levels of PE has

been observed during seizures [42] and it can be observed with enhanced sensitivity through polarization transfer [43].

- Determination of the Inorganic phosphate (Pi) signal frequency and amplitude can be used to measure the cardiac intracellular pH (pH_i) and the free energy of ATP hydrolysis [44].
- Phosphodiesterase (PDE) have been studied extensively in a wide range of disorders as they breakdown second messengers, rendering them as crucial regulators [45]. The signal detected as PDE in spectra is often assumed as the sum of signals from Glycerophosphocholine (GPC) and Glycerophosphoethanolamine (GPE) [46], but it can also be other metabolites and not GPC and GPE [47].

Two factors that can affect the ppm value of a metabolite in MR spectra are temperature and pH. Almost all metabolites increase their ppm value when the pH decreases. How much depends on the different metabolites, and it can also vary within a metabolite, such as ATP. The three phosphorus atoms in ATP vary different to change in pH. γ-ATP has the largest change and α-ATP has the smallest change in ppm value. Most of the change in ppm value for all metabolites happens around pH 5 to 7 [48]. There is also a change in the ppm value for metabolites when changing the temperature. The ppm value either increases or decreases depending on the metabolite. For example, the ppm value of creatine and PCr decreases with increasing temperature while other metabolites increase with increasing temperature [49].

2.3 High resolution magic angle spinning MRS

The main idea with high resolution magic angle spinning (HR MAS) is spinning a sample in solid state at an magic angle equal to 54.74° relative to the magnetic field. This achieves narrowing of line widths in MRS. Figure 2.4 shows how a rotor filled with sample is placed in the magnetic field. Spinning of the sample narrows the broad resonance through a transformation at the isotropic resonance frequency [12, 16]. MAS is a technique commonly used in solid-state NMR/MRS because this technique applies line-narrowing which is needed for NMR-based metabolomics studies to other heterogeneous specimens than brain tissue. Brain tissue analyzed with ^{1}H MRS have relatively narrow signals in its spectra because of characteristics like fast molecular tumbling which partially averages any susceptibility effects [50].

^{1}H HR MAS is used to study a large amount of different diseased and healthy tissues. It is highly sensitive and have the possibility to measure a large number of metabolites. ^{31}P HR MAS has the advantage that it can get well resolved resonances of many different phosphate metabolites as for example GPC, GPE, PE and PC. These resonances can easily be resolved and measured in a 1D spectrum, while with a 1D ^{1}H HR MAS spectrum it is harder to observe PE and GPE, while PC and GPC are possible to observe. To be able to detect PE and GPE more accurately 2D spectra are required in order to visualize these two metabolites [51].

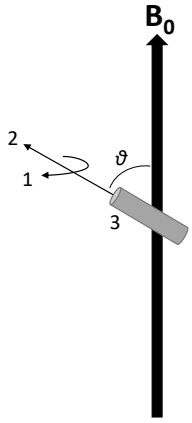

Figure 2.4: A rotor filled with sample spinning at the magic angle (54.74°) compared to the magnetic field. 1) The rotor spinning direction around its own axis. 2) The magic angle axis. 3) The MAS rotor simplified. θ is the magic angle equal to 54.74°.

2.3.1 Magic angle spinning

The magnetic field that a sample experiences in an MRS experiment is called the effective magnetic field and can be expressed as:

$$B = \mu_0 H_0 + M, \tag{2.8}$$

where M is the magnetization of the sample per unit volume, μ_0 is the permeability of the free space and H_0 is the external magnetic field. M can also be defined as χB_0 if the magnetic susceptibility is isotropic, where the χ is a scalar component of the susceptibility and B_0, which is the magnetic field induction, is equal to $\mu_0 H_0$. From this, equation (2.8) can be changed to:

$$B = \mu_0 H_0(1 + \chi) = \mu H_0, \tag{2.9}$$

where the permeability of the sample $\mu = \mu_0(1 + \chi)$. By looking at the two equations above, (2.8) and (2.9), it can be seen that the effective field B experienced in a sample has a direct dependence on χ, which emerges from the local dipole moment M. This dependence can lead to a shift the NMR signals of a sample if the sample is combined with a homogeneous liquid. The reason for this is that the susceptibility of the liquid medium can induce an additional homogeneous magnetic field in the sample. This effect is called susceptibility broadening and its magnitude can be estimated by determining the induced dipolar magnetic field.

Now consider a dipolar magnetic moment m placed in a spherical volume with permeability $\mu_m = 1+\chi_m$ and radius a. Then consider a point K placed in a medium with permeability $\mu_2 = 1 + \chi_2$ at a distance R from the magnetic moment m. The magnetic moment m generates a magnetic field B_z at point K, which is dipolar. The B_z field is the factor that essentially causes the line broadening and the magnitude of the induced effect can be estimated with the equation

$$B_z = -\frac{\Delta\chi \cdot a^3}{3 \cdot R^3} B_0(3cos^2\delta - 1), \tag{2.10}$$

where $\Delta\chi$ represents the difference $\chi_2 - \chi_1$ and δ is the angle between B_0 and the dipolar vector between the dipolar magnetic moment in the spherical volume and the point K.

The angle contribution in equation (2.10) can be canceled out by spinning the sample at a certain angle $\theta_{\text{MAS}} = cos^{-1}(1/\sqrt{3}) = 54.74°$ relative to B_0. Spinning the sample at this angle was introduced in 1959 by Lowe [10] and Andrew [11], and is now known as MAS. MAS eliminates the broadening by susceptibility and results in an isotropic signal that has a chemical shit that depends on the nuclear spin chemical shift interaction [50].

2.3.2 Shimming

When the rotor capsule with the sample is placed inside the magnet for analysis, both the sample and the rotor capsule perturb the B_0 field. This perturbation of the field leads to a non-homogeneous B_0 field across the sample, which will lead to broadening of the resulting specter signals. The B_0 field needs to be corrected across the sample in order to minimize the effect, which can be done by B_0 field shimming. B_0 shimming for a HR MAS analysis is different compared to a standard liquid-state NMR analysis because of the changed orientation of the sample. The shimming is done along the magic angle axis in HR MAS [52]. In standard NMR experiments the shimming system usually consist of two types of shim coils: 1) cylindrical symmetric coils around the sample axis in order to reduce B_0 variations on-axis, called zonal shims, and 2) tesseral shims which are used to alter the B_0 variations that are off-axis. Examples of zonal shims are B_{z^1}, B_{z^2} and B_{z^3}, while examples og tesseral shims are B_x, B_y, B_{x^2}, B_{y^2}, B_{xy}, B_{zx} etc. For HR MAS it is a bit different because the inhomogeneity of the B_0 field is almost averaged to zero in the transverse plane, which implies that no corrections are necessary along the magic angle axis for the tesseral shims. The inhomogeneities along the magic angle axis can be corrected up to the third order using the zonal shims $B_{z^1}^{\text{MAS}}$, $B_{z^2}^{\text{MAS}}$ and $B_{z^3}^{\text{MAS}}$, and it can be done by adjusting conventional shims in a linear combination. As an example, if the stator containing the MAS rotor lies along the yz plane, the magic angle zonal shims are:

$$B_{z^1}^{\text{MAS}} = \frac{1}{\sqrt{3}} B_z - \frac{\sqrt{2}}{\sqrt{3}} B_y, \tag{2.11}$$

$$B_{z^2}^{\text{MAS}} = B_{X^2-y^2} - 2\sqrt{2} B_{zy}, \tag{2.12}$$

$$B_{z^3}^{\text{MAS}} = -\frac{2}{3\sqrt{3}} B_{z^3} - \frac{1}{\sqrt{6}} B_{z^2 y} + \frac{5}{\sqrt{3}} B_{z(x^2-y^2)} - \frac{5}{3\sqrt{6}} B_y. \tag{2.13}$$

The MAS notation indicates that the field follows the magic angle axis. One thing to note is that there are no x-directional shims, as seen in the example described by equation (2.11), (2.12) and (2.13), because the exact weighting is not important under MAS of these linear combinations. The optimal shim setup will often be different for different solvents and samples because the can have different susceptibilities. For a sample that is static, the tesseral shims in the magic angle axis directions would have to be considered as well [53], and from a practical point of view, three more shims ($B_{x^2-y^2}$, B_{z^3} and $B_{z(x^2-z^2)}$) needs the correct setting in order to obtain a correct lineshape. A good practice is to perform the shimming directly on a strong metabolic signal. A strong metabolic signal could be the doublets of alanine, glucose or lactate [50, 54].

2.3.3 Sample preparation

HR MAS experiments are usually performed on NMR spectrometers that are of a standard liquid-state type with a rotor that allows the sample to spin a the magic angle. Sample

preparation for an HR MAS MRS experiment is done manually. The sample, typically a type of tissue, is cut into usable sizes and placed in a rotor. A HR MAS rotor have a design made to minimize the different sources of magnetic field perturbations close to the sample. This feature keeps the resonance line widths similar to those obtained on a normal liquid-state HR rotor [54]. The rotors used in HR MAS usually has a range from 50 to 80 μL. Together with the sample is also a small amount of buffer, based on D_2O, added in order to achieve field lock without leading to metabolite extraction. The amount of buffer added is often in the range of 2-10μL. In order to keep the sample with added buffer inside the rotor during the analysis a sealing consisting of a taper and a screw cap is placed at the open end of the rotor to keep it from leaking [16]. Standard types of caps are usually made of Kel-F (fluoropolymer) that can be used in a temperature range of -20°C to 50°C. Other types of caps are made from macor and boron nitride. These caps can be used for temperatures from -150°C to 250°C and -150°C to 150°C, respectively [14].

Field locking
Field locking is used to stabilize the B_0 magnetic field in the region around the sample during the acquisition of data. This is important in order to be able to acquire an acceptable result, especially from long acquisitions, because even the slightest drift in the B_0 field could affect the final resolution of the spectra. The signal from the added deuterated water, D_2O, is constantly monitored by the field lock system. Whenever the ^2H signal from the deuterated water shifts due to drift of the B_0 magnetic field, the field lock system alters the total magnetic field strength in order to keep the signal from D_2O constant. This also explains why the D_2O-based buffer is added together with the sample in the rotor, because by keeping it close to the sample it is possible to ensure that the B_0 magnetic field adjustment is within the sample region [50].

Another feature with the HR MAS rotor is that the radio-frequency circuits used on these rotors are designed to withstand only the power on a liquid-state NMR spectrometer that is classically available. Because of this, HR MAS rotors cannot be used in other typical solid-state experiments like cross-polarization [54].

2.3.4 Temperature

Temperature in the rotor during an HR MAS experiment can influence the resulting NMR signal. This can happen if the ^1H shift of the sample is temperature-dependent, which can cause a broadening signal acquired. The change in temperature can come from heat caused by friction on the rotor surface from air bearing, which can induce a local temperature gradient inside the rotor. For water this temperature gradient has a chemical shift temperature dependence equal to 6 Hz per degree centigrade at 500 Hz [50, 55]. This is especially important to consider when working with samples consisting of water, like cells or biopsies, because the temperature gradients present will not always allow for the use of field lock level as a reliable measure of the homogeneity of the field [54].

2.3.5 Pulse programs

There exists a large amount of different pulse sequences to use for HR MAS MRS. Here we are presenting three different pulse programs used for this master's thesis. All the pulse programs for HR MAS MRS have different abbreviations that explains something about its field of usage. One pulse program used was a 1D ^1H MRS called noesygppr1D. This program is a 1D version of a collection of 2D experiments named NOESY. NOESY stands

for Nuclear Overhauser Effect SpectroscopY and consists of experiments that provides proton-proton connectivities. The specific pulse program noesygppr1D is described as follows in the Pulse Program Catalog for Bruker Biospin [56]:

> 1D NOESY with presaturation during d1 and mixing time and spoil gradients.

In this master's thesis 1D ^{1}H spectra were acquired of a sample from a phantom made for the specialization project. 1D NOESY is a pulse sequence that has become one of the standard pulse sequences for NMR-based studies [57]. 1D NOESY specks creates high quality spectra with good water suppression [58]. d1 describes the time before the first pulse in the pulse sequence and this period allows for relaxation to the original position before the read pulse is applied, and the mixing time describes the time between the first pulses and the last pulse producing the fid. The gppr in the abbreviation means that the pulse sequence includes presaturation both during the pre-scan relaxation time d1, and during the mixing time between the read-pulses. The spoil gradients are applied at the end of both the d1 and the mixing time [56].

The second pulse program used for the analysis of the phantom from the specialization project was a 1D ^{31}P MRS named zgpg (Bruker Biospin). Zgpg is a basic 1D pulse sequence with multinuclear applications that consists of a pre-scan delay which allows for relaxation to the original position of the sample before the read scan is applied and the signal is acquired from the fid. This sequence produces a ^{31}P spectra by decoupling the ^{1}H signal [56].

The third pulse program used was a 2D ^{1}H /^{31}P MRS program. This program has the abbreviation hsqcetgpprsisp2.2 (Bruker Biospin). The first part of the abbreviation, HSQC, stands for Heteronuclear Single-Quantum Correlation. This is a group of experiments/pulse programs that is designed to use proton-detection to obtain heteronuclear correlations between proton and other heteronuclei through a scalar coupling constant. The other heteronuclei could for example be ^{31}P or ^{13}C. The resulting spectra from this pulse program is a 2D spectra that shows markings where there are heteronuclear correlations [56]. Geoffrey Bodenhausen and D. J. Ruben was in 1980 the first to describe an experiment using HSQC [59]. An example is shown in Figure 2.5.

The representation of the data in a 2D spectra is called a correlation map. Two types of peaks can be observed in correlation maps, diagonal peaks and cross peaks, depending on if the NMR experiment is homonuclear or heteronuclear. Diagonal peaks can only be found in homonuclear correlation maps, while cross peaks can be found in both types of 2D spectra. The diagonal peaks corresponds to the absorption from a 1D NMR experiment and can be found along the diagonal of the spectra, where both axes have the same frequency values. Cross peaks are visible in both versions since they give information about the coupling of two nuclei. HSQC NMR experiments creates stronger signal from nuclei like ^{15}N and ^{31}P compared to traditional 2D NMR. These nuclei have a very low gyromagnetic ratio that is detected indirectly during HSQC experiments by transferring polarization through a ^{1}H nucleus [60]. From the Pulse Program Catalog for Bruker Biospin [56] this pulse program is listed under gradient-based programs and has the description:

> Phase-sensitive ge-2D HSQC using PEP and adiabatic pulses for inversion and refocusing with gradients in back-inept and presaturation.

Using PEP pulses (Preservation of Equivalent Pathways) in HSQC experiments is a

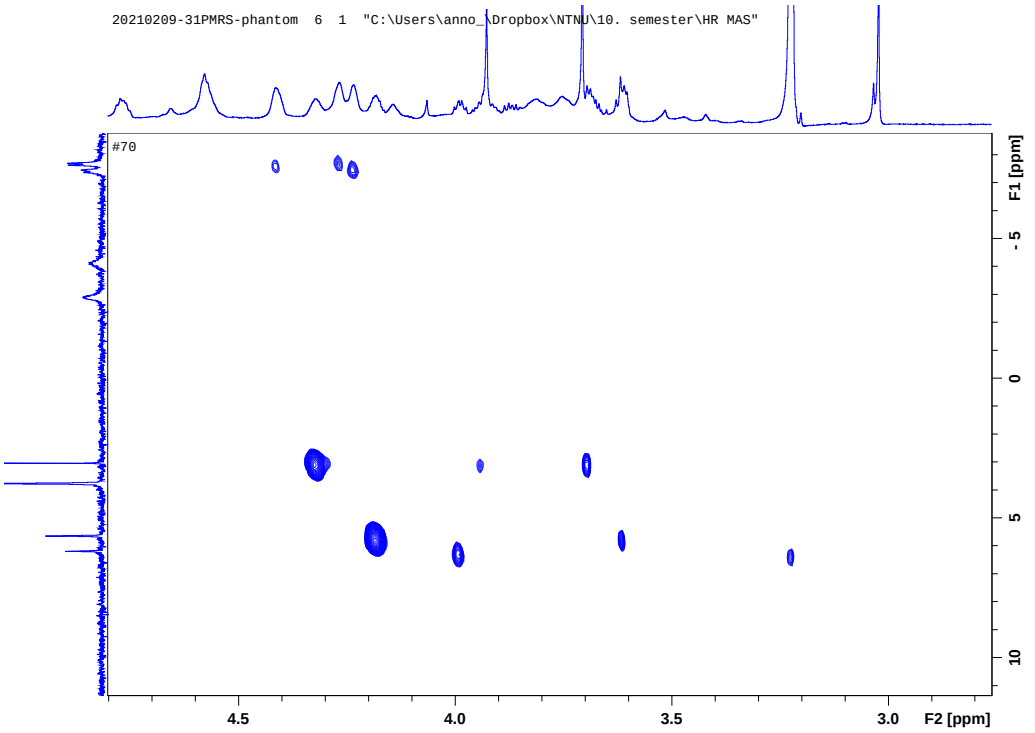

Figure 2.5: Resulting 2D spectra after running hsqcetgpprsisp2.2.

methodology that is based on the implementation of a second shifted 90°pulse in the regular HSQC pulse sequence. This methodology leads to a sensitivity enhancement of the signal. The shifted 90°is a refocused INEPT (Insensitive Nuclei Enhanced by Polarization Transfer) pulse sequence. An INEPT pulse sequence is widely used in 2D NMR because it facilitates for sensitivity improvements by polarization transfer from ^{1}H , which is a high-sensitive nuclei, to low-sensitivity nuclei as ^{31}P and ^{13}C [61, 62]. A standard INEPT pulse sequence consists of three parts:

- 90°^{1}H pulse in order to create transverse magnetization
- An heteronuclear spin-echo fixed period. This is to allow the evolution of heteronuclear coupling constants. Simultaneously should there be applied a 180°^{1}H and i.e. ^{31}P pulse in the middle of this period to refocus the evolution of chemical shift.
- Transfer polarization from ^{1}H to i.e. ^{31}P by simultaneous 90°^{1}H and i.e. ^{31}P pulses.

This can be seen in Figure 2.6.

The second pulse type named in the description of the pulse in addition to PEP pulse is the adiabatic pulse. Adiabatic pulses differ from other pulses because the carrier frequency varies with time and they are much more tolerant to field inhomogeneities compared to other pulses. Adiabatic pulses are also capable of refocusing heteronuclear spin that has a large chemical shift range, which is convenient when working with high-field spectroscopy [62].

The scalar coupling constant, also called J-coupling constant, describes something about the distance between and the angle between to atoms in a molecule. This is then used to

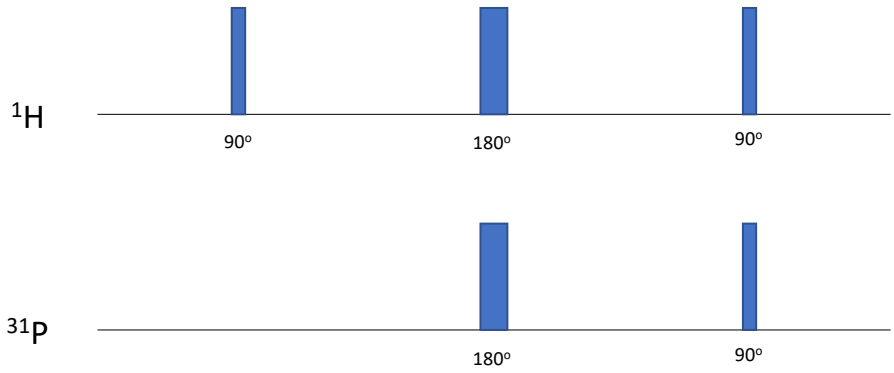

Figure 2.6: Simplified Insensitive Nuclei Enhanced by Polarization Transfer (INEPT) pulse sequence.

determine the interaction between two nuclei in the molecule containing spin. In NMR, the J-coupling constant can be used to validate what the different peaks in a NMR spectra represents. This can be especially important when doing a NMR experiment of a complex molecule. J-coupling is in comparison to the Zeeman interaction considered to be a weak interaction. The J-coupling is often used in combination with chemical shift to derive the through-bond connectivity in different kinds of proteins and other small molecules. J-couplings can either be heteronuclear or homonuclear. Heteronuclear J-coupling describes the bond between two different atoms, i.e. phosphorus and hydrogen, while homonuclear J-coupling describes the bond between hydrogen atoms with different chemical shifts. The magnitude of the J-coupling reduces with increased number of bonds between the atoms in question. The notation for J-coupling comes with a number describing the number of bonds between the atoms before J and thereafter the notation describing the coupling nuclei. For example, 1JHP describes the J-coupling of a phosphorus and hydrogen atom separated with one bond between them. In addition to the length between the atoms, some other properties that also affect the J-coupling constant are the hybridization of atoms, substituent electronegativities, dihedral angles etc [63, 64].

The determination of one-bond heteronuclear J-coupling constants with HR NMR spectroscopy is of interest for configuration-identification and molecular structure, but the measurement heteronuclear J-coupling constant is challenging due to i.e. low sensitivity and phase distortions etc. Because of this, the accurate measurement of J-coupling constants remain an important task. One advantage by 2D experiments when measuring this constant is the separation of chemical shift and J-coupling into two dimensions, but these experiments also suffer from phase-twist lineshape and must be displayed in magnitude mode, and therefore reducing spectral resolution and the accuracy of the J-coupling constant measurements [63, 65].

2.4 MRS parameters

When doing MRS there are several parameters that can be altered in order to optimize the spectra. The choices done for each of these parameters involves trade-offs in scanning time, visibility of different metabolites, and spatial and spectral resolution. Some of the parameters that can be altered in a ^{31}P MRS are repetition time (TR), number of signal averages, bandwidth, vector size and the pulse type.

Repetition time
The repetition time is defined as the time from the application of an excitation RF pulse to the application of the next excitation RF pulse for each slice. The TR time is measured in milliseconds or seconds, and it determines the amount of longitudinal magnetization that recovers between each pulse, which affects the peak height as seen in Figure 2.7. This means that the TR determines how much T_1 relaxation that has occurred before the signal is acquired [37]. Long TR time gives the longitudinal magnetization time to fully recover before the next RF pulse excitation, which is useful for quantification. Short TR time can introduce steady-state, where the longitudinal magnetization never fully recovers before the next RF pulse. After several pulses the maximum longitudinal magnetization that is possible to achieve will be the same, which means that it has reach a steady-state.

Varying the TR time for different scans can also be used to determine the T_1 relaxation time for the object in question. This can be done by doing several scans for increasing TR time, from very short to five-six times the assumed T_1 relaxation time and measure the magnitude of the integrated area under the peak. If done right, these different magnitudes of the integrated areas will follow a logarithmic line when plotted against the repetition time.

Ideally would long TR time always be used because better spectra would be produced for all metabolites. However, since the scanning time is directly related to the TR time, it is often considered that the benefits from a much longer TR time does not overcome the drawback of longer scanning time. For normal, clinical scans, the TR time is usually between 1500-2000 milliseconds as sort of a compromise [66, 67].

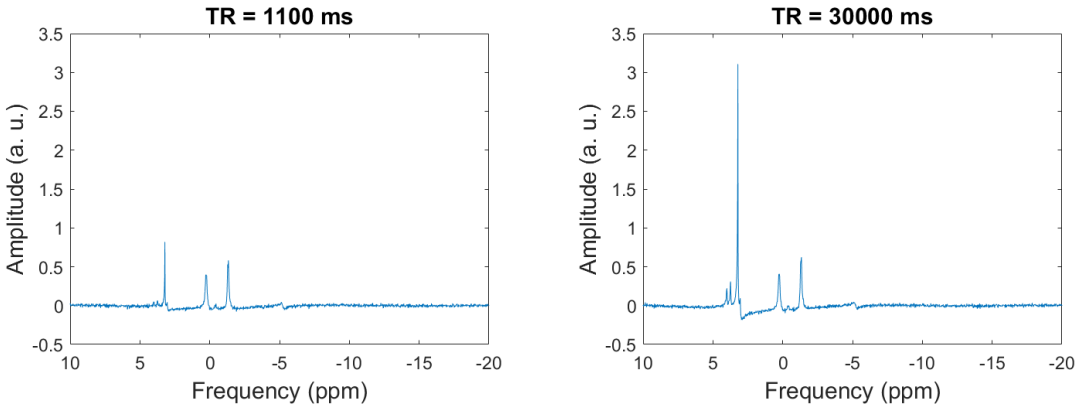

Figure 2.7: Longer TR leads to increasing recovery of longitudinal magnetization which leads to increased peak height.

The chosen repetition time for a scan can be used to find the optimal nutation angle for a specific tissue if the T_1 relaxation time for the tissue is already known. This optimal

nutation angle is known as the Ernst angle, α_{opt}, and can be found using the following equation:

$$\alpha_{\text{opt}} = arccos(\exp^{-\text{TR}/\text{T}_1}). \tag{2.14}$$

By following this equation, the optimal nutation angle becomes 90° for TR > $5T_1$, because this makes the exponential term vanish. For shorter TR times the optimal nutation angle reduces in size in order to maximize the acquired signal and reduce the saturation of longitudinal magnetization. The Ernst angle is also the nutation angle which produces the highest SNR for the given TR/T_1 ratio. Data acquisition with a short TR time and a corresponding Ernst angle found using equation (2.14) is often used for low-sensitivity nuclei in MRS, like ^{31}P. One effect to be aware of when using a short TR time and corresponding Ernst angle is that the short TR time introduces significant T_1 weighting. This weighting varies for the different metabolites because of different T_1 relaxation times, which in the end can influence the quantitative interpretation of the resulting metabolite spectra. Figure 2.8 shows the relationship between Ernst angle and the TR/T_1 ratio [35, 68].

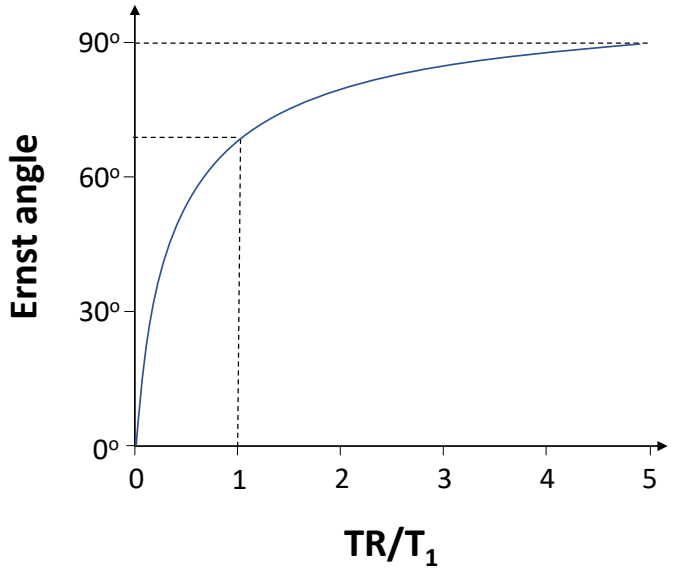

Figure 2.8: The graph shows the relation between the Ernst angle and the TR/T_1 ratio. Ernst angle is known as the optimal nutation angle for a chosen TR/T_1 ratio.

Number of signal averages

The parameter number of signal averages (NSA), also known as number of excitations (NEX), is the total number of times the FID-signal is acquired. This parameter mainly affects the signal-to-noise ratio and the scan time. Signal-to-noise ratio is increased by the square root of the NSA, SNR $\propto \sqrt{\text{NSA}}$, while the scan time increases proportional to the NSA. Increasing number of signal averages is also contributing to sharper and more defined peaks in the frequency spectrum, and the baseline noise is reduced significantly, as can be seen in Figure 2.9. The scan time is as mentioned also affected by the NSA, and it is directly proportional, so it increases with the increase in signal averages. This means that also here it must be compromised between sharper peaks and higher SNR, and increasing scan time [37, 66].

Bandwidth

The dependence of bandwidth occurs twice in an MR sequence, during transmission of the RF pulse and during reception of the MR signal. A typical range for bandwidth lies around a few kilohertz (kHz) in the transmission phase. In the reception phase is the

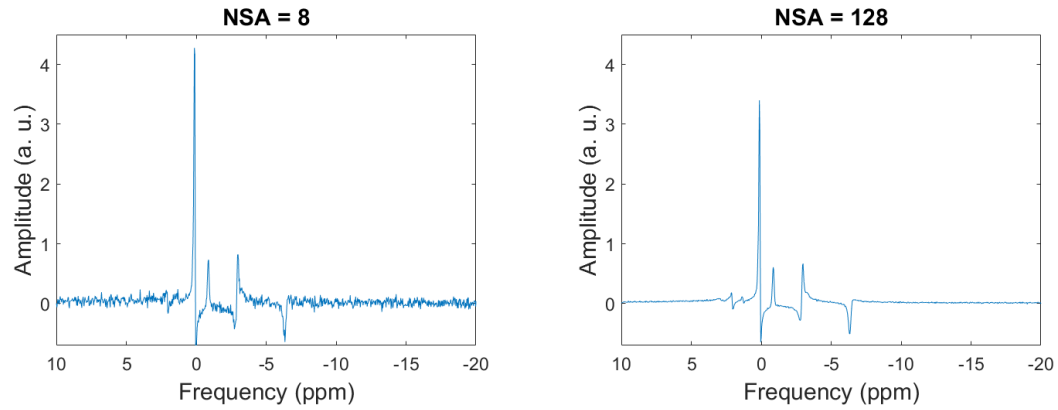

Figure 2.9: Increasing NEX leads to sharper peaks and reduced baseline noise.

bandwidth equal to the reciprocal of the total sampling time. Advantages with increasing the bandwidth is that it leads to a reduced sampling time which allows for shorter TE and TR times. Lower SNR is one of the disadvantages with increasing bandwidth, because of the large amount of noise that is sampled due to larger frequency range. Some of the advantages with lower bandwidth is higher SNR due to smaller frequency range to sample noise from, while some of the disadvantages with lower bandwidth are longer sampling time, which leads to longer TE and TR times [69].

Nuclear Overhauser Enhancement

The Nuclear Overhauser Enhancement (NOE) is a mechanism similar to proton decoupling which can lead to improved peak definition in a ^{31}P spectrum by selective RF-irradiation of proton nuclei. This NOE mechanism can be explained in the way that it saturates proton resonance in a system where these protons undergo a dipolar interaction with ^{31}P nuclei. This interaction contributes to a disturbance in the thermodynamic balance between spin up states and spin down states. The RF-saturation of the proton spins leads to a zero difference between the proton spins which therefore leads to an increase in the population difference for ^{31}P. The combination of these to effects can lead to an increase in the ^{31}P signal amplitude of up to 120%, but the increase is practically around 40-80%, which can be seen in Figure 2.10 [70, 71].

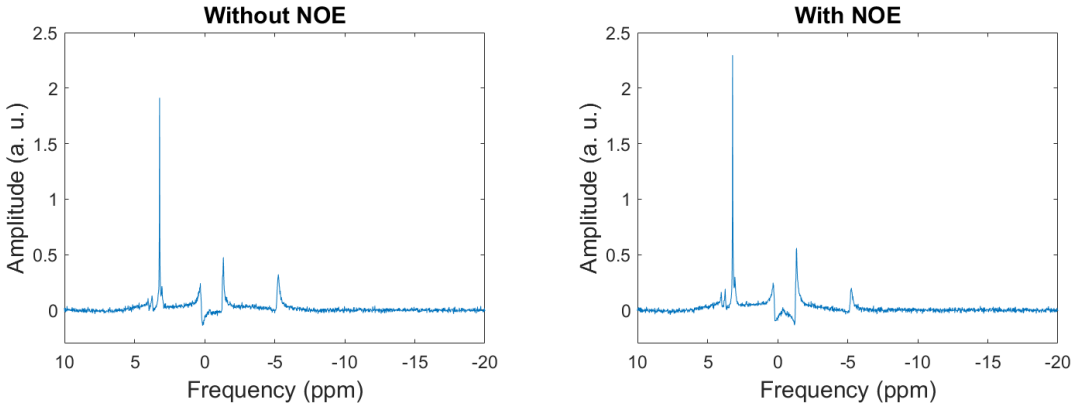

Figure 2.10: ^{31}P MRS spectra without and with NOE.

Full width half maximum
The measurement full with at half maximum (FWHM) describes the spectral width of a peak at its half amplitude. This measurement is one of the main indices of how well the shimming is for a scan. The peaks will be narrower with good shimming, which means that the FWHM will be smaller, and the other way around for poor shimming. The desired value for the FWHM is as small as possible [72].

Repeatability
Repeatability in an experimental study is a measure of the ability to reproduce results several times in series when the same quantity is measured [73]. The *Association for Computing Machinery* has stated the following definition on repeatability [74]:

> The measurement can be obtained with stated precision by the same team using the same measurement procedure, the same measuring system, under the same operating conditions, in the same location on multiple trials. For computational experiments, this means that a researcher can reliably repeat her own computation.

The precision of two subsequent measurements under repeatability conditions may be expected to be within the difference

$$\mathrm{R} = 2.8 \cdot \mathrm{SD}, \tag{2.15}$$

where SD is the standard deviation of the results obtained under repeatability conditions. The number 2.8 refers to that the test results lie within the 95% probability interval [75, 76].

2.5 RF pulses

MR spectroscopy is performed with a variety of pulse sequences, ranging from simple sequences consisting of only a 90 degree RF pulse without any gradients to complex sequences with multiple RF pulses and gradients in multiple directions [31].

The most basic pulse and acquire sequence is a free induction decay (FID) signal. FID is a damped oscillation at the resonance frequency recorded when the net magnetization is tipped into the transverse plane. FID is damped by the T_2^* decay. The most used RF pulse for FID is a 90° pulse, but a FID will be created by an RF pulse of almost any flip angle. This is because some component of the longitudinal magnetization will always be tipped into the transverse plane. The only theoretical exception is an RF pulse with a flip angle of 180°, since this pulse in principle does not generate any transverse components because all longitudinal magnetization is only inverted. However, since no RF pulse is 100% perfect in practice, will also 180° RF pulses produce FID signals [77].

FID's are recorded by a receive coil immediately after a single RF pulse is transmitted by a transmit coil, without any gradients applied. This pulse sequence is fast and simple, and is often used in dynamic muscle exercise studies of high-energy phosphate metabolism with ^{31}P MR spectroscopy. The method of sampling a frequency-encoded FID signal was one of the earliest projection-acquisition MRI methods performed [78].

RF pulses are required for all Fourier transform MRI and MRS experiments. They are used to perform chosen spin modulations like excitation, inversion and refocusing. One

of the most used RF pulses is the 'square' RF pulse. It achieves an uniform excitation of the spins because of its constant amplitude. Several more sophisticated RF pulses are also used in *in vivo* MRS experiments. These more selective RF pulses can be designed using Fourier transform theory and are often more well-defined than a regular 'square' RF pulse, and has a more limited range of frequencies to excite [35]. Here three pulse types; rectangular, adiabatic half-passage and B_1-insensitive rotation will be presented.

2.5.1 Rectangular pulse

The rectangular RF pulse is a common pulse type and goes under several names like rectangular, square or 'hard' pulse. This pulse type is commonly used as a non-selective pulse, which is a pulse that affects all the tissues within the transmitting coil. The transmit power in this type of pulse is often relatively high, so that it can be delivered with a short pulse length with a wide bandwidth for a given nutation angle. Experiments involving rectangular pulses needs to be performed on-resonance to avoid creating off-resonance phase shifts [35]. The largest signal can be acquired from a 90° pulse with a sufficiently long TR time, TR $\geqslant$ 4-5 T_1. This is to avoid saturation because of incomplete T_1 relaxation, since short TR give T_1 weighting.

2.5.2 Adiabatic Half-Passage pulse

Adiabatic Half-Passage (AHP) pulses are one type of adiabatic pulse design which are often used to generate uniform excitation and inversion in applications with surface coils. Adiabatic pules are a class of pulses that are characterized by specific modulation functions describing RF frequency $\omega(t)$ and amplitude $B_1(t)$. Adiabatic pulses can be used, even when B_1 is very inhomogeneous, to rotate the magnetization vector $\mathbf{M}$ by a constant flip angle. AHP pulses are often 90° excitation pulses. It is practical to represent AHP pulses in a reference frequency frame, $x'y'z'$, that rotates around z' at an instantaneous frequency $\omega(t)$ of the pulse. The difference from other pulses represented in a rotating reference frame is that the rotating frame varies with time for adiabatic pulses, and in this reference frame the $B_1(t)$ does not precess in the transverse plane. Since adiabatic pulses have frequency and amplitude modulation, the spins affected by the adiabatic pulse will encounter an additional magnetic field along the z' axis with magnitude $\Delta\omega(t)/\gamma$ because the pulse frequency deviates from the Larmor frequency ω_0 as a function of time. This $\Delta\omega(t)$ is defined as $\omega(t)$ - ω_0. The change in B_1 and frequency $\Delta\omega(t)$ can in the frequency frame be expressed as:

$$B_1(t) = B_{1max} f_b(t)[x'] \tag{2.16}$$

$$\Delta\omega(t) = \Delta\omega(t) f_\omega(t)[z'] \tag{2.17}$$

where $f_b(t)$ and $f_w(t)$ are unitless, normalized modulation functions. Some examples of the combinations used for $f_b(t)$ and $f_w(t)$ are sin/cos and tan/tanh. $[x']$ and $[z']$ are the unit vectors that identify the axes of the frequency frame, and B_{1max} and $\Delta\omega_{max}$ represents the modulation amplitudes of $B_1(t)$ and $\Delta\omega(t)$. It is also possible to represent the modulations as a phase modulation which gives more insight into the complex rotations involved, but it does not give the same insight in the applications and principles. Therefore are the

modulation functions given in equation (2.16) and (2.17) preferred [35, 79]. Figure 2.11 shows an example for how B_1 and $\Delta\omega$ changes during an AHP RF pulse.

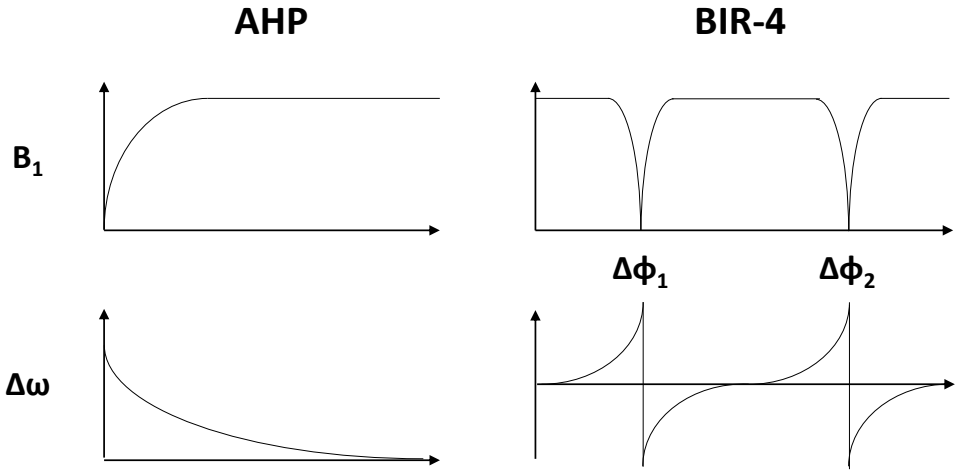

Figure 2.11: The x-axis represents the time from the excitation of the pulse for both graphs. *Left*: Example of how the B_1 and $\Delta\omega$ changes during an AHP pulse. $\Delta\omega$ is defined as the difference between the instantaneous frequency ω(t) and the Larmor frequency ω_0. *Right*: Example of how the B_1 and $\Delta\omega$ changes during a BIR-4 pulse. The two phase shifts $\Delta\phi_1$ and $\Delta\phi_2$ values can be used to determine the nutation angle generated by a BIR-4 pulse and are defined as $\Delta\phi_1 = 180° + \theta_1$ and $\Delta\phi_2 = -(180° + \theta_2)$, where $\theta_1 + \theta_2$ can be expressed by the rotation of the plane.

2.5.3 B_1-insensitive rotation pulse

B_1-insensitive rotation (BIR-4) pulse is an adiabatic pulse that consists of four adiabatic segments. These four segments can be placed in two groups (A, B), where group A is composed of segment 1 and 3 and group B is composed of segments 2 and 4. The segments in group A are equal to a time-reversed AHP pulse, while the segments in group B equals AHP pulses. As shown in Figure 2.11, the BIR-4 pulse exhibits two dips in the amplitude of B_1. These two dips happens after T/4 and 3T/4 where T equals the pulse length. As previously stated, a frequency modulation is equivalent to phase modulation for all adiabatic pulses. This is because the phase ϕ(t) is equal to the time integral of frequency $\Delta\omega$(t), also seen in Figure 2.11. The two phase shifts $\Delta\phi_1$ and $\Delta\phi_2$ values can be used to determine the nutation angle generated by a BIR-4 pulse. These two phase shifts occurs at the same time as the dips in the B_1 amplitude, at T/4 and 3T/4. The nutation angle θ can be used to describe the total plane rotation the BIR-4 pulse achieves. This total plane rotation can be expressed as $\theta_1 + \theta_2$ where the two nutation angles comes from $\Delta\phi_1 = 180° + \theta_1$ and $\Delta\phi_2 = -(180° + \theta_2)$. The BIR-4 pulse can change its phase shifts within the pulse to generate any arbitrary nutation angle [35].

2.6 pH

Intracellular pH can be measured using ^{31}P MRS to find the chemical shift difference between Pi, which is pH-dependent, and a reference peak that is pH-independent. Pi is used as the pH-dependent metabolite because the chemical shift of Pi is most sensitive to pH-changes around neutrality. This can be explained by the dissociation constant (pK) of Pi, which is the pK of $H_2PO_4^{2-} \rightleftharpoons H^+ + HPO_4^{2-}$, because it is approximately 7. The peak is chosen based on what the tissue or gel in question consists of.

Three often used reference peaks are (PCr), α-ATP, and water when using ^{1}H MRS. PCr is often used due to its strong non-overlapping single resonance, especially in muscles [80, 81], but it can not be used as a reference in all tissues, due to its low concentration. Some examples where PCr is not detectable are in kidney or liver, or for severe pathological conditions such as ischemia, anoxia, hypoxia and tumors [35]. The second reference peak, α-ATP [82, 83], is often used as an alternative when the PCr concentrations are low. This is because the α-ATP is somewhat insensitive to pH and its signal is visible in most spectra. Using water as the reference peak is a third method to measure the pH. This method is based on acquiring the water signal in the same region with ^{1}H MR [84], and then using its resonance frequency to create a 'virtual reference' peak in the ^{31}P spectrum for the same region. One main difference with this method compared with PCr and α-ATP as reference peak is that a dual-receiver is needed for the last method [22]. One way to calculate the intracellular pH with PCr as the reference peak is to use the modified Henderson-Hasselbach equation:

$$\mathrm{pH} = \mathrm{pK_A} + log[\frac{\delta - \delta_{\mathrm{HA}}}{\delta_{\mathrm{A}} - \delta}], \tag{2.18}$$

where $\mathrm{pK_A}$ is the dissociation constant [85] equal to 6.75. δ_{HA} and δ_{A} represents the chemical shifts for the protonated form of Pi, equal to 3.27, and for the non-protonated form of Pi, equal to 5.69, in cardiac and skeletal muscles, respectively [86]. These values are slightly different in other tissues such as the brain, where these values are 6.77, 3.29 and 5.68, respectively [6]. The δ in equation (2.18) represents the chemical shift difference between PCr and Pi [87]. If α-ATP is used as the reference peak instead of PCr, the δ is calculated from the chemical shift difference between α-ATP and Pi

$$\delta = \delta_{\mathrm{Pi}} - \delta_{\alpha-\mathrm{ATP}} - 7.56. \tag{2.19}$$

The 7.56 ppm represents the expected difference in frequency from the center of the α-ATP peak relative to PCr in equation (2.19).

For the third method mentioned the frequency of the PCr peak is estimated in the ^{31}P spectrum with the following equation:

$$\delta_{\mathrm{PCr}} = \delta_{\mathrm{H_2O}} \cdot \mathrm{k}, \tag{2.20}$$

where k is a constant that describes the relation between the frequency of PCr and H_2O. This constant can be calculated by defining the absolute frequency for PCr and H_2O and divide the two equations (2.21) and (2.22). The proportionality between the absolute frequency positions for PCr and H_2O and the local magnetic field is what this method build on. The absolute frequency of PCr can be defined as

$$\delta_{\mathrm{PCr}} = \frac{\gamma_{^{31}\mathrm{P}} \cdot B_{local} \cdot (1 - \sigma_{\mathrm{PCr}})}{2\pi}, \tag{2.21}$$

where $\gamma_{^{31}\mathrm{P}}$ is the gyromagnetic ratio and the chemical shielding effect for PCr is represented by σ_{PCr}. B_{local} is the local magnetic field B_0 affected by local susceptibility effects. For H_2O it can be defined as

$$\delta_{^1\mathrm{H}} = \frac{\gamma_{^1\mathrm{H}} \cdot B_{local} \cdot (1 - \sigma_{\mathrm{H_2O}})}{2\pi}. \tag{2.22}$$

Then the constant k can be represented in the following way:

$$k = \frac{\gamma_{^{31}\mathrm{P}} \cdot B_{local} \cdot (1 - \sigma_{\mathrm{PCr}})}{\gamma_{^1\mathrm{H}} \cdot B_{local} \cdot (1 - \sigma_{\mathrm{H_2O}})} = constant. \tag{2.23}$$

After calculations for the constant k, it is possible to estimate the frequency for PCr from the water frequency, as shown in equation (2.20) [22, 84].

Chapter 3

Methodology

3.1 The Phantom

The ^{31}P metabolites phantom was constructed to imitate a human calf muscle. Relevant phosphorus metabolites, common in a calf muscle, were added to the phantom. The metabolites were dissolved in water and mixed with 3% agarose (agar) and 0.12% sodium acid. Total volume of the phantom was set to be 400 g. The MRS phantom was constructed in the following way:

- Two phosphate buffered saline (PBS) tablets were dissolved in 200 g of deionized water by the use of a magnetic stirrer to produce a phosphate buffer that controls the pH value in the phantom. One dissolved tablet in 200 mL deionized water equals 0.01 M phosphate, 0.0027 M KCl and 0.1137 M NaCl.
- The agar-sodium-acid solution was prepared by dissolving 3% agar (12 g Bakto-agar, DIFCO) and 0.12% NaN_3 (0.483 g) in 200 g of deionized water. This solution was heated at around 100°C while stirred with a magnetic stirrer to create a homogeneous solution. When bubbles appeared the temperature was regulated to 50°C for 15 minutes.
- The relevant metabolites for the phantom was prepared, weighted and poured into the solution already containing PBS tablets from the first step. This solution was made homogeneous by the magnetic stirrer and heated to around 50°C to have the same temperature as the agar-sodium-acid.
- The metabolite solution was then poured into the agar-sodium-acid solution and stirred gently for a few minutes to become a homogeneous mixture. The final mixture was then poured into a cylinder bottle and set to cool and solidify.

The different metabolites used in the phantom, and the target and true concentrations are shown in Table 3.1. The target and true masses used to make the concentrations listed in Table 3.1 can be found in Table A.1 in Appendix A. A picture of the '^{31}P metabolites phantom' can be seen in Figure 3.1.

Table 3.1: Target concentrations and true concentrations of the relevant metabolites used in the constructed ^{31}P metabolites phantom.

Metabolite	Molecular weight [g/mol]	Normal concentration from literature	Target concentration [mM]	True concentration [mM]
ATP	507.18	5-8 mM [88]	6	5.64
PCr	211.114	16-32 mM [88]	4	3.84
PBS	141.96		2.03	2.03
GPC	257.221	2.47 ± 0.98 mM [89]	2	2.09
PE	141.063	0.84 ± 0.21 mM [90]	1	1.01
PC	184.151	1.18 ± 0.41 mM [90]	2	2.04
NAD	663.43	104.6 ± 13.35 uM [91]	0.2	0.19

Figure 3.1: The ^{31}P metabolites phantom.

3.2 NMR Spectroscopy

The MR Core Facility at NTNU, located at St. Olavs Hospital, offers the newest technology in MR-scanning as well as expertise and technical support to support the research performed at the facility. Some of the research areas are *in vivo* MR spectroscopy and imaging in disease models in small animals, MR metabolomics of biofluids or human tissue samples and *ex vivo* HR NMR spectroscopy. In addition to three NMR spectroscopes, the MR Core Facility also provides access to a clinical 3T Siemens Skyra MR scanner and a preclinical 7T Bruker Biospec (small animal MRI) MR scanner [92]. A small sample from the '^{31}P metabolites phantom' was analyzed using a 600 MHz Bruker Avance III NMR spectrometer that is dedicated for solid samples. It has a MAS probehead, dual probehead (^{1}H / ^{13}C), and triple probehead (^{1}H / ^{31}P / ^{13}C). 'Minispec' is a mq20 Bruker NMR analyzer for relaxation time measurements [93].

3.3 HR MAS MRS

For the HR MAS experiment the sample was prepared in a 50 μL rotor. The rotor was first filled with 7 μL of a buffer consisting of D_2O (used to correct for B_0 field drift) and format (used for manual B_0 shimming). Then a sample of 5.2 mg from the '^{31}P metabolites phantom' was placed inside the rotor before adding 3 μL extra of buffer to make a total of 10 μL of buffer. The total weight of the rotor with buffer and sample was equal to 52.8 mg. Before the rotor was inserted into the NMR spectrometer half of the bottom was mark black by a marker in order for the software to be able to count the number of spins it does.

The first test was a KBr-test. The KBr-test is used in order to check or adjust the magic angle. KBr is used for this test because a sample with a single NMR line, which is very sensitive to angle adjustments, is needed. A deviation from the magic angle would lead to a splitting of each sideband as well as the center band, and this splitting should then be adjusted by the use of a micrometer screw at the probe bottom. The adjustment is correctly done when the band-splitting disappears [94].

Shimming was performed manually for HR MAS MRS. The main goal for the shimming was to get the FWHM to be under 1-1.5 Hz for the format peak in the acquired proton spectrum. This was done by adjusting the current in four different shim coils: Y, YZ, YZ^2 and Z^4. The Y shim is optimal when the peak is as tall as possible. For the YZ shim the optimal setting is when the peak is as symmetric as possible and that the sides of the peak are smooth and continuous. After the YZ shims are altered, the YZ^2 shim is used to flatten/smoothen out the 'shoulders' for the peak. Then the Z^4 shim is altered to adjust for unsymmetrical 'shoulders'/broadening of the peak. When all the shims are altered, it is important to check some of the shims again in order to see if they can be altered into giving better results after the other shims has been optimized. Afterwards the FWHM for the format peak was 1.1 Hz.

After shimming the next thing to do was to find the 90° pulse and the 360° pulse. The 90° pulse was found after first finding the length of the 360° pulse. The 360° pulse gives zero signal when applied, and after finding the length of that pulse, the length of the 90° pulse could be found by dividing the length of the 360° pulse by four. The last preprocessing step was water suppression. Different Hz values were tried before the optimal water suppression was achieved.

Now the main experiments could be performed. Three different pulse sequences were used. For the 1D ^{1}H (quantitative spectra) spectra the pulse sequence used was called noesygppr1D, the pulse sequence called hsqcetgpprsisp2.2 was used for the 2D (proton phosphor coupled) spectra, and a pulse sequence called zgpg was used for acquiring the 1D ^{31}P (proton decoupled) spectra. The 2D experiment was done in order to more accurately determine which metabolites was present in the '^{31}P metabolites phantom'. The 1D ^{31}P spectra was acquired in order to have a spectra that was directly comparable with the spectra acquired of the phantom from the 7T MR, while the 1D ^{1}H spectra was acquired to provide with extra information on the contents of the phantom.

3.4 7T MRS

The 7 Tesla MR system at NTNU/St. Olavs Hospital is a Siemens MAGNETOM Terra System [95]. The installed system is equipped with dual mode (Clinical and Research), 8 channel RF-transmit chain in research mode and a 80/200 gradient system. It is equipped with a 32RX/1TX head coil (clinical mode), 32RX/8TX head coil (research mode only), 28RX/1TX knee coil (clinical mode), ^{13}C and ^{31}P loop coils, multinuclear option and fMRI equipment. The bore size is 60 cm and the magnet length is 270 cm. It has both active and passive shimming, and the helium consumption is zero helium boil-off technology.

The B_0 shim system at the 7T MR scanner at NTNU consists of three linear channels (1^{st} order), five non-linear channels (2^{nd} order) and four 3^{rd} order channels for advanced high order shim [96]. Three different methods for B_0 shimming were used in this project and all of them were already installed at the 7T scanner. They were: a standard B_0 shim, Foot/ankle, and DESS_Adv. The standard B_0 shimming and the Foot/Ankle shimming consists of a gradient echo (GRE). This method calculates the B_0 inhomogeneities by doing several GRE recordings, both a phase image and a magnitude image, with two or more echos, and subtracts one phase image from the other to create the final results. DESS in DESS_Adv stands for Double Echo Steady State and Adv describes that this method performs measurements in two directions compared to the standard one direction. The sequence produced by DESS acquires two echos between consecutive RF pulses [97]. After the measurements is the amount of voltage to be used in the different B_0 shim-coils calculated and applied.

3.5 7T MRS of healthy volunteers

One of the main goals for the Master's thesis was to look at the repeatability in ^{31}P MRS spectra acquired with the ^{31}P loop coil at the 7T MR scanner at St. Olavs Hospital. Figure 3.2 shows the protocol found from the scan of the first healthy volunteer. This protocol will then be used during several scans of the same or other healthy volunteers, both for multiple scans on the same day, and for scans on different days. After these scans it is possible to look at the variations between the scans on the same day, variations between scans done on different days, and variations between scans acquired from different healthy volunteers on different days.

Four healthy volunteers (all male, mean age = 24.5 $\pm$ 0.5 years) were included in the this study regarding testing and optimization of MR protocols. The Regional Committee for Medical and Health Research Ethics (REK) has assessed this project, and has in a decision of 16.05.2019 decided that testing and optimization of MR protocols does not need to be applied for at REK [2014/1289/REK midt]. We thus not have a REK approval, but REK says that we do not need this for this project. This project has a legal basis in the EU Privacy Regulation article 6 (1a) and article 9 (2a). The volunteers have agreed to participate in the optimization project, but also have the right to have the data deleted unless the information has already been included in analyzes or publications. The volunteers have the right to complain about the processing of privacy information to the Norwegian Data Protection Authority. The Department of Circulation and Imaging (ISB) at NTNU is responsible for ensuring that this information is processed on a legal basis.

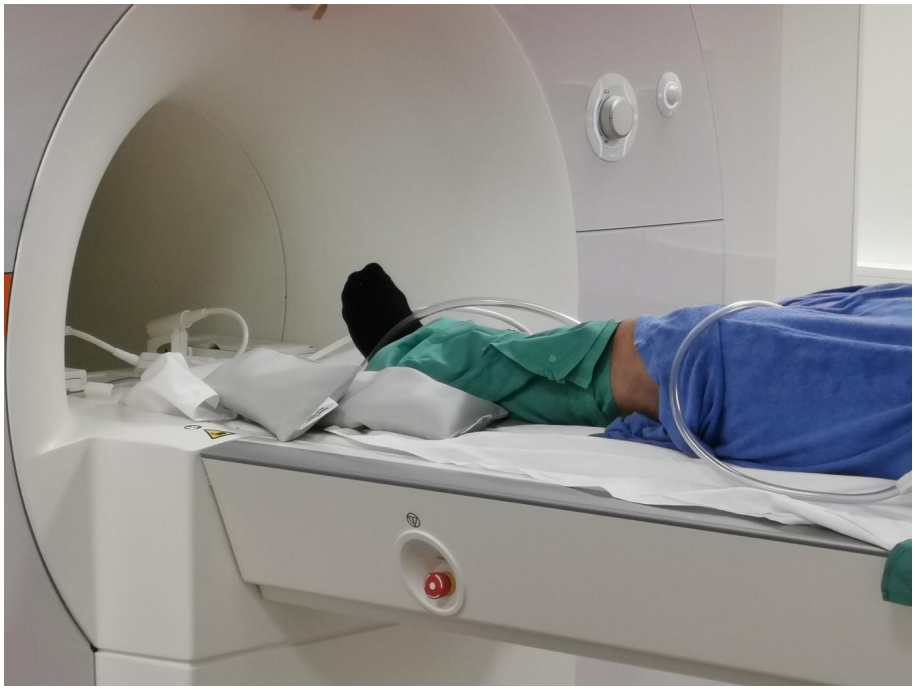

Figure 3.2: The ^{31}P loop coil is placed under the left calf muscle and stabilized. Photo taken by Maria T. Grinde.

3.5.1 Protocol optimization

The first scan of a healthy volunteer was used to find a protocol which would give good enough spectra to be able to analyze the repeatability of the scanner. The procedure to find a working protocol was to do qualitative comparisons regularly between each step after a parameter was changed. The list below describes how the protocol was found:

- First a preparatory scan was done in order to define the sensitivity area and perform B_0 shimming. The B_0 shimming used was a shimming called Foot/Ankle from Siemens.
- Then the first MRS spectra was acquired using the optimal protocol found for the phantom in the specialization project. Pulse type: BIR-4, Flip angle (fa): 60°, NSA: 16, TR: 4000 ms, Vector size (VS): 2048, Bandwidth (BW): 10000 Hz.
- The next scan was done with the Siemens built-in ^{31}P protocol. Pulse type: Rect, fa: 90°, NSA: 256, TR: 400 ms, VS: 1024, BW: 10000 Hz.
- A third scan was also performed before the first comparison. This scan protocol had the following specifications: Pulse type: Rect, fa: 90°, NSA: 16, TR: 8000 ms, VS: 2048, BW: 10000 Hz.
- After the third scan, the acquired spectra were qualitatively compared, and it was decided that the spectra from the second scan (with TR: 400 ms) was the best of the three. Before going forward to test flip angles, it was decided to check if any of the other pulse types at TR = 4000 ms with flip angle equal to 90° could match the spectra from the Siemens protocol with TR = 400 ms.
- Three scans were done with different pulse type for each scan. First BIR-4, then rectangular, and lastly AHP. All other parameters where kept constant for these

scans. fa: 90°, NSA: 32, TR: 4000 ms, VS: 1024, BW: 10000 Hz.

- After comparison with the Siemens protocol spectra, it was decided that none of these spectra was better than the one acquired from the Siemens protocol. Then the next parameter to be tested was flip angle.
- Three new flip angles (10°, 30° and 60°) were tested in addition to the 90° used in the second scan. Pulse type: Rect, NSA: 256, TR: 400 ms, VS: 1024, BW: 10000 Hz. Again it was decided to keep the original protocol from Siemens.
- NOE was the next parameter to be tested. Pulse type: Rect, fa: 90°, NSA: 256, TR: 400 ms, VS: 1024, BW: 10000 Hz. After comparing the acquired spectra with the Siemens spectra it was yet again decided to keep the protocol parameters from the Siemens ^{31}P protocol.
- The two next parameter tested were vector size and bandwidth. Here two scans where performed, one with vector size equal to 2048 and one with bandwidth equal to 5000 Hz. Except for the parameter that was changed, all other parameters were kept the same as the setup of the original Siemens protocol in step two. Again the original Siemens protocol was kept after comparison with the two new spectra.
- The last parameter that was scheduled to be tested was TR, but due to insufficient time, it was only possible to test one alternative TR time, TR = 800 ms.

3.5.2 Repeatability

When the parameters were chosen, based on the scans listed above, the next step was to scan three healthy volunteers several times with the chosen parameters too test its repeatability. The parameters chosen were: TR: 800 ms, NSA: 128, fa: 90°, VS: 1024, BW: 10000 Hz. With these parameters, each scan lasted 1 minute and 42 seconds. The scanning protocol used for this part was:

- First placing the ^{31}P coil on the left calf of the healthy volunteer and doing preparatory scans like B_0 shimming and localization. Then three ^{31}P MRS scans were performed with the parameters mentioned.
- After the three scans, the volunteers were taken out of the MR and the ^{31}P coil was repositioned again at the calf before the volunteer was placed inside the MR again for preparatory scans. Again three scans were performed with the parameters mentioned.
- The volunteers were after that taken out of the MR again, the ^{31}P coil was repositioned at the calf before the volunteer again was placed inside the MR for first preparatory scan and then for three scans with the chosen parameters.
- After the three scans the volunteer was asked to flex the calf muscle during the next three scans, for a total time of five minutes and six seconds. When the five minutes was passed, the volunteer could again relax the calf muscle while another five scans with the chosen parameters were performed.

To be able to check the repeatability of the ^{31}P MRS spectra, it was decided to use three healthy volunteers and to scan each of them two times with the protocol with a one week interval, called week 1 and week 2. Figure 3.3 shows the scanning protocol visualized.

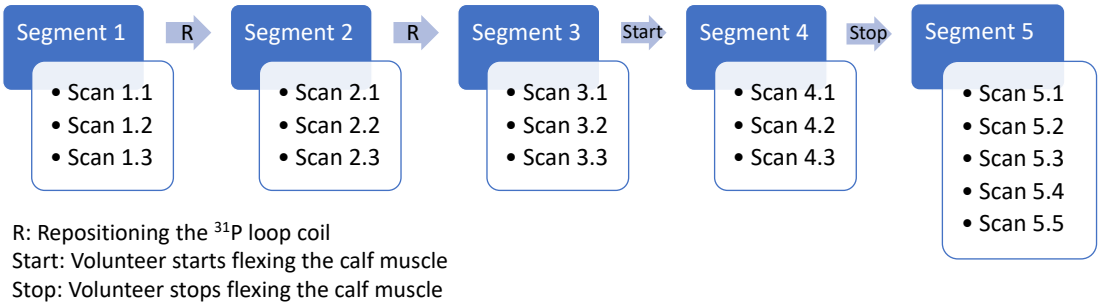

Figure 3.3: The scanning protocol used for both weeks of scanning for all volunteers. Each scan lasted 102.4 seconds.

3.6 Analysis software

In the following section a description of the different softwares used for analysis of the experimental results acquired from the different experiments performed during the Master's thesis. TopSpin and Chenomx were used to analyze the results from the HR MAS MRS experiment, while FID-A and SIVIC were used to analyze the results from the 7T MRS experiments.

TopSpin

TopSpin (ver. 4.1.1) is an integrated software package from Bruker BioSpin, available at `https://www.bruker.com/en/products-and-solutions/mr/nmr-software/topspin.html`, for visualization and analysis of NMR data. Some of the functionalities available with TopSpin are [98]:

- Importing and displaying NMR data from various formats.
- Processing spectra and fid's: phase correction, peak picking, integration, smoothing etc.
- Exporting plots and displays in different graphical formats.
- Automatic 1D-3D peak picking and integration.

The TopSpin Interface is shown in Figure 3.4. The Interface shows the main applications like process, analyze, applications and manage. Under process it is possible to process the spectra by adjusting phase, baseline, calibrating the axes etc, and under analyze some of the options are peak picking, integration, line shaping and quantifying. Process and analyze were the two most used parts of TopSpin for the analysis of the HR MAS MRS data, and some of the main applications used were calibrating the axes, phase and baseline adjusting, and peak picking.

In addition to the standard Bruker data format, TopSpin can both read and display numerous of other formats [98]:

- Bruker TopSpin data stored in JCAMP-DX format.

- Bruker TopSpin data stored in ZIP format.
- Bruker WINNMR data.
- Bruker ASpect 3000 data.
- Varian VNMR spectrometer data.
- Jeol JNMR spectrometer data.
- FELIX 1D data, FID or spectra.

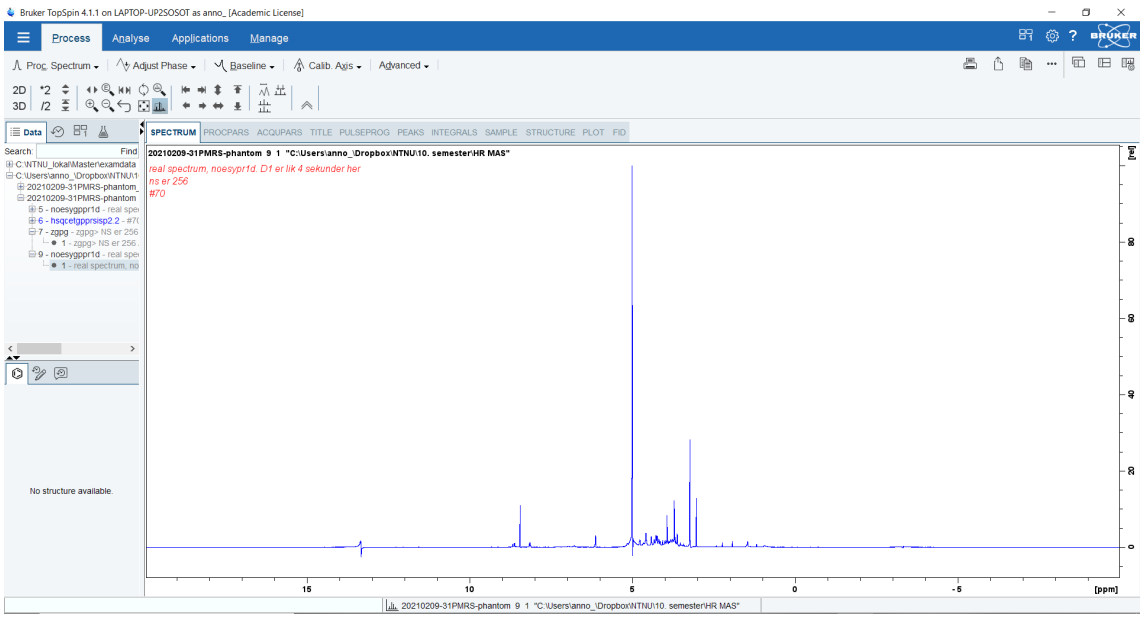

Figure 3.4: TopSpin Interface.

3.6.1 Chenomx

The NMR analysis software Chenomx NMR Suite is an easy to use software that, among other things, allows for manual adjustment of peak fitting. It also provides a utility to identify metabolites and can do absolute quantification in the presence of an internal reference chemical. One thing Chenomx is well known for is for metabolic profiling in order to identify and quantify metabolites with peak deconvolution in NMR spectra of complex samples. There exists a full version and an evaluate version. The evaluate version is free for use, but then the user is restricted in several ways. One restriction is that it is only possible to highlight and view five different metabolites in the same spectra at the same time. Another restriction was that it was not allowed to save any modified spectra. Despite of the restrictions, this software proved to be very useful for our analysis. It was useful in the way that it gave good indications on which metabolites that were present in the phantom based on the 1D ^{1}H spectra acquired from the HR MAS MRS experiment An example can be seen in Figure 3.5, were the metabolite ATP is highlighted. The blue peaks are created by the software and shows where and how the ^{1}H signals from ATP are expected to show. To the right in the figure, a reference card shows the molecular structure of the metabolite, and when selecting one of the blue peaks in the spectra the phosphorus

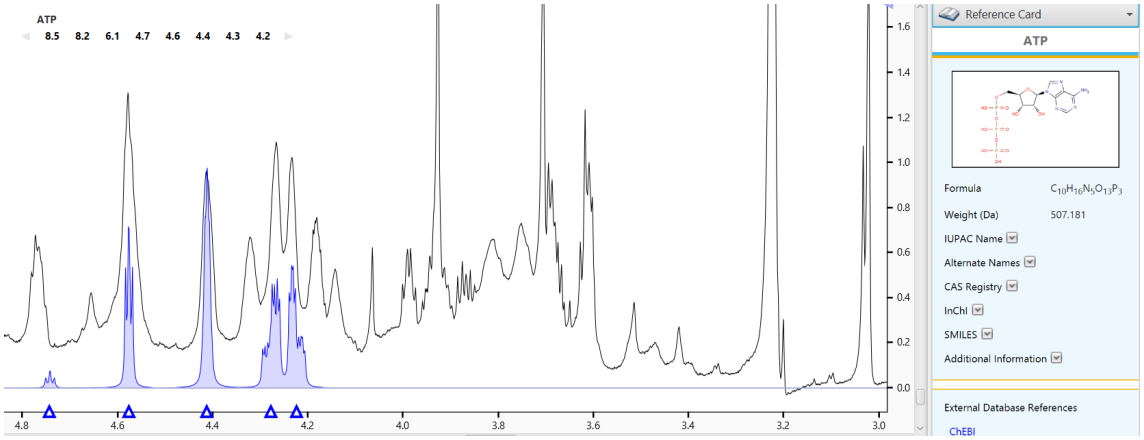

Figure 3.5: A part of the Chenomx Interface when when selecting a specific metabolite during analysis of a 1D ^{1}H spectra. ATP is the metabolite chosen for analysis.

atom for that specific peak gets marked in the molecular structure. The Chenomx software can mainly be used for proton spectra [99].

The Chenomx NMR suite supports raw data from four file formats and processed data from six file formats [100], shown in Table 3.2.

Table 3.2: File formats supported by Chenomx NMR suite for raw data and processed data.

	File formats	
Vendor	**Raw data**	**Processed data**
Aglient	fid	phasefile
Bruker	fid	1r
JEOL	.jdf	.jdf
NMRPipe	.fid	.ft2
JCAMP_DX		.jdx*
Mestrelab		MNOVA

3.6.2 FID-A

FID appliance (FID-A) is an open source, MATLAB-based software package that is made for simulation of different MRS experiments, analysis and design of RF pulses, and MRS data processing. One of the things FID-A is especially designed for is managing raw MRS data sets. These data sets contains often multiple dimensions of data resulting from the presence of multiple RF channels, averages, and sub-spectra. This software also has the function that it can import MRS data of most MRI/MRS vendors, such as Siemens, Philips, Agilend, GE, etc. FID-A uses primarily a command-line structure which provides a high level of flexibility and efficiency to the users. Table 3.3 shows an overview over which file formats that can be used by FID-A to load, read, and/or write data.

Table 3.3: Overview over which file formats that can be used by FID-A to load, read, and/or write data.

Format	**Load**	**Read**	**Write**
jMRUI	Yes	Yes	Yes
LC Model	Yes	Yes	Yes
GE P file	Yes	No	No
Siemens IMA	Yes	No	No
Siemens RDA	Yes	No	No
Siemens TWIX	Yes	No	No
Siemens PTA	No	Yes	Yes
Philips MRS	Yes	No	No
Bruker MRS	Yes	Yes	No
Varian	Yes	Yes	No
RF pulse	No	Yes	Yes

The toolkit available from the FID-A software consists of four different toolboxes, and these four are:

- The Input-Output Toolbox consists of functions for reading and writing data between data formats from different MRS vendors to MATLAB, and functions for exporting or importing data formats from different MRS vendors, as mentioned above. The functions in this toolbox can be divided into three different categories: load-, read-, and write-functions. The load-functions are the functions described above which is used to accept MRS data from other data processing or analysis software packages. For exporting the processed data back to the other data processing or analysis software packages one uses the write-functions. The read-functions read different file types. All functions in this toolbox starts with the prefix 'io_'.

- The Processing Toolbox contains over 50 different processing operations and can be used once the data has been loaded into MATLAB using the Input-Output Toolbox. These different operations can be applied to both experimental and simulated data, and many of the processing operations available are specially designed for use on data sets with higher dimensionality. Many of the processing operations can be nested with one another, so that multiple operations can be done with one line of code. Prefix: 'op_'. An example could be to first load data, then chose one of the averages from the data set, apply auto-phasing, before plotting the processed spectra:

  Example 3.6.1. out = op_plotspec(op_autophase(op_takeaverages(io_loadspec_twix ('filename. dat'), 1), 2, 7, 0), 2, 7, 'Label x-axis', 'Label y-axis', 'Title');
  where the argument '1' determines which averages is chosen from the data set, the arguments '2' and '7' both times represents lower and higher bound for the spectra, and the argument '0' is the desired phase value in degrees.

- The Simulation Toolbox contains built-in functions for simulating basic components of an MRS pulse sequence. The toolbox is based on an implementation of the density matrix formalism, in which the MRS experiment is modeled by successive evolution's of the density matrix by time-independent Hamiltonian operators. Some of the basic components that can be simulated with this toolbox are excitation, rotation using ideal RF pulses and signal readout. By using these basic pulse sequence elements it is possible to implement common *in vivo* MRS pulse sequences like FID, STEAM

and PRESS. Also included in the toolbox is a full set of metabolite spin system definitions. Prefix: 'sim_'.

- The RF Pulse Toolbox enables the creation of basic RF pulse waveforms, as well as Bloch simulations to be able to determine the resulting excitation-, refocusing-, or inversion profiles. It also has functions for manipulating existing RF waveforms, including resampling, frequency shifting, and the time-bandwidth product. This toolbox can be used in combination with the Simulation toolbox, this to enable simulations that incorporate fully shaped RF waveforms. Prefix: 'rf_'.

FID-A also has different example run scripts, and a few graphical user interfaces (GUI) that are provided to assist with processing tasks [101].

3.6.3 SIVIC

Spectroscopic Imaging, VIsualization, and Computing (SIVIC) is an open-source, standard-based software framework and application suited for processing and visualizing DICOM MRS data. SIVIC was developed to address the limitations of existing strategies for analyzing MRSI data, and is designed to support all aspects of MRSI data analysis and visualization. This software consists of different libraries that support the various stages of analysis including algorithm pipelines, data input-output, and visualization. The most important application of the SIVIC software is the SIVIC GUI. This GUI supports reading, visualization and reconstruction of MRI, MRS and MRSI data. SIVIC is also able to convert between different formats with command line tools, and for applying reconstruction, post processing, and quantification algorithms. The different supported file formats for SIVIC are presented in Table 3.4 [1].

Table 3.4: Overview of the supported file formats for SIVIC. Adapted from [1]

Format	Read	Write
DICOM MR spectroscopy storage	Yes	Yes
DICOM MR image storage	Yes	Yes
DICOM raw storage	No	Yes
GE P files	Yes	No
Siemens RDA	Yes	No
Siemens IMA	Yes	No
Philips MRS	Yes	No
Varian	Yes	No
JPEG	No	Yes

When opening the SIVIC GUI environment, several options are possible. It is possible to either load raw MRS data by using the 'spectra' label in the toolbar, loading images by selecting 'images', or chose the 'exam' button to examine both images and spectra combined. For this master's thesis, the mainly used option was 'spectra'. Choosing 'spectra' gives a drop-down menu to select from two different options, either 'load data' or 'load single file'. The main difference between these two is that with 'load data' it is possible to choose several files, while for 'load single file', as it is stated in it's name, it is only possible to chose a single file to analyze. The MRS data selected is shown in a trace view where the FID from the selected data comes up as a default view. Below this trace view there is a panel that contains nine different tabs that is used to manage loaded data

in SIVIC and provides controls to perform processing on the chosen datasets. The trace view and the panel with the different tabs can be seen in Figure 3.6.

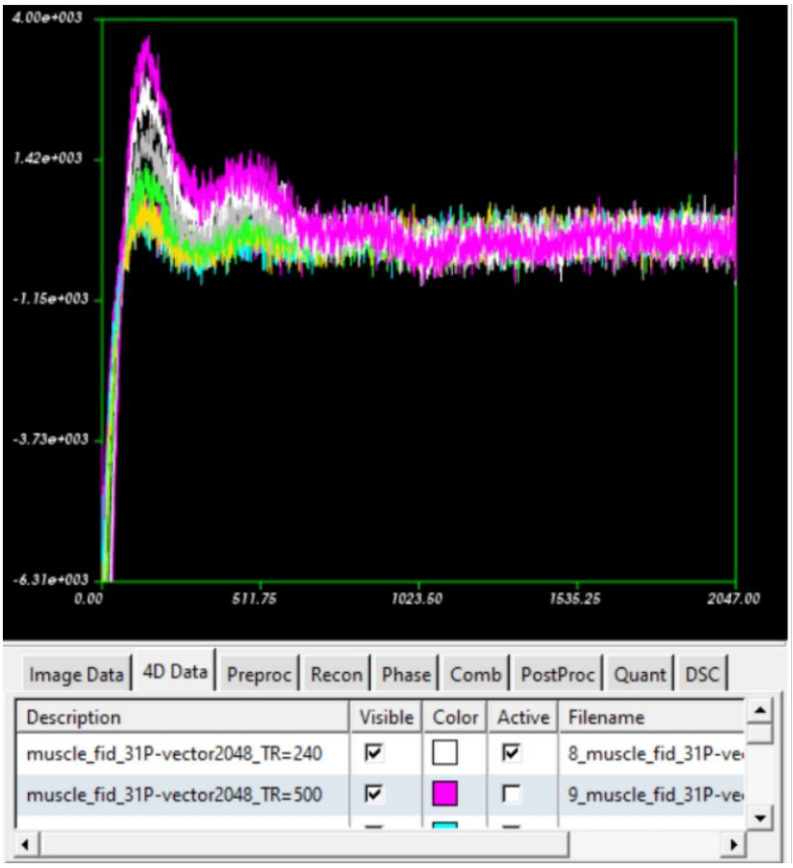

Figure 3.6: The trace view and processing panel in SIVIC GUI.

Reconstructing spectroscopic data is possible by using the 'recon' tab. Both spectral and spatial FFT's (Fast Fourier Transform) can be applied, and this functionality only applies to the 'active' data. After the reconstruction, phasing of the spectroscopic data can be done manually in the 'phase' tab. Two different slider parameters can be changed here, zero-order phase and first-order/linear phase. These are applied about a chosen pivot point, which can be modified. It is also possible to apply two different automatic phasing algorithms. The first one phases data using the water peak, if there is one, and the second applies a first point phase algorithm. Quantification of the spectroscopic data is done with the 'Quant' tab. There the software lists the metabolites it finds from the spectrum, and a slider is used to define the minimum and maximum range used for quantification. The slider for each metabolite will be set to default ranges defined from a directory in the SIVIC software. When the range is defined for the metabolite of interest, different types of quantification can be performed: Peak height, magnitude peak height, integrated area, magnitude integrated area, ppm-value, z-scores, and ratios of other maps.

Chapter 4

Results

4.1 HR MAS MRS

Figure 4.1a shows the resulting 2D spectra from the HR MAS analysis of the '^{31}P metabolites phantom' that was made during the specialization project last fall. The spectra shown on the two axes are 1D ^{1}H spectra along the x-axis (F1-axis) and 1D ^{31}P spectra along the y-axis (F2-axis). These two spectra are shown in Figure A.1 and A.2 in Appendix A, respectively. The 2D spectra was used to verify which metabolites were present in the '^{31}P metabolites phantom'. By comparing the expected ppm value of the metabolites in the 1D ^{1}H and ^{31}P MR spectra [6, 102, 99] and the spectra acquired during the HR MAS MRS analysis, it was possible to label the different peaks in the 2D spectra. 10 peaks were visible in the part of the spectra shown in Figure 4.1a: 3 representing α-ATP, 3 representing GPC, 2 representing PC and 2 representing PE. The numbering of the different protons in Figure 4.1b and peaks in Figure 4.1a was done by using the analysis software Chenomx to compare theoretical placements of different metabolites in a 1D ^{1}H spectra with the spectra acquired from the HR MAS MRS analysis.

Labeling of metabolites showed that the '^{31}P metabolites phantom' contained these metabolites: PE, PC, Pi, GPC, γ-ATP, NAD, α-ATP and β-ATP. No PCr was found in the phantom. The magnitude of the peaks in Figure 4.1a could be explained by the difference in distance between the phosphorus atoms and the proton atoms in the metabolites. Figure 4.1b shows the chemical structure of the four different metabolites PE, PC, GPC and ATP that had visible peaks in the 2D spectra in Figure 4.1a.

Figure 4.2 shows the ^{31}P MR spectra from the '^{31}P metabolites phantom' acquired by HR MAS MRS and on the 7T MR scanner, respectively. A major difference between the two spectra was that the peaks, especially the four to the left of zero ppm, were more well-defined and separated in the HR MAS spectra compared to the 7T MR spectra. Another difference was the baseline which was much smoother in the HR MAS experiment compared to the 7T experiment. The two peaks γ- and α-ATP, between 0 and -10 ppm, were more visible in the 7T MRS spectra, but this could be due to the large Pi signal registered in the HR MAS spectra, making the ATP peaks between 0 and -10 ppm visibly smaller compared to the peaks in the 7T spectra. The large difference in intensity between the HR MAS and 7T MR spectra could come from the large differences in the protocols used or the acquisition parameters.

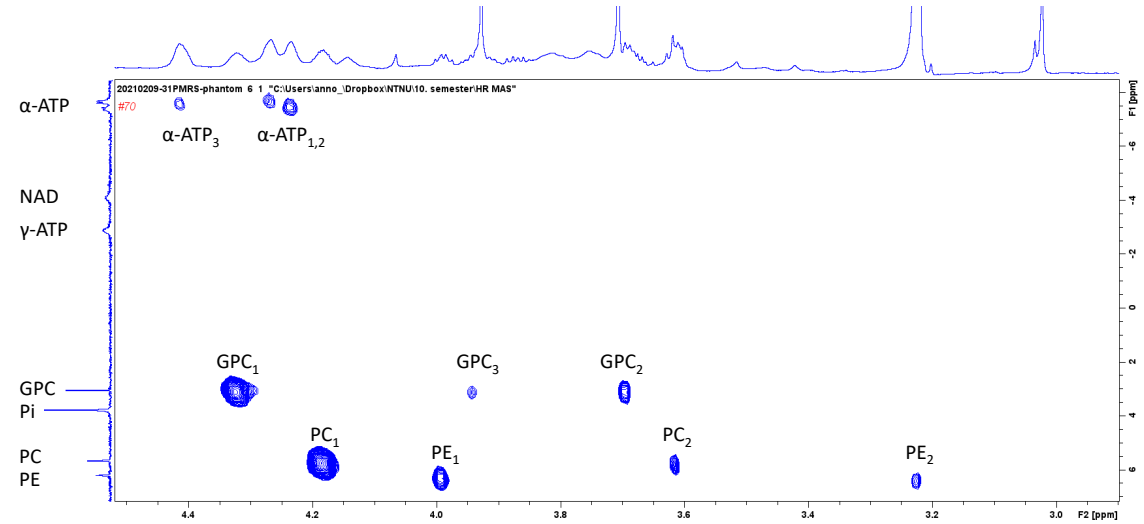

(a)

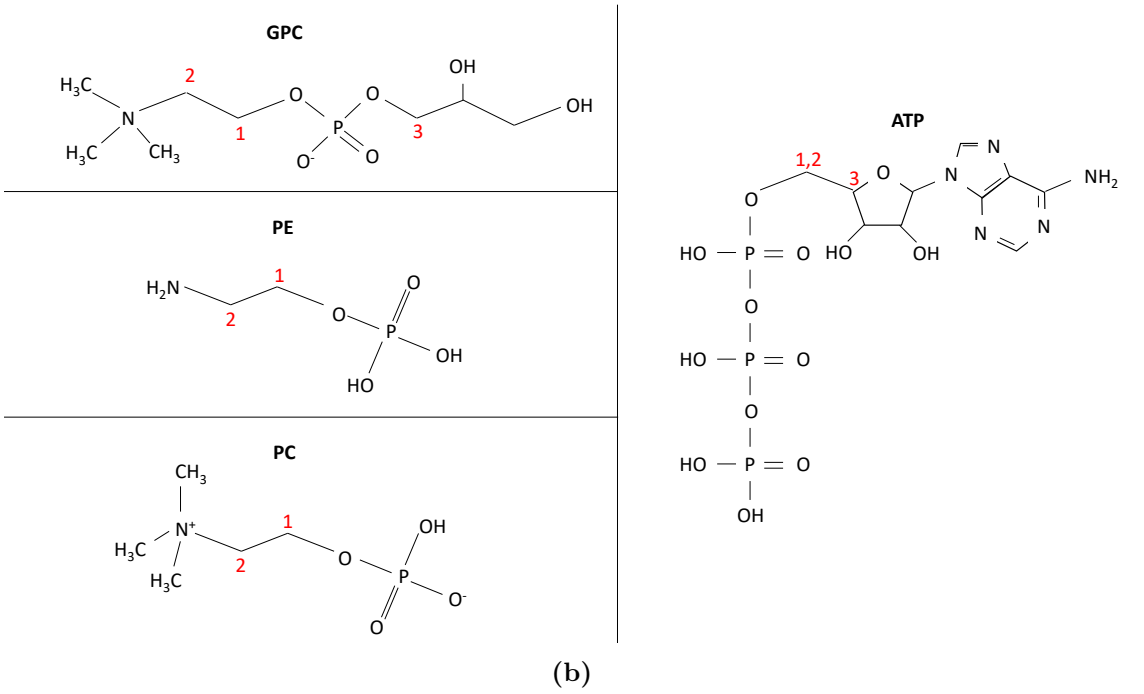

(b)

Figure 4.1: (a) Resulting 2D spectra from HR MAS MRS of the ^{31}P metabolites phantom with labeled peaks in the 1D ^{31}P spectra along the y-axis (F1-axis). The subscript numbers refers to the different protons labeled in Figure 4.1b. (b) Chemical structure for GPC, PE, PC and ATP.

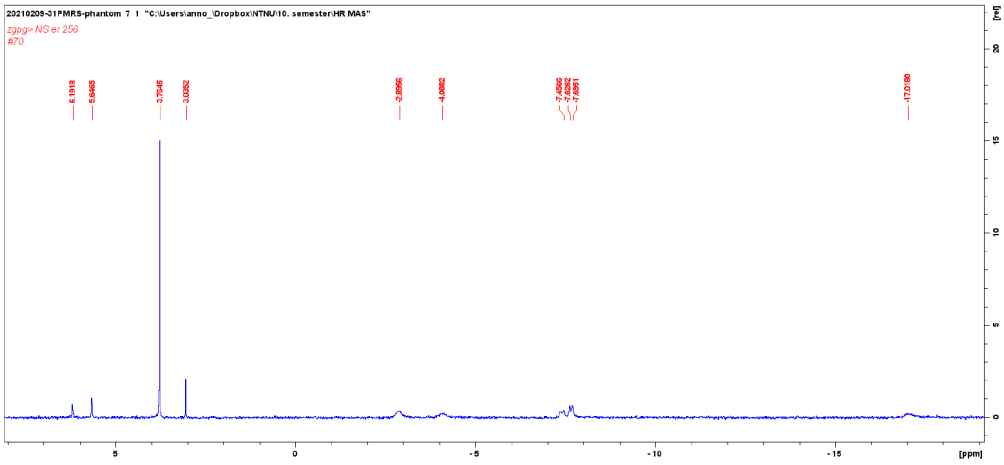

(a)

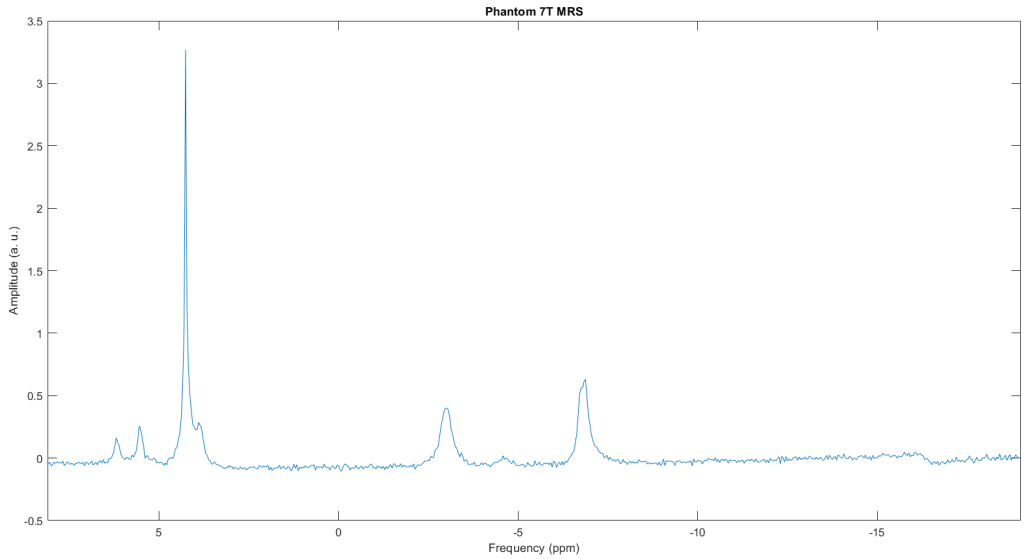

(b)

Figure 4.2: (a) HR MAS MRS spectra of the '^{31}P metabolites phantom' made for the specialization project. (b) 7T MRS spectra of the '^{31}P metabolites phantom' made for the specialization project. Protocol details can be seen in Appendix B. a.u.: arbitrary unit.

4.2 Protocol optimization in calf muscle

The scan protocol was optimized for the ^{31}P loop coil at the 7T MR in a healthy volunteer. The chosen protocol was later used to test the repeatability of the scanner. Figure 4.3 shows spectra acquired with the protocol optimized for the phantom and a spectra acquired with Siemens standard protocol for ^{31}P MRS, details described in Appendix B. Both spectra were averaged, calibrated and phased with FID-A. The phantom protocol spectra had a larger PCr signal at 0 ppm, but the baseline showed more noise and it was not possible to achieve a good phase. The three ATP peaks to the right of PCr (0 ppm) was larger for the Siemens protocol, but this could be because of the sub-optimal phasing for the phantom protocol spectra.

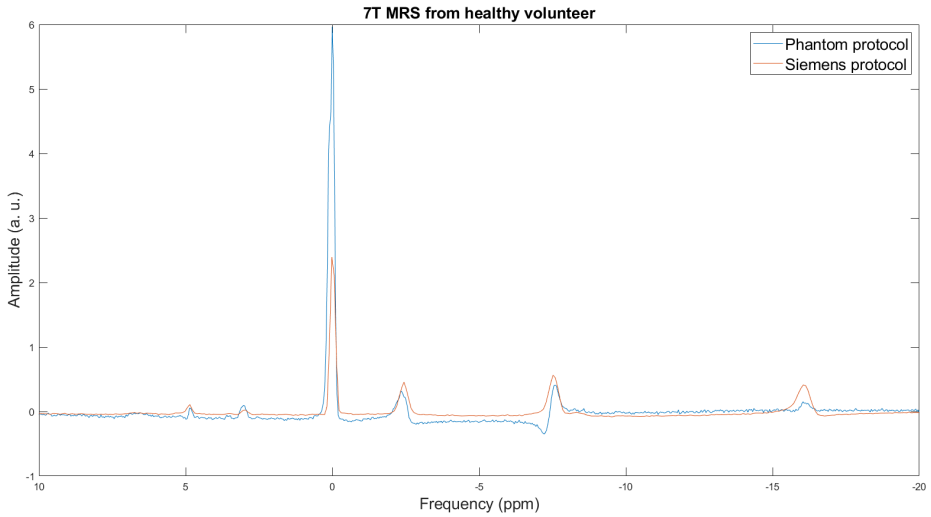

Figure 4.3: The blue spectra was acquired using the protocol found optimal for the phantom made for the specialization project. The orange spectra was acquired using Siemens protocol for ^{31}P MRS. Both spectra were averaged, calibrated and phased with FID-A. a.u.: arbitrary unit.

Figure 4.4 shows two spectra from the protocol optimization using the spectroscopy viewer at the 7T scanner. The left spectra was acquired using the Siemens standard protocol and the right spectra was acquired using the optimal protocol chosen to be used for further analysis of the repeatability. This protocol was largely based on Siemens protocol for ^{31}P MRS at 7T and only the repetition time was changed from 400 ms to 800 ms. By a qualitatively inspection of the two spectra, it could be seen that all peaks had increased intensity. This also means that each peak was more well-defined and that the protocol was able to acquire more signal from the volunteer during the scan. The total scan time was shorter for the Siemens standard protocol compared to the optimized protocol, but the T_1-effect was reduced by increasing TR. The measured peak area for the three different protocols can be seen in Table 4.1 for PCr, Pi and β-ATP. The peak area for PCr and Pi were largest for the Phantom protocol, while the peak area for β-ATP was largest for the Optimal protocol.

Figure 4.5 shows three of the spectra acquired during the protocol optimization using different RF excitation pulse types, i.e. BIR-4, rectangular and AHP pulse. They all had a repetition time of 4000 ms, a flip angle of 90° and 32 NSA. Some of the metabolites, like PCr, γ-ATP and α-ATP, had very good signals from these protocols, but all these spectra

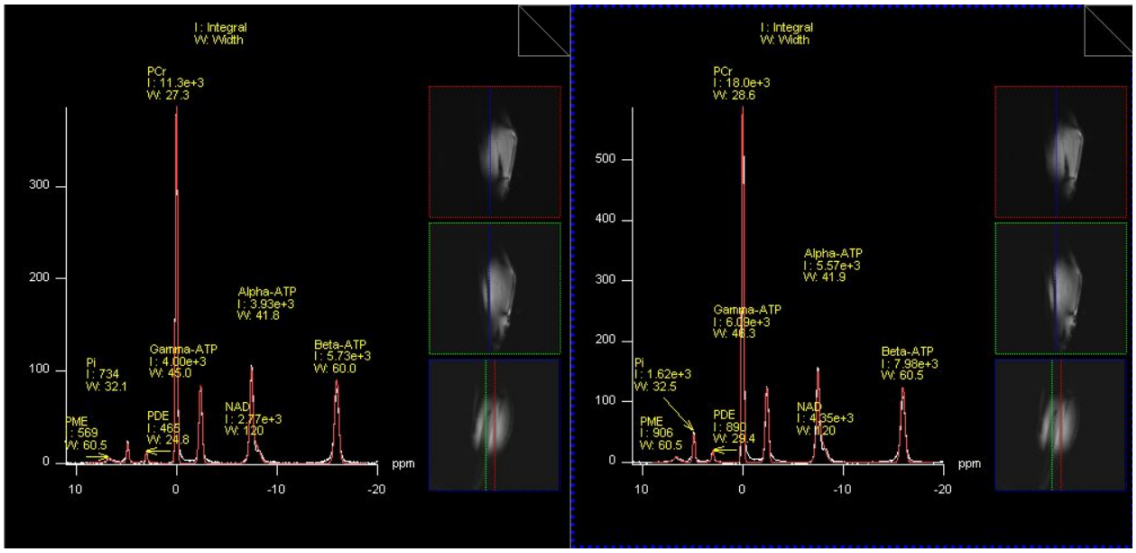

Figure 4.4: *Left:* Spectra acquired using the Siemens standard protocol (TR = 400ms, acquisition time = 102.4s). *Right:* Spectra acquired with the protocol found optimal for a volunteer (TR = 800 ms, acquisition time = 204.8s).

Table 4.1: Measured peak area for the metabolites PCr, Pi and β-ATP for the three different protocols: Phantom, Siemens and Optimal. Details for the protocols can be seen in Appendix B

	Peak area		
Protocol	**PCr**	**Pi**	**β-ATP**
Phantom	83.2	3.8	3.1
Siemens	16.2	0.9	5.7
Optimal	25.3	2.1	8.0

were discarded due to the inadequate signal from some of the metabolites, especially the β-ATP signal.

Figure 4.6 shows the comparison between the theoretical and calculated SNR ratio between spectra with different numbers of NSA. Table B.1 in Appendix B shows the data used in Figure 4.6. Both ratios were calculated with NSA = 16 as the base, this can be seen in the figure since both the theoretical and the calculated SNR ratio were equal to one. Spectra with a higher number of NSA had a lower calculated SNR ratio compared to the theoretical values, while spectra with a lower number of NSA had a higher calculated SNR ratio compared to the theoretical values.

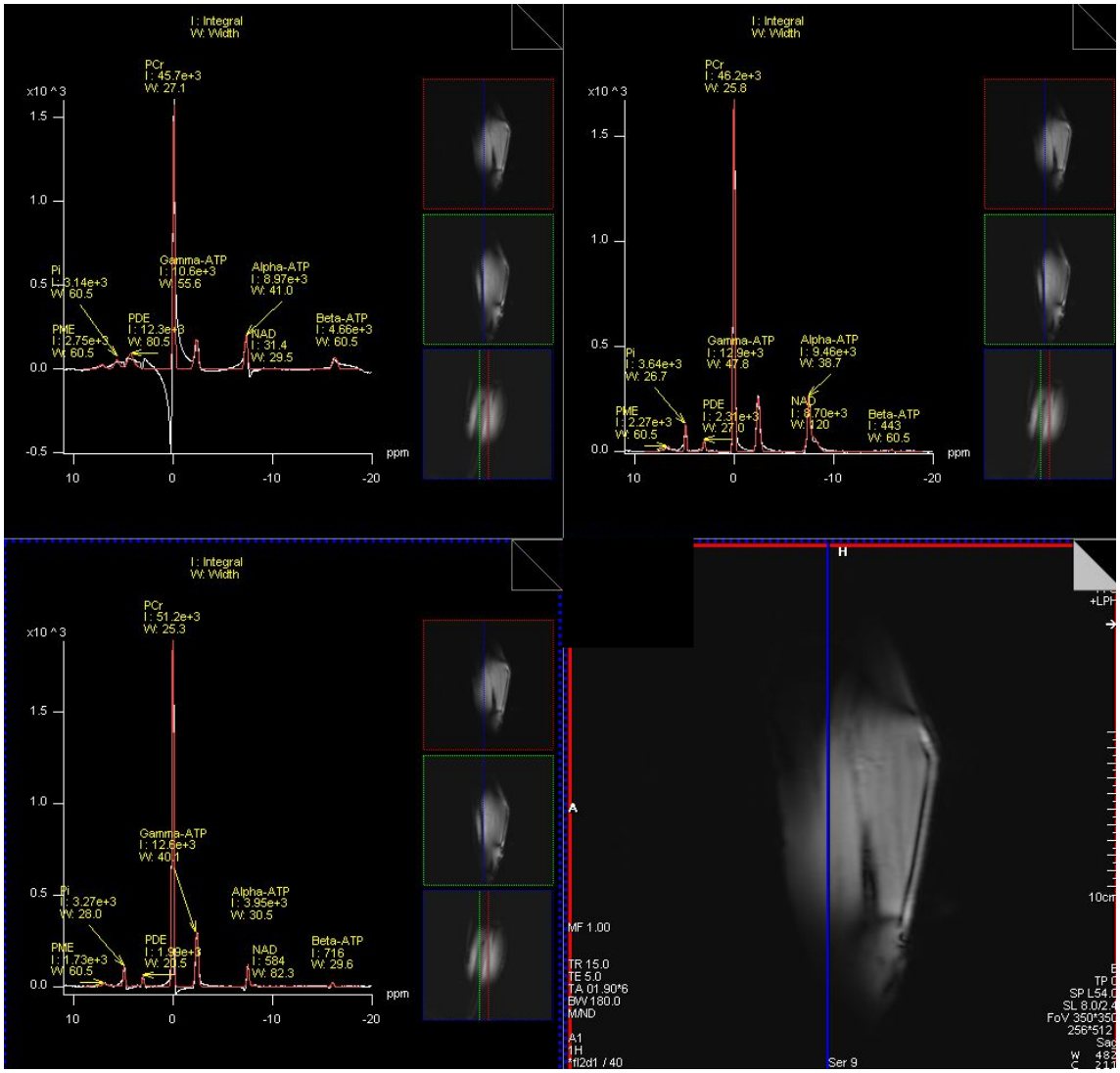

Figure 4.5: Three spectra acquired in the calf muscle in a healthy volunteer using different RF pulse types. The repetition time for all spectra is equal to 4000 ms, and they all had 32 NSA and 90° flip angle. Upper left: BIR-4, upper right: Rectangular and bottom left: AHP.

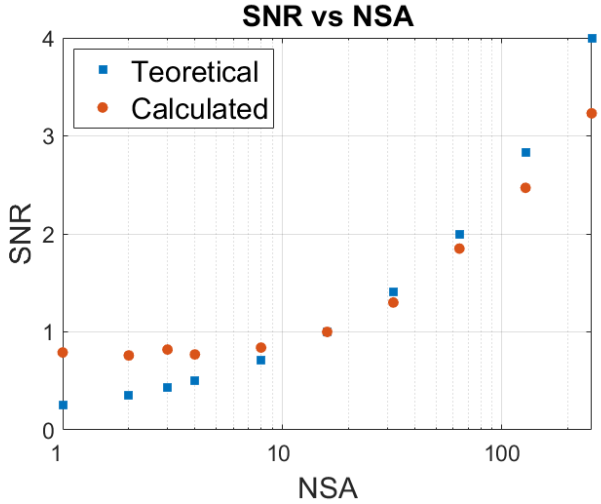

Figure 4.6: Theoretical and calculated ratio of the SNR values for one spectra with different numbers of NSA.

4.3 Repeatability

The optimized protocol was used to produce spectra from the 7T scanner to evaluate repeatability in healthy volunteers. As described in chapter 3.5.2, three healthy volunteers were scanned several times with the optimized protocol at two different days, one week apart. Repeatability describes how well a measurement or experiment could be repeated and produce similar results. For the scans of the healthy volunteers this could be looked at by comparing the three scans taken for each placement of the ^{31}P loop coil, and by comparing the results from the segments when the ^{31}P loop coil was repositioned.

4.3.1 Comparing scans acquired without repositioning the coil

Figure 4.7 shows spectra acquired from the three scans from the first segment for volunteer 1. The spectra to the left in the figure was acquired one week before the spectra to the right. There are no major differences between the spectra, as expected, since the three spectra in each subfigure were acquired without any changes in protocol, shimming or coil placement. The peaks, from left to right, are: PME (barely visible), Pi, PDE, PCr, γ-ATP, α-ATP, NAD and β-ATP. One way to check that the peak intensities in Figure 4.7 were at an expected size was to compare ratios of different metabolites with reported mean values in healthy cohorts from other studies. Table 4.2 shows some metabolite ratios from segment 1 for volunteer 1 compared with reported mean values for the same ratios in a resting calf muscle. When comparing the calculated ratios with the theoretical ratios it is seen that only the PDE/β-ATP ratio was larger than the theoretical value and six out of eight calculated ratios were within the range of means when also considering the standard deviation.

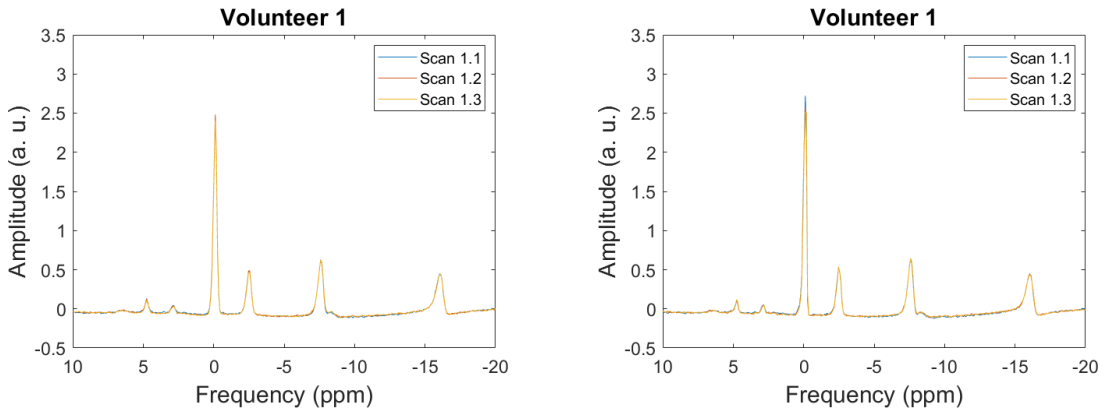

(a) Week 1 **(b)** Week 2

Figure 4.7: Spectra from scan 1.1, 1.2 and 1.3 from volunteer 1. The spectra i Figure (a) and (b) were acquired with one week interval.

Peak area is a measurement that is possible to compare from scan to scan, and from average to average. Figure 4.8 shows the measured peak area of PCr from three scans of a volunteer while the coil was left unmoved. The data presented in the two graphs was acquired with a one week interval. The peak area of PCr was relatively consistent in both graphs between each scan, which starts at 0, 102.4 and 204.8 seconds, marked with the red dotted lines. The only irregularity, which could be seen in both graphs, was the larger peak at the beginning of each scan. This irregularity comes from that steady-state was achieved first after 4-6 averages, which can be seen in Figure 4.8. It took some averages to

Table 4.2: Peak area ratios for volunteer 1 from segment 1 for both weeks. The theoretical values shows the reported mean values in healthy cohorts with the range of means shown in the square brackets [2].

	Volunteer 1		
Ratio	**Week 1**	**Week 2**	**Theoretical**
PCr/β-ATP	3.10 ± 0.15	3.34 ± 0.16	4.23 ± 0.24 [3.22-5.20]
Pi/β-ATP	0.30 ± 0.03	0.29 ± 0.04	0.56 ± 0.13 [0.37-0.81]
PDE/β-ATP	0.27 ± 0.03	0.28 ± 0.04	0.19 ± 0.05 [0.07-0.43]
Pi/PCr	0.10 ± 0.01	0.09 ± 0.01	0.13 ± 0.01 [0.09-0.17]

reach steady-state since TR<T_1, which means that the magnetization in the z-direction had not fully recovered before the next RF excitation pulse was applied. Therefore, in later presentations of data from each average, the first 4-6 averages of each scan segment were omitted.

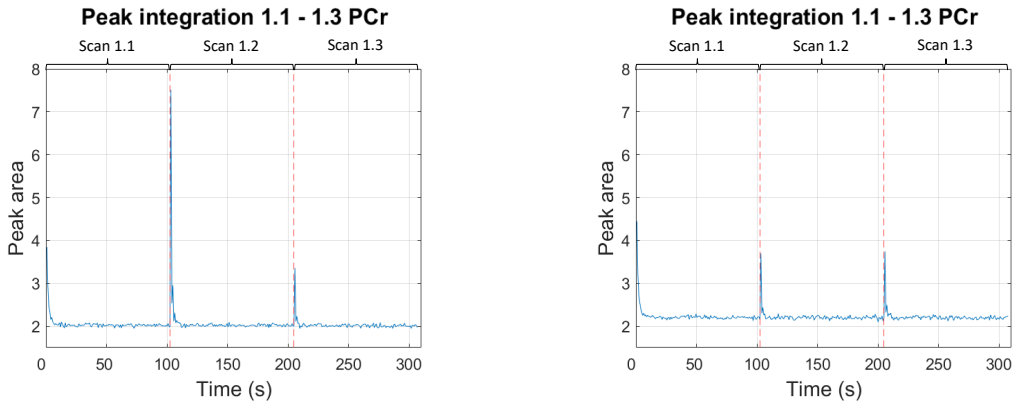

(a) **(b)**

Figure 4.8: Calculated peak area of PCr for every average for scan 1.1-1.3 in volunteer 1. The two spectra (a) and (b) were acquired with a one week interval.

The consistency between each scan of the peak area from PCr seen in Figure 4.8 from volunteer number one was also seen in the two other volunteers, shown in Figure B.1 in Appendix B. This was also seen for the second and third segment of scans for all volunteers. These results could point in the direction that there was no significant change in the spectra between successive scans with the ^{31}P loop coil for MRS at the 7T MR.

Another measurement to consider when comparing the scans within one segment was pH. Figure 4.9 shows pH measurements for the three first segments of scans for all the volunteers. pH was calculated using equation (2.18) where it depends on the chemical shift difference between the metabolites PCr and Pi. The only difference between the three first segments was that the coil was repositioned. The variations in measured pH was low. Most scans produced stable pH around 7.03 or 7.04, except for the first segment from the first volunteer that had pH values between 7.06 and 7.07, and in the last scan of the third segment for volunteer 2's second week. These results showed that there were good stability in the ppm values that were measured from scan to scan. The ppm values used for the calculations are shown in Table D.1 and Table D.2 in Appendix D.

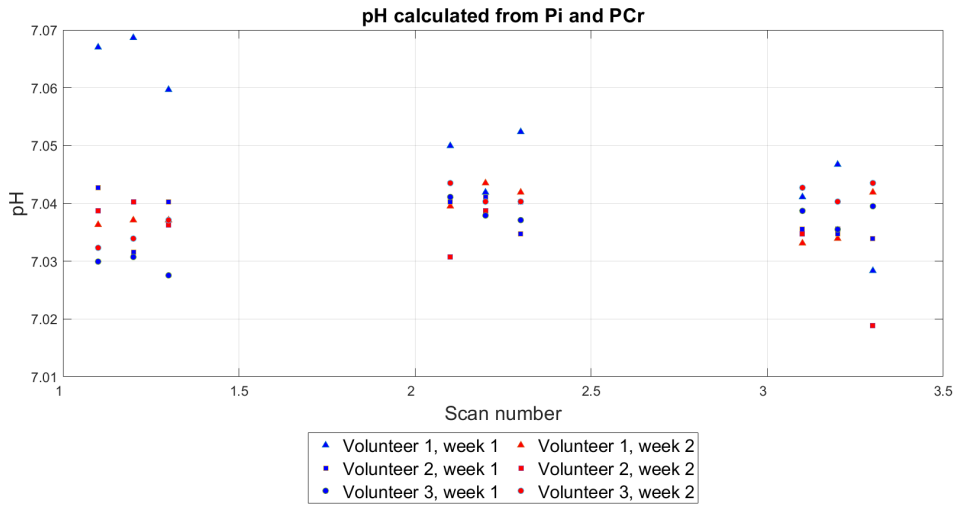

Figure 4.9: pH calculated for all scans from the three first segments for all volunteers. ppm-values used for the calculations can be seen in Tables D.1 and D.2 in Appendix D.

Table 4.3 shows the difference in mean value between two subsequently scans in segment 1 for all volunteers. The precision difference is the precision which states that the absolute difference between two test results may be expected to lie within a difference of 2.8·SD (standard deviation) when obtained under repeatability conditions. All differences were within the precision difference. Mean values and standard deviation used in the calculations are shown in Table C.1 in Appendix C.

Table 4.3: Actual difference and precision difference between scan 1.1-1.2 and 1.2-1.3 for the mean value of measured peak area of PCr in all volunteers.

	Scan 1.1-1.2 difference	**Precision difference**	**Scan 1.2-1.3 difference**	**Precision difference**
Vol 1, week 1	0.01	0.08	0.01	0.08
Vol 1, week 2	0.01	0.08	0	0.08
Vol 2, week 1	0	0.11	0	0.11
Vol 2, week 2	0	0.11	0.01	0.11
Vol 3, week 1	0.01	0.11	0.01	0.11
Vol 3, week 2	0.02	0.11	0.01	0.11

4.3.2 Comparing segments after repositioning of the coil

Figure 4.10 shows three spectra in each subfigure where each spectra is the average of the three first segments for the actual volunteer and week. All spectra were averaged and phased with the analysis software FID-A [101].

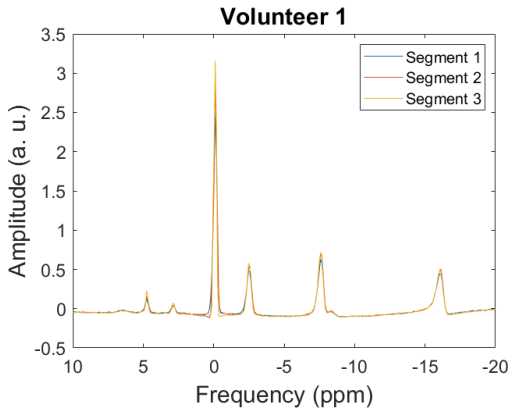

(a) Volunteer 1, week 1

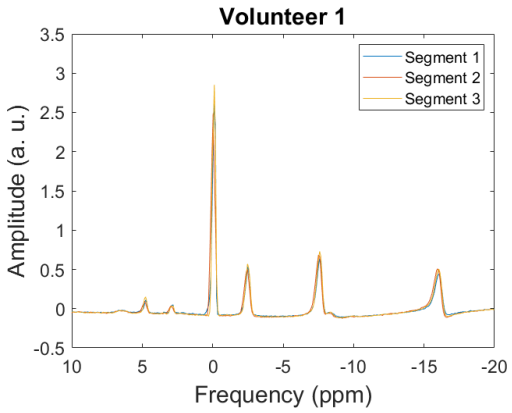

(b) Volunteer 1, week 2

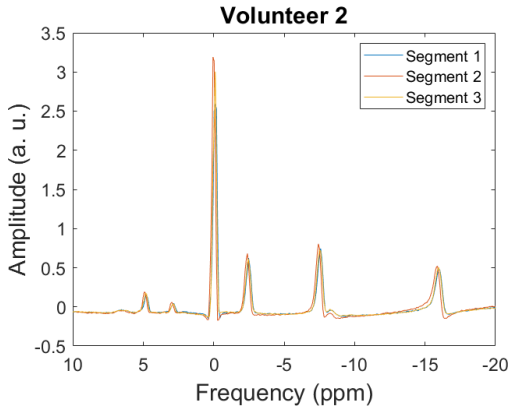

(c) Volunteer 2, week 1

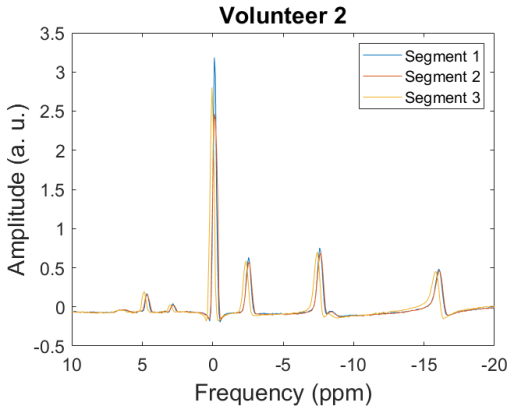

(d) Volunteer 2, week 2

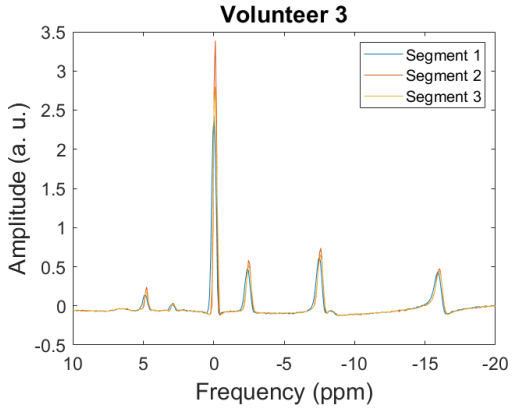

(e) Volunteer 3, week 1

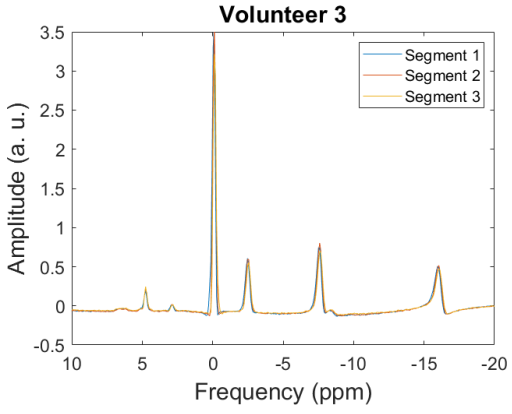

(f) Volunteer 3, week 2

Figure 4.10: Each Figure shows three spectra that was the average spectra for each of the three first segments for each week of scanning for all volunteers.

Figure 4.11 shows the measured peak area for PCr after repositioning of the coil for all volunteers. There was a one week interval between week 1 and week 2 for each volunteer.

From these box plots it could be seen that the measured peak area had some variation when the coil was repositioned between the segments. A dynamical plot for all volunteers can be seen in Figure C.1 in Appendix C.

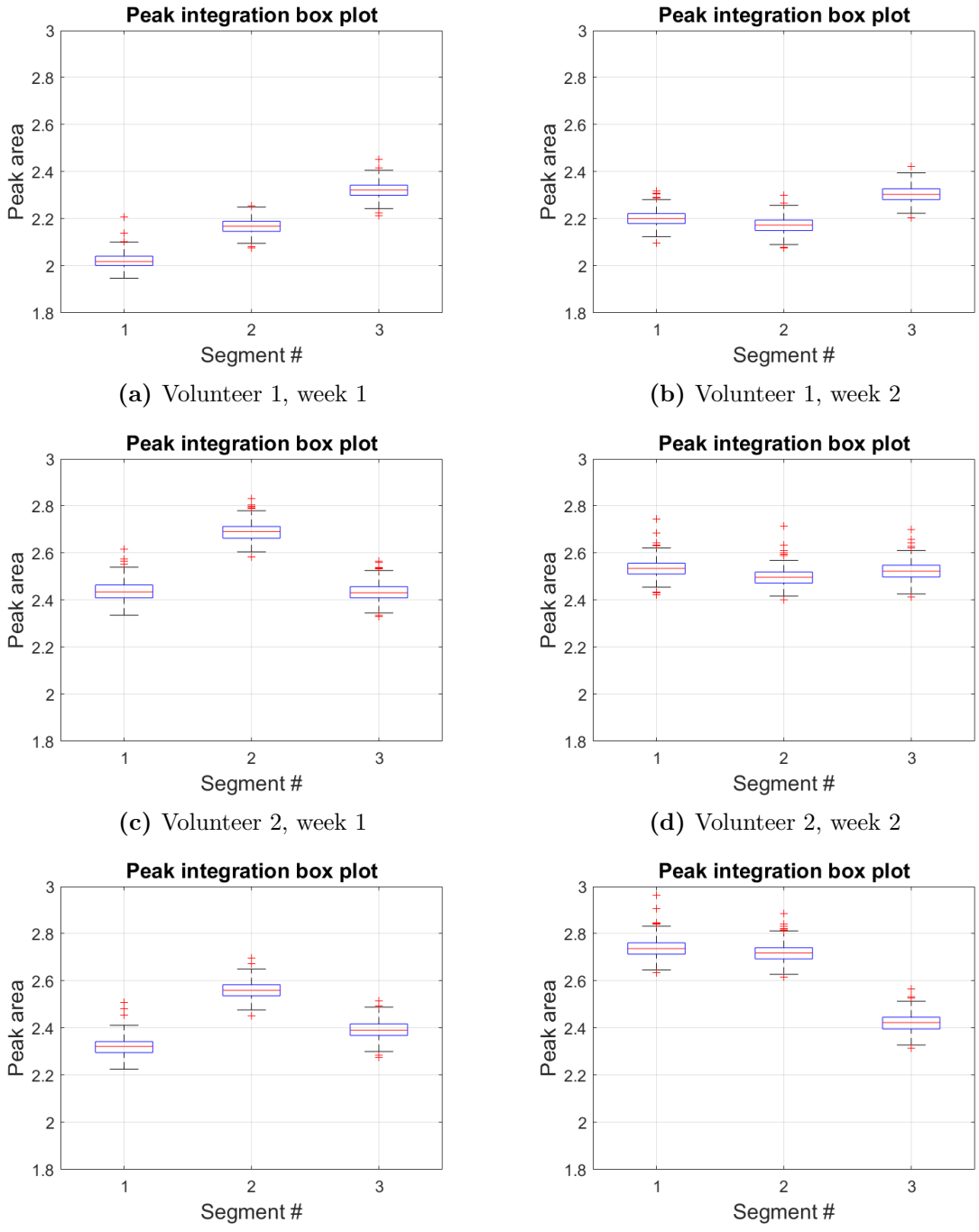

(a) Volunteer 1, week 1

(b) Volunteer 1, week 2

(c) Volunteer 2, week 1

(d) Volunteer 2, week 2

(e) Volunteer 3, week 1

(f) Volunteer 3, week 2

Figure 4.11: Box plot of measured peak area for PCr for the three first segments for all volunteers. The red central mark indicates the median, while the top and bottom edges of the box indicate the 75^{th} and 25^{th} percentiles, respectively. The black lines extended from the box represents the data points not considered outliers, while the red + signs marks the data points considered as outliers.

Figure 4.4 shows the calculated mean value and standard deviation for Pi/PCr for the

three first segments for all volunteers. The variations are small for all volunteers. Only volunteer 3's second week had a variation larger than 0.01 in mean value between the three segments. Theoretical value for this ratio in healthy cohorts, with the range of means shown in the square brackets, is 0.13 ± 0.01 [0.09-0.17] [2].

Table 4.4: Mean values with standard deviation for the Pi/PCr ratio for the three first segments for all volunteers.

	Volunteer 1		**Volunteer 2**		**Volunteer 3**	
Seg	**Week 1**	**Week 2**	**Week 1**	**Week 2**	**Week 1**	**Week 2**
1	0.10 ± 0.01	0.09 ± 0.01	0.10 ± 0.01	0.10 ± 0.01	0.10 ± 0.01	0.09 ± 0.01
2	0.10 ± 0.01	0.10 ± 0.01	0.10 ± 0.01	0.11 ± 0.01	0.11 ± 0.01	0.10 ± 0.01
3	0.10 ± 0.01	0.10 ± 0.01	0.11 ± 0.01	0.11 ± 0.01	0.11 ± 0.01	0.11 ± 0.01

As mentioned earlier, the pH calculations from the scans of the volunteers for the three first segments can be seen in Figure 4.9. After looking at the pH values measured without repositioning, we then compared the pH values measured with repositioning of the coil. It was mainly the first segment from scan number one of the first volunteer that stood out. The variations for the other segments were relatively small for all volunteers.

Table 4.5 shows the difference in mean value for measured peak area for PCr between segments 1-2 and 2-3 and the calculated precision difference, which was the absolute difference allowed between the two values in order to be obtained under repeatability conditions. The same were done for the Pi/PCr ratio for the same segments, shown in Table 4.6. The precision difference was calculated using equation (2.15). The values used for the difference calculations for Table 4.5 and 4.6 are shown in Table C.2 in Appendix C and Table 4.4, respectively.

Table 4.5: Actual difference and precision difference between segment 1-2 and 2-3 for the mean value of measured peak area of PCr for all volunteers.

	Segment 1-2 difference	**Precision difference**	**Segment 2-3 difference**	**Precision difference**
Vol 1, week 1	0.15	0.08	0.15	0.08
Vol 1, week 2	0.03	0.08	0.13	0.08
Vol 2, week 1	0.26	0.11	0.27	0.11
Vol 2, week 2	0.04	0.11	0.03	0.11
Vol 3, week 1	0.24	0.11	0.16	0.11
Vol 3, week 2	0.02	0.11	0.30	0.11

Table 4.6: Actual difference and precision difference between segment 1-2 and 2-3 for the mean value of measured peak area ratio of Pi/PCr for all volunteers.

	Segment 1-2 difference	**Precision difference**	**Segment 2-3 difference**	**Precision difference**
Vol 1, week 1	0	0.03	0	0.03
Vol 1, week 2	0.01	0.03	0	0.03
Vol 2, week 1	0	0.03	0.01	0.03
Vol 2, week 2	0.01	0.03	0	0.03
Vol 3, week 1	0.01	0.03	0	0.03
Vol 3, week 2	0.01	0.03	0.01	0.03

4.3.3 Before, during and after flexing of the calf muscle

For the last part of the scans of the volunteers they were asked to flex their calf muscle. Figure 4.12 shows the peak area for PCr for all volunteers for the segments of scans before, during and after flexing the calf muscle.

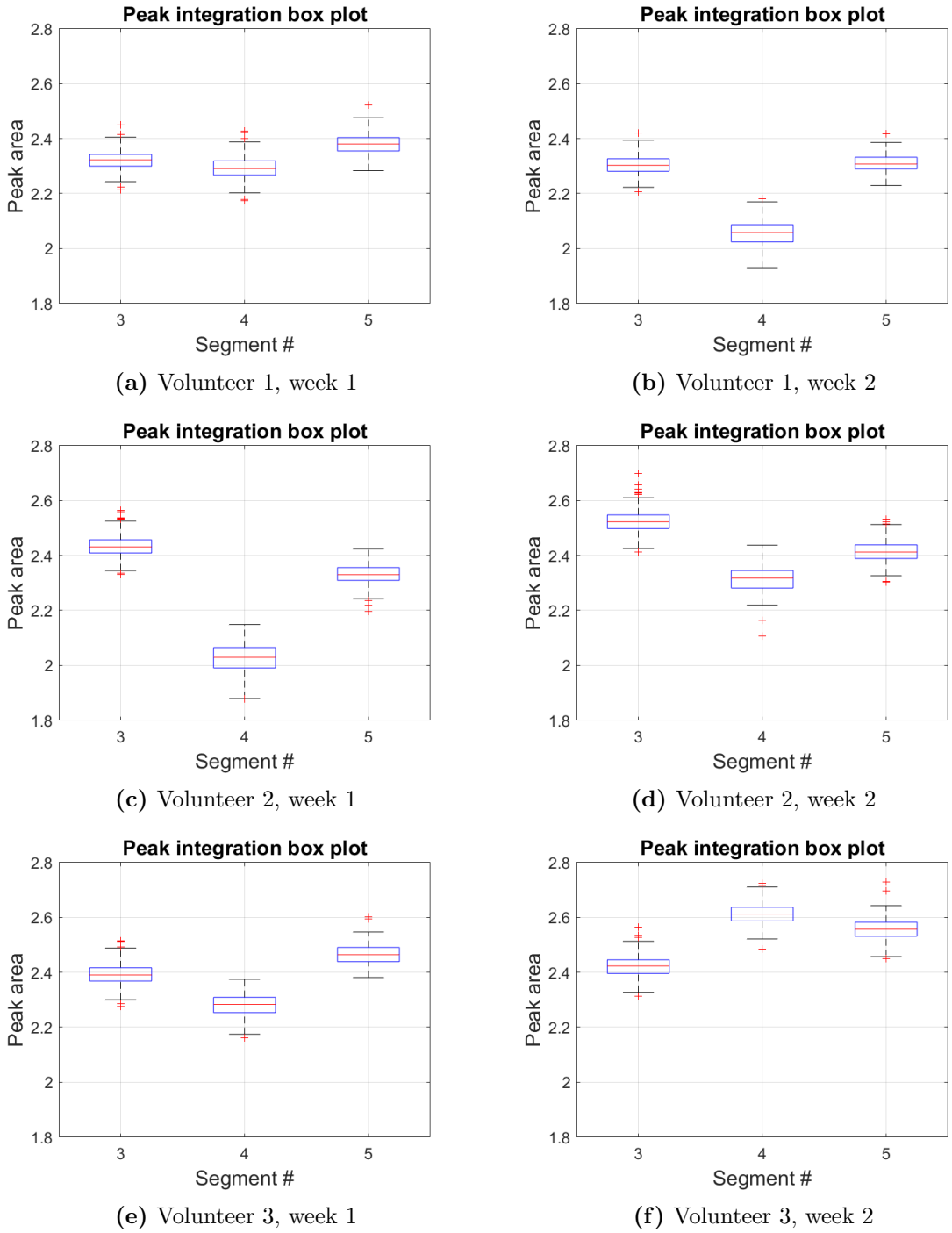

(a) Volunteer 1, week 1

(b) Volunteer 1, week 2

(c) Volunteer 2, week 1

(d) Volunteer 2, week 2

(e) Volunteer 3, week 1

(f) Volunteer 3, week 2

Figure 4.12: Box plot for the segment before (3), during (4) and after (5) flexing of the muscle for all volunteers. The red central mark indicates the median, while the top and bottom edges of the box indicate the 75^{th} and 25^{th} percentiles, respectively. The black lines extended from the box represents the data points not considered outliers, while the red + signs marks the data points considered as outliers.

Four of the Figures (4.12b, 4.12c, 4.12d and 4.12e) had a clear decrease in peak area for PCr during the segment where the muscle was flexed, while the first scan for volunteer 1, Figure 4.12a, had almost no dip in the peak area. The exception of these six Figures was Figure 4.12f where the peak area increased during flexing of the muscle, before decreasing for the last segment, where all the other increased. Figure 4.13 shows a dynamic representation of the measured peak area for PCr for the segments before (3), during (4) and after (5) the muscle was flexed.

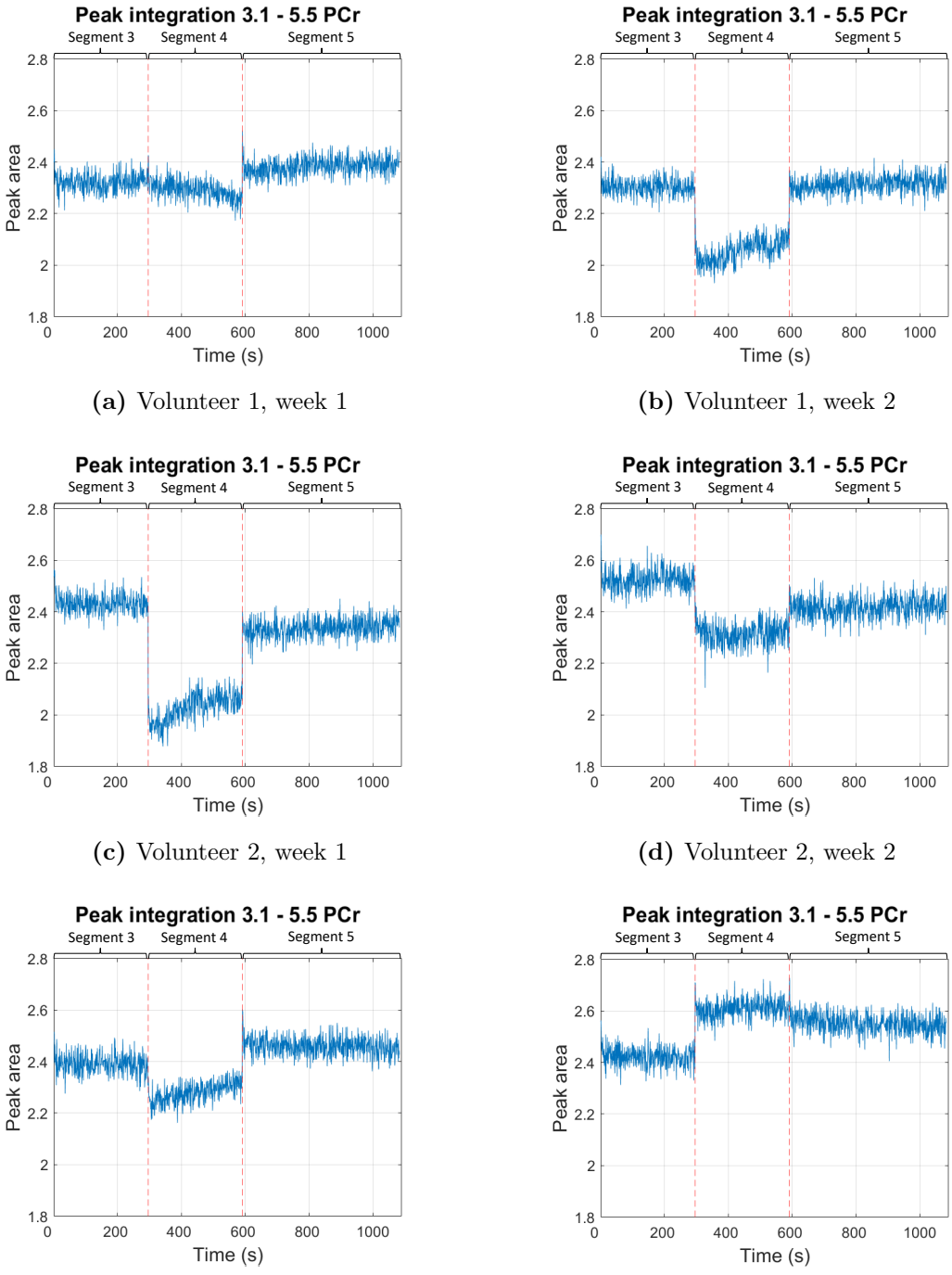

(a) Volunteer 1, week 1

(b) Volunteer 1, week 2

(c) Volunteer 2, week 1

(d) Volunteer 2, week 2

(e) Volunteer 3, week 1

(f) Volunteer 3, week 2

Figure 4.13: Integrated peak area for the metabolite PCr before, during and after flexing of the muscle for all volunteers.

Figure 4.14 shows the pH calculated from the chemical shift between Pi and PCr before, during and after flexing of the calf muscle. All scans in this part were done without changing the placement of the ^{31}P loop coil in order to get comparable results. From the figure it can be seen that there was a large degree of coherence of the pH calculations between the different weeks of scanning for the same volunteer and between the volunteers. From the three segments displayed in the figure, there were two single scans that stood out the most, scan 3.3 from the second week for volunteer 2 and scan 4.3 from the second week for volunteer 1, both of which had a lower pH value compared to the other scans in the same segment.

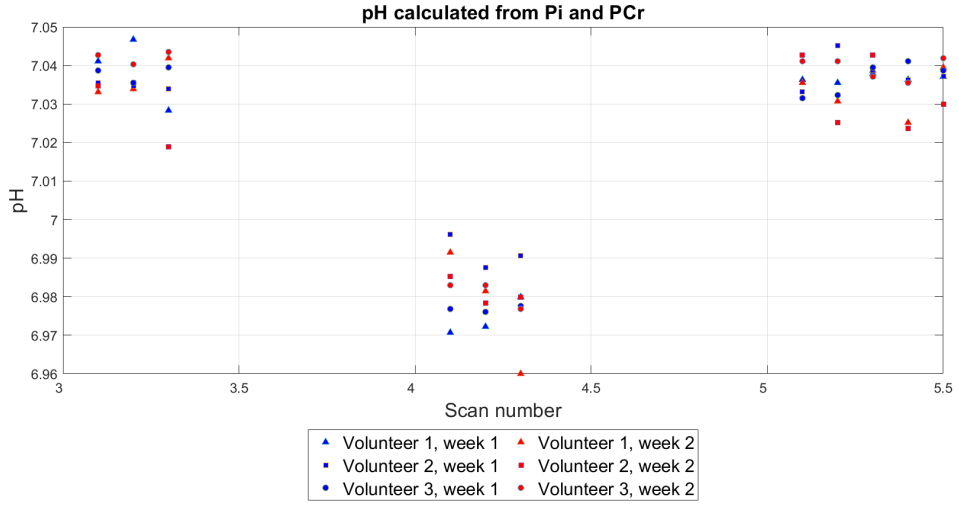

Figure 4.14: pH calculated for scans from the last three segments for both weeks of scans for all volunteers. ppm-values used for the calculations can be seen in Tables D.1 and D.2 in Appendix D.

Chapter 5

Discussion

5.1 The '^{31}P metabolites phantom'

A phantom containing ^{31}P metabolites normally found in different kinds of tissue in the human body, such as muscle or liver, was made for different types of use during the specialization project and the master's thesis. This phantom was intended to be used in testing and/or optimizing of ^{31}P MRS-protocols at the 7T MR. Furthermore, we analyzed the phantom both using high resolution magic angle spinning MRS (HR MAS MRS) and on 7T MR, to compare. HR MAS MRS analysis were performed to confirm which metabolites were present in the '^{31}P metabolites phantom' made during the specialization project fall 2020. The same ^{31}P metabolites were identified both on the HR MAS spectrometer (Figure A.2) and the 7T MR scanner (Figure 5.1). To identify the peaks in the 1D ^{31}P spectra from the HR MAS experiment, both the software Chenomx and TopSpin were used. Chenomx analyzed the different metabolites in the 1D ^{1}H spectra, while TopSpin was used to analyze the 2D ^{1}H /^{31}P spectra. Metabolite peaks in the 2D spectra fitted well with the expected ppm values for both the ^{1}H and ^{31}P axes.

Figure 4.1a and 4.1b shows that the largest peaks in the 2D spectra refers to protons located closest to the phosphorus atom, and that the second closest proton refers to the second largest peak etc. This is the case for three of the four metabolites in Figure 4.1b. ATP, PE and PC all have peaks in the 2D spectra according to the nearest proton in the structure, while for GPC, the second largest peak is not the second closest proton in the structure. The reason for this could be the triplet to the left of the proton in question. ATP has three phosphorus atoms but only the first one, seen from the top, creates a peak in the 2D spectra. This is because the two other phosphorus atoms are too far away from the closest proton atom to create a phosphorus proton coupling which would have been visible in the 2D spectra. From top to bottom are the three phosphorus atoms in the ATP structure referred to as α, β and γ. The peak for β-ATP is not visible along the F2 axis in Figure 4.1b because its ppm-value was outside the sweep width for the experiment. It is usually found around a ppm value of -16 to -20 depending on the calibration of the NMR spectra and the structure/tissue of the sample [103, 104]. For the 1D ^{31}P spectra displayed along the F2 axis, the β-ATP peak is located at -17.02 ppm, which can be seen in Figure A.2.

Something that can be compared when the correspondence between the HR MAS MRS (Figure 4.2a) and the 7T MR (Figure 4.2b) is to be assessed is whether the peaks in the two spectra are in the same place or not. When comparing the two figures it can be seen

that the peaks to the left of -5 ppm have a more negative ppm value in the HR MAS spectra, while the peaks to the right of 0 ppm has a slightly more positive ppm value in the 7T MR spectra. These changes could be made from the fact that ppm values may be sensitive to temperature [49], since the HR MAS scan was run at 4-5°C while the 7T MR scan was run at 22°C.

The '^{31}P metabolites phantom' made during the specialization project did not contain any PCr. PCr was expected to produce a clear and defined peak between GPC and γ-ATP in the ^{31}P MR spectra as shown Figure 5.1, but no peak was present. This was one of the motivations to do the HR MAS MRS of the phantom, in order to get spectra with higher spectral resolution. Another reason to use HR MAS MRS was that the use of 2D spectra makes the identification of peaks in the ^{31}P MRS spectra more secure, since we then have two axes to do the identification from. One hypothesis is that we had received a different metabolite than expected and that this could then be creatine (Cr), or that PCr had split into inorganic phosphate and Cr. To see if the phantom contained Cr or PCr, we analyzed the 1D ^{1}H spectra, seen in Figure A.1. In a 1D ^{1}H spectra both Cr and PCr are expected to have two peaks around 3.95 and 3.0 ppm [35, 105], and in the 1d ^{1}H spectra in Figure A.1 two peaks can be seen at the ppm values expected for both metabolites. But since there is no peak where PCr is expected to have it, neither in the 1D ^{31}P spectra (Figure A.2) nor in the 2D spectra (Figure 4.1a), then it is more natural to assume that the two peaks visible in the 1D ^{1}H spectra (Figure A.1) represent Cr and not PCr.

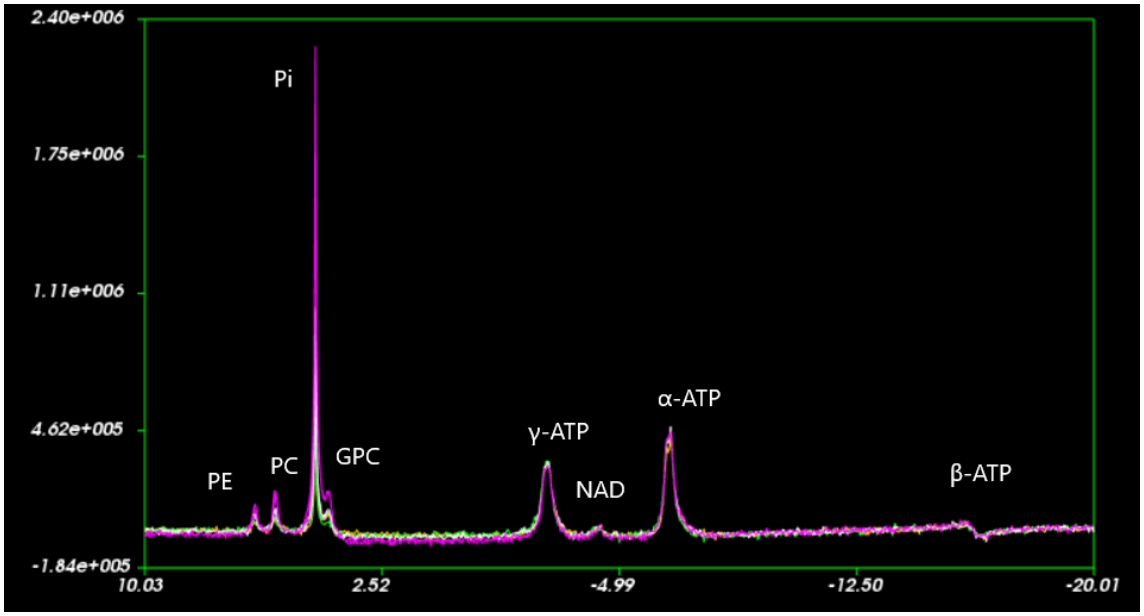

Figure 5.1: 1D ^{31}P spectra of the '^{31}P metabolites phantom' using 7T MR at St. Olavs Hospital. The spectra is presented using the analysis software SIVIC. The x-axis has the unit ppm and the y-axis has an arbitrary magnitude unit.

One thing that should be considered after creating and using a phantom for a study is its usefulness. The phantom was created for the specialization project and the master's thesis to be used for testing and/or optimization of MRS protocols on the 7T MR. A phantom could be very useful when testing different parameters in a protocol to see and learn what those changes do to a spectra. The use of a phantom also means that it is possible to do simple examinations/tests without having to get a volunteer or patient, and the tests can be done more on the fly if needed. Some of the disadvantages with the phantom is that

it can be difficult to recreate the composition of metabolites that are in a typical tissue, such as muscle or liver. It also turned out that the optimal protocol for the phantom, found during the specialization project, did not produce the same quality when used on a healthy volunteer. For the volunteer there had to be made changes in the protocol, which will be discussed later.

5.2 Protocol optimization in muscle

The protocol optimization was performed on a calf muscle on one of the healthy volunteers. Based on the peak area values in Table 4.1 it could look like the Phantom protocol would have been the best protocol out of the three represented in the table. The main reason for the large PCr and Pi peaks from the Phantom protocol is because of the long repetition time used, which was 8000 ms compared to 400 ms and 800 ms for the two other protocols. Since PCr and Pi both have relatively long T_1 times at 7T, 4.0 ± 0.2 s and 6.5 ± 1.0 s respectively [2], the long repetition time would reduce the t_1 weighting from these metabolites. The decision to use a much shorter repetition for the optimal protocol was based on several factors. A shorter repetition time allowed for a larger number of NSA within the same scan time, which could contribute to better SNR, as shown in Figure 4.6. This protocol was also chosen because it produced a better signal from the ATP metabolite, especially the β-ATP. The resulting spectra from the optimal protocol was also easier to phase correctly compared to the phantom protocol. The reason for this could be that the optimal protocol used a rectangular pulse while the phantom protocol used an adiabatic pulse, but it could also be because of the analysis software used for the 0^{th} and 1^{st} phasing of the spectra.

Different RF excitation pulse types were also tested in muscle using a repetition time of 4000 ms, as shown in Figure 4.5. They had twice the number of signal averages as the Phantom protocol which resulted in larger peaks for some of the metabolites even though the repetition time was halved. An equal effect happened for all these spectra as for the Phantom protocol, namely that the signal from the β-ATP was significantly weaker compared to the other peaks from the ATP metabolite. A reason why the signal from β-ATP was weaker could be that the transmission bandwidth was too narrow for the pulse to be able to excite the full spectra range [106]. One solution that could improve the signal is to shift the center-frequency up-field, but doing this change would potentially weaken the signal from the metabolites (Pi, PE, PC) at the other side of the spectra. Another solution could be to increase the transmission bandwidth, but this was not possible at the 7T MR scanner used in this thesis. It had a maximum transmission bandwidth of 10000 Hz for ^{31}P MRS.

Considering the large difference in signal for β-ATP for the two repetition times, the steady-state signal equation [107] could be used in order to check what kind of signal intensity that was expected for the two repetition times, given a theoretical T_1 value equal to 1.6 seconds for β-ATP [2]. The steady-state equation is considered for this case because the short repetition time induces a longitudinal steady-state after a few repetitions. This means that the magnetization in the z-direction had not completely returned in the z-direction before the next RF pulse excitation. The hypothesis is that the flip angle was too low for the β-ATP because of the small transmission bandwidth. If, on the other hand, one uses a short repetition time to get more frequently pulses, the flip angle will increase slightly for each RF pulse excitation, as the signal has not completely returned to the z-direction before the next pulse is applied.

Figure 5.2 shows the signal intensity for the two repetitions times 0.4 s and 4 s for β-ATP. Based on the calculations shown in this figure the β-ATP should be much more visible in the spectra with 4 seconds repetition time compared to the spectra with 0.4 seconds repetition time for a flip angle of 90°. Figure 5.2 does not take into consideration the fact that the scan with TR = 0.4 seconds had 256 NSA while the scan with 4 seconds repetition time had 32 NSA. This difference in NSA would in theory give a SNR difference of $\sqrt{256/32} = 2.83$, which clearly could contribute to the difference in signal for β-ATP in the two spectra. Another remark from Peter Lundberg [106] was that the PDE and PME resonances could be enhanced and sharpened if NOE was applied to the system, without affecting the ATP or PCr-resonance amplitudes.

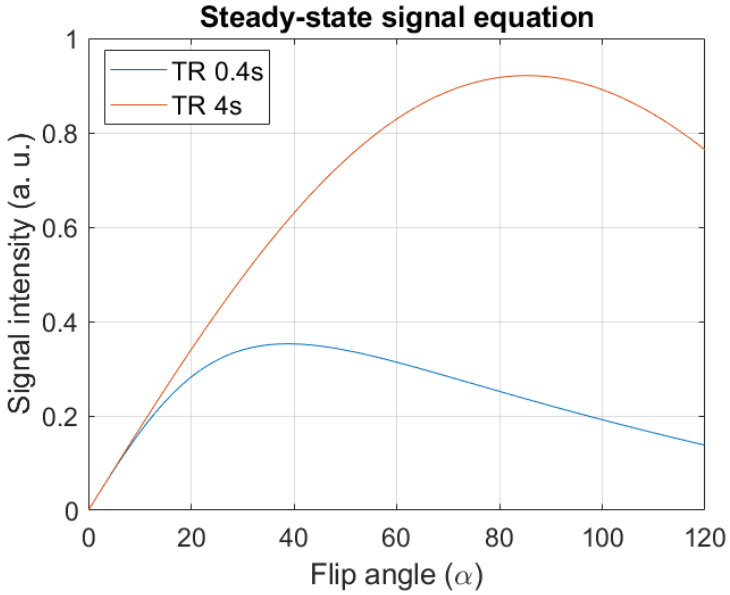

Figure 5.2: Steady-state signal equation used to calculate the expected signal intensity for β-ATP for different flip angels and repetition times. The T_1 used for β-ATP is 1.6 seconds. a.u.: arbitrary unit.

The optimal protocol found for ^{31}P MRS when scanning a healthy volunteer in the 7T MR had NSA equal to 256. A higher number of NS results in a higher SNR but will also increase the duration of the scan. Because of this, the NSA chosen in the protocol used for the repeatability scans were 128 to reduce the scan time. Proton decoupling is a technique that could have been used in order to increase the SNR for split metabolites. Proton decoupling causes split peaks such as doublets and triplets, which split due to protons being close to phosphorus atoms, to become singlets [35].

5.3 Repeatability

5.3.1 Comparing scans acquired without repositioning the coil

The peak area measured for PCr for the three scans in the same segment gave very consistent results for each volunteer when the 4-6 first signal averages were removed, as shown in Figure 4.8. This consistency between each scan within the same segment was somewhat expected since there are no changes between the scans and the scans was acquired almost directly after each other.

The main reason for a drop in SNR after 4-6 averages is that steady-state is achieved after a few averages. Since the repetition time (800 ms) was shorter than the T_1 relaxation time for PCr (∼4 seconds at 7T [2]), it would take a few periods of TR before the signal would settle down into steady-state. It takes a few TR periods for the metabolites magnetization vectors to recover to the same longitudinal magnetization after each TR period, and when this is achieved (steady-state) they will always recover to the same point of magnetization [37].

The differences in calculated mean value of the peak area for PCr between scan 1.1-1.2 and 1.2-1.3, listed in Table 4.3, were below 0.02 for all volunteers while the lowest calculated precision difference limit was 0.08. This means that all scans done subsequently without repositioning of the coil had good repeatability.

The variations in measured pH value within each segment is low for all volunteers, as shown in Figure 4.9. This shows that when the calf muscle is at rest and no other factors is changed, the ^{31}P loop coil gives consistent data for PCr and Pi concentrations and pH measurements. The average pH for each segment, calculated using equation (2.19), is approximately 7.04 which is in good agreement with other experiments performed by others and calculations that have pH $\sim 7.03 \pm 0.01$ [2, 81, 108].

Concentration or peak area ratios can be used to evaluate metabolic change in a range of diseased conditions [109, 110]. Typical ratios used for these studies are Pi/PCr, PCr/ATP, Pi/ATP etc [6]. Pi/PCr and PCr/ATP ratios from ^{31}P MRS of calf muscles could for example produce interesting and different analysis in the evaluation of heart failure patients [18]. The theoretical ratio values presented in Table 4.2 represents mean and range of mean for healthy volunteers from other studies [2]. Lower values from the calculated ratios from volunteer 1 could for example come from differences in the experimental setup or software analysis program used. The comparison was only used to confirm that the spectra acquired from the scans were representative and in accordance with other studies.

5.3.2 Comparing segments after repositioning of the coil

The changes in peak area value after repositioning of the coil for all graphs in Figure 4.11 and 4.13 were expected since placing the coil at the exact same place each time could be difficult. Differences in peak areas could come from variations in the part of the calf muscle that was analyzed. The changes in peak area between segments seen for PCr can also be found for most of the other metabolites like all three resonances for ATP, Pi and PDE for the different volunteers. The relative changes are somewhat smaller since the peaks also are visibly smaller in size, and some of the mentioned metabolites does not follow the changes to PCr perfectly. They have some variations, but all have the same main features in their peak area figures.

The number and size of the outliers around the box plots in Figure 4.11 would have been larger if the first six averages had not been removed. Apart from that, the number of outliers are varying from volunteer to volunteer, and from scan to scan, but a clear trend is that most of the outliers are above the mean value. The reason for this could be inaccurate phasing of some of the averages in a scan since the 0^{th} and 1^{st} order phasing was found based on the spectra created from all the averages within one of the three scans in a segment.

Changes in pH from segment to segment, as shown in Figure 4.9, were small for all the volunteers, which shows that the measured ppm is less affected of the repositioning of the

^{31}P loop coil compared to for example the measured peak area in Figure C.1. The pH values measured for almost all volunteers are within the expected range for pH values in a resting calf muscle, which is $\sim$7.03 $\pm$ 0.01 [2, 108, 81]. The problem with not achieving perfect repositioning of the coil between the scans was also mentioned as a minor effect from a study by Valkovic *et al.* [111]

pH calculated from the chemical shift difference between Pi and PCr was the preferred method here due to PCr's strong non-overlapping single resonance in the spectra. For spectra without PCr signal, e.g. liver, other methods are more suitable for pH calculations. For example, the chemical shift between Pi and α-ATP using equation 2.19 [22].

The spectra acquired after repositioning of the coil (Figure 4.10) had larger variations compared with the spectra acquired without repositioning of the coil (Figure 4.7). This was expected because each spectra in Figure 4.10 were the average for a segment, and between each segment the coil was repositioned. A slightly different shim was applied since the volunteer was removed and replaced in the isocenter of the scanner. The variations are present for all volunteers and the most visible variation between the segment spectra is the amplitude of the PCr peak at approximately 0 ppm. Metabolite concentrations or ratios can be used to get further information about a volunteer or a patient. This ratio is therefore dependent on the measurements from two different metabolites and that both of them are credible. Variations in measured peak area could affect the ratios, and therefore also the interpretation of the results. The average spectra viewed in Figure 4.10 shows that a calculated ratio, e.g. PCr/β-ATP, would depend on which spectra one chose to do the calculations from. This can of course be avoided to some extent by using the total average of all the spectra for the same volunteer. It would at the same time give a slightly larger standard deviation compared to using only a single spectrum for the calculations.

The Pi/PCr ratios listed in Table 4.4 shows that although the measurements of peak area for PCr vary when the coil is repositioned, the other metabolites vary reasonably equally. There are very small variations in the average value for all the volunteers in Table 4.4. The largest variation is in the second week for volunteer 3. This variation is due to the fact that measured peak area for PCr and Pi did not change equally when the coil was repositioned, which can be seen by comparing Figure 4.11f and C.2f. The rest of the box plots in Figure 4.11 and C.2 agrees well with comparison as suggested by the ratios in Table 4.4. There are advantages and disadvantages with the use of ratios versus peak area measurements. When using ratios you only discover changes that stands out from the rest, while with only peak area measurements you discover all changes between the segments. Table 4.5 and 4.6 shows quantitative measurements if two subsequent segments had good repeatability or not, based on equation 2.15. The calculations in these two tables shows that there is a clear difference between whether two of the segments in the study have good repeatability or not. This is based on whether one look at the measurements from a single metabolite or a ratio. Only using Table 4.6 would say that all segments had good repeatability compared to each other, while Table 4.5 only consider four of the combinations to have good repeatability. This shows the importance of deciding whether the goal for the repeatability study is to get repeatability of a single metabolite or a ratio.

Some measurements of the mean values of FWHM were made for the PCr peak for scan 1.1, 1.2, 1.3, and for all segments for all volunteers. This is shown in Table E.1 and E.2 in Appendix E. The FWHM values for the first three scans for each volunteer are almost identical. This was expected since the three scans were performed directly after each other with minimal delay. No changes were made to the setup or the placement between the scans.

The average FWHM for the three first segments for all volunteers shown in Table E.2 have some variations between the segments. These changes could come from the coil repositioning, meaning that the part of the muscle visible in the field of view is changed, or it could be because of a slightly changed shimming, which is always done after repositioning of the coil. The FWHM values of PCr in a calf muscle in Table E.1 are slightly larger than the FWHM value Meyerspeer *et al.*[112] found for PCr, which was 16 ± 7 Hz at 7T. FWHM values from PCr increased during flexing (segment 4) for volunteer 2 while it decreases for volunteer 1 and 3. This may indicate that the change in the measured FWHM is affected by the person being scanned, and not just by whether the muscle is flexed or not. For these segments, the coil was not repositioned and the volunteer was not taken out of the scanner between the segments, so the changes in FWHM does not come from altered shimming. The change could still come from that different parts of the muscle is in the field of view for the coil because of small changes in placement when the muscle is flexed

5.3.3 Before, during and after flexing of the calf muscle

The percentage decrease in the peak area for PCr before compared to during flexing of the calf muscle varies both between the volunteers and the scans of the same volunteers. As shown in Figure 4.12, the peak area decreases between 7% and 20% in five cases. An increase of 10% is observed in one case. Comparing these numbers with literature values is difficult because there is great variation in how the exercise of the muscle takes place in each of the different studies. It is not always done in the same way or with the same intensity, so the expected decrease in PCr signal intensity varies from 10% up to 80% depending on the method and length of flexing/training the muscle [2, 18, 113].

For this experiment it is not possible to see the all parts of the recovery for the PCr peak area after the muscle flexing because there was a small pause between scan 4.3 and scan 5.1 in order to assure that the volunteer had stopped flexing of the muscle. The recovery is dependent both on the type of exercise and if the volunteer has any diseases or not. Some types of exercises, e.g. low impact plantar flexion exercise, will typically increase the change in PCr signal while the pH stays relatively constant. Other types of exercise, like static flexion over time, might cause a dip in pH [2]. A study from Menon *et al.* [18] showed that increased recovery time of PCr after a low impact plantar flexion exercise may indicate that a patient has a heart failure. Measured recovery time for PCr in the healthy volunteers was 26.73 ± 4.49 s, while the recovery time for PCr in the heart failure cohort was 50.1 ± 8.51 s. Dynamic ^{31}P MRS studies could also give unique information that could be of interest for heart failure patients, e.g. different types of metabolic ratios and changes in ATP [18].

The values in Figure 4.14 represents the calculated pH before, during and after the volunteers flexed their calf muscle. The change in pH for all volunteers are almost the same with only some minor differences. A dip in the pH was expected when the muscle was flexed due to creation of lactate during the exercise [114]. How large the dip is, may depend on several factors like the total exercise time, the physiology of the muscle for the volunteer, the exercise/flexing method, and differences in how much each volunteer flexed their muscle etc. Other, and more advanced, exercise methods could be to have the volunteers do plantar flexion exercise by, for example, using a MR compatible ergometer [18, 115]. The dip in calculated pH for these measurements are around 0.6 between segment 3 and 4, and between segment 4 and 5. In a study by Rossiter *et al.* [116] used the same calculation method for measuring pH during skeletal muscle exercise. They measured an

average resting pH of 7.05 ± 0.04 while the average measured pH from the exercise was 6.95 ± 0.09. Their exercise consisted of the subject laying prone inside the bore using an ergometer which permitted high-intensity exercise. Each round of exercise started with 4 minutes rest, then 6 minutes exercise, and finished with 6 minutes recovery. The study of Rossiter *et al.* was similar to the one we have conducted in terms of both the length before, during, and after exercise, and the variations found in pH during the exercise. The main difference was how the training was performed in the scanner. Rossiter *et al.* also concluded that the main contribution to the dip in pH during exercise was the production of lactate.

The actual exercise in the MR scanner could have been more controlled for a future study, to get even more comparable results where you could control how hard each volunteer does the exercise given. This was not controlled well enough during this master's thesis. The volunteers were only asked to flex the muscle so hard that they would get tired, but at the same time they managed to keep the same flex for the total duration of five minutes. The exercise part of the study was done in order to see the metabolic changes and to have some alternative data to compare between the different volunteers. It was also done to be able to calculate the pH based on the chemical shift between Pi and PCr and to see if or how much it would change when a volunteer flexed its muscle for approximately five minutes.

Chapter 6

Conclusion

The main objective for this thesis was to optimize a protocol and investigate the repeatability effect for ^{31}P MRS in calf muscle of healthy volunteers at a clinical 7T MR scanner. A sample from '^{31}P metabolites phantom' was first analyzed by HR MAS MRS to confirm the findings from the 7T MR scanner during the specialization project from the fall semester of 2020. The metabolites found were PC, PE, Pi, PCr, α-ATP, β-ATP, γ-ATP and NAD. The ^{31}P MRS scan protocol was optimized in a healthy volunteer, where we started with the protocol found optimal for the '^{31}P metabolites phantom' during the specialization project. We tested both the optimal protocol from the phantom and Siemens standard protocol for the protocol optimization. After testing these protocols with different acquisition parameters, we ended up with a protocol more similar to the Siemens standard protocol for muscle tissue, where the repetition time was increased from 400 ms to 800 ms to decrease the T_1 weighting effect.

The repeatability experiment was then performed with three volunteers, each scanned two times with one week interval. The analysis was performed mainly using the analysis software FID-A. It could be concluded that the ^{31}P MRS at the 7T MR has a good repeatability, and that the main source leading to deviations in the repeatability is repositioning of the coil between scans.

As a part of the repeatability experiment, the volunteers were asked to flex the calf muscle to analyze the ability to detect changes in pH and in the signal from the individual metabolites in ^{31}P MR spectra. The results showed that the ^{31}P MRS had a very good ability to detect the change in pH during flexing of the calf muscle. The measured peak area from PCr was found decreasing, as expected, in five out of six scans of the volunteers.

6.1 Future work

There are many different tests, adaptions and experiments that could have been done, but these are left for future work. A larger homogeneous group of healthy volunteers could be used for the test of repeatability. This would have made the data stronger statistically. A study using a more heterogeneous group of volunteers could be used to look at the biological variations in the population.

Another interesting study for the future would be to do an exercise study with more volunteers over a longer period. The group of volunteers could, for example, be a training

group where the objective could be to look after changes in ^{31}P metabolites and pH in calf muscle after some weeks of training. The volunteers could be divided into groups depending on the intensity of the training. One could choose to have one group of well-trained volunteers measured against a group of more average or poorly trained volunteers, where the objective could be to see what kind of impact these parameters would have on the results.

Bibliography

[1] J. C. Crane, M. P. Olson, and S. J. Nelson, "Sivic: Open-Source, Standards-Based Software for DICOM MR Spectroscopy Workflows," *International Journal of Biomedical Imaging*, vol. 2013, p. 12 pages, 2013.

[2] M. Meyerspeer, C. Boesch, D. Cameron, M. Dezortová, S. C. Forbes, A. Heerschap, J. A. Jeneson, H. E. Kan, J. Kent, G. Layec, J. J. Prompers, H. Reyngoudt, A. Sleigh, L. Valkovič, G. J. Kemp, and E. W. G. on 31P MR Spectroscopy of Skeletal Muscle, "31p magnetic resonance spectroscopy in skeletal muscle: Experts' consensus recommendations," *NMR in Biomedicine*, vol. 34, no. 5, p. e4246, 2021.

[3] M. Cohn and T. J. Hughes, "Phosphorus magnetic resonance spectra of adenosine di- and triphosphate. I. Effect of pH," *J Biol Chem*, vol. 235, pp. 3250–3, 1960.

[4] J. Ackerman, T. Grove, G. Wong, D. Gadian, and G. Radda, "Mapping of metabolites in whole animals by 31P NMR using surface coils," *Nature*, vol. 283, pp. 167–170, 1980.

[5] P. Bendel, C. Lai, and P. Lauterbur, "P-31 Spectroscopic Zeugmatography of Phosphorous Metabolites," *J Magn Reson*, vol. 38, pp. 343–356, 1980.

[6] Y. Liu, Y. Gu, and X. Yu, "Assessing tissue metabolism by phosphorous-31 magnetic resonance spectroscopy and imaging: a methodology review," *Quant Imaging Med Surg*, vol. 7, pp. 707–726, 2017.

[7] F. Bloch, "Line-narrowing by macroscopic motion," *Phys. Rev.*, vol. 94, pp. 496–497, 1954.

[8] W. A. Anderson and J. T. Arnold, "A line-narrowing experiment," *Phys. Rev.*, vol. 94, pp. 497–498, 1954.

[9] H. S. Gutowsky and D. E. Woessner, "Nuclear magnetic spin-lattice relaxation in liquids," *Phys. Rev.*, vol. 104, pp. 843–844, 1956.

[10] I. J. Lowe, "Free induction decays of rotating solids," *Phys. Rev. Lett.*, vol. 2, pp. 285–287, 1959.

[11] E. Andrew, A. Bradbury, and R. Eades, "Removal of dipolar broadening of nuclear magnetic resonance spectra of solids by specimen rotation," *Nature*, vol. 183, p. 1802–1803, 1959.

[12] Y. J. Jiang and J. K. Harper, "An explanation of magic angle spinning nmr experiments in the time domain," *Concepts in Magnetic Resonance Part A*, vol. 34A, no. 5, pp. 249–263, 2009.

[13] W. E. Maas, F. H. Laukien, and D. G. Cory, "Gradient, high resolution, magic angle sample spinning nmr," *Journal of the American Chemical Society*, vol. 118, no. 51, pp. 13085–13086, 1996.

[14] H. Farooq, D. Courtier-Murias, R. Soong, W. Bermel, W. M. Kingery, and A. J. Simpson, "Hr-mas nmr spectroscopy: A practical guide for natural samples," *Current Organic Chemistry*, vol. 17, pp. 3013–3031, 2013.

[15] E. R. Andrew, R. E. Richards, and K. J. Packer, "Magic angle spinning in solid state n.m.r. spectroscopy," *Philosophical Transactions of the Royal Society of London. Series A, Mathematical and Physical Sciences*, vol. 299, no. 1452, pp. 505–520, 1981.

[16] S. Moestue, B. Sitter, T. F. Bathen, M.-B. Tessem, and I. S. Gribbestad, "Hr mas mr spectroscopy in metabolic characterization of cancer," *Current Topics in Medicinal Chemistry*, vol. 11, pp. 2–26, 2011.

[17] B. Chance, J. Im, S. Nioka, and M. Kushmerick, "Skeletal muscle energetics with pnmr: personal views and historic perspectives," *NMR in Biomedicine*, vol. 19, no. 7, pp. 904–926, 2006.

[18] R. G. Menon, D. Xia, S. D. Katz, and et al, "Dynamic 31p-mri and 31p-mrs of lower leg muscles in heart failure patients," *Sci Rep*, vol. 11, 2021.

[19] I. Cresshull, M. Dawson, R. Edwards, D. Gadian, R. Gordon, G. Radda, D. Shaw, and D. Wilkie, "Human muscle analysed by 31p nuclear magnetic resonance in intact subjects," *J Physiol*, vol. 317, p. 18P, 1981.

[20] J. Griffiths, A. Stevens, R. Iles, R. Gordon, and D. Shaw, "31p-nmr investigation of solid tumours in the living rat," *Biosci Rep*, vol. 1, no. 4, pp. 319–25, 1981.

[21] R. B. Moon and J. H. Richards, "Determination of intracellular ph by 31p magnetic resonance," *Journal of Biological Chemistry*, vol. 248, no. 20, pp. 7276–7278, 1973.

[22] M. Rata, S. L. Giles, N. M. deSouza, M. O. Leach, and G. S. Payne, "Comparison of three reference methods for the measurement of intracellular ph using 31p mrs in healthy volunteers and patients with lymphoma," *NMR in Biomedicine*, vol. 27, no. 2, pp. 158–162, 2014.

[23] Y. Lian, W. Zhang, L. Ding, X. Zhang, Y. Zhang, and X. dong Wang, "Chapter 8 - nanomaterials for intracellular ph sensing and imaging," in *Novel Nanomaterials for Biomedical, Environmental and Energy Applications* (X. Wang and X. Chen, eds.), Micro and Nano Technologies, pp. 241–273, Elsevier, 2019.

[24] G. Layec, A. Bringard, Y. Le Fur, C. Vilmen, J.-P. Micallef, S. Perrey, P. J. Cozzone, and D. Bendahan, "Reproducibility assessment of metabolic variables characterizing muscle energetics in vivo: A 31p-mrs study," *Magnetic Resonance in Medicine*, vol. 62, no. 4, pp. 840–854, 2009.

[25] K. K. McCully, T. N. Turner, J. Langley, and et al., "The reproducibility of measurements of intramuscular magnesium concentrations and muscle oxidative capacity using 31p mrs," *Dyn Med*, vol. 8, no. 5, 2009.

[26] R. G. Miller, P. J. Carson, R. S. Moussavi, A. Green, A. Baker, M. D. Boska, and M. W. Weiner, "Factors which influence alterations of phosphates and ph in exercising human skeletal muscle: Measurement error, reproducibility, and effects of fasting, carbohydrate loading, and metabolic acidosis," *Muscle & Nerve*, vol. 18, no. 1, pp. 60–67, 1995.

[27] R. G. Miller, D. Giannini, H. S. Milner-Brown, R. B. Layzer, A. P. Koretsky, D. Hooper, and M. W. Weiner, "Effects of fatiguing exercise on high-energy phosphates, force, and emg: Evidence for three phases of recovery," *Muscle & Nerve*, vol. 10, no. 9, pp. 810–821, 1987.

[28] N. M. A. van den Broek, H. M. M. L. De Feyter, L. d. Graaf, K. Nicolay, and J. J. Prompers, "Intersubject differences in the effect of acidosis on phosphocreatine recovery kinetics in muscle after exercise are due to differences in proton efflux rates," *American Journal of Physiology-Cell Physiology*, vol. 293, no. 1, pp. C228–C237, 2007.

[29] L. M. Edwards, D. J. Tyler, G. J. Kemp, R. M. Dwyer, A. Johnson, C. J. Holloway, A. M. Nevill, and K. Clarke, "The reproducibility of 31-phosphorus mrs measures of muscle energetics at 3 tesla in trained men," *PLOS ONE*, vol. 7, pp. 1–7, 06 2012.

[30] "MR Spectroscopy." Available from: `https://www.cedars-sinai.edu/Patients/Programs-and-Services/Imaging-Center/For-Physicians/Neuroradiology/MR-Spectroscopy.aspx`, Accessed: 2020-09-25.

[31] D. M. G. A. da Veiga and A. P. F. Gaillard, "MR spectroscopy." Available from: `https://radiopaedia.org/articles/mr-spectroscopy-1`, Accessed: 2020-09-25.

[32] J. S. Grewal, "Spin-Spin coupling in NMR." Available from: `https://conductscience.com/spin-spin-coupling-in-nmr/`, Accessed: 2020-10-25.

[33] J. Hornak, *The Basics of NMR*. 01 1997.

[34] "Precession." Magnetic Resonance - Technology Information Portal, Member of SoftWay's Medical Imaging group. Available from `https://www.mr-tip.com/serv1.php?type=db1&dbs=Precession`. Accessed: 2021-04-26.

[35] R. A. D. Graaf, *In Vivo NMR Spectroscopy - 2nd Edition: Principles and Techniques*. John Wiley and Sons, Ltd, 2007.

[36] "Spin-lattice and spin-spin relaxation." Available from: `https://www.ucl.ac.uk/nmr/sites/nmr/files/L5_3SH_web_shortened.pdf`. [homepage on Internet]. University College London, UCL Chemistry NMR Instruments (LectureNotes): London, 2014. [Accessed 2020-12-14].

[37] C. Westbrook and J. Talbot, *MRI in Practice, fifth edition*. John Wiley and Sons, Ltd, 2019.

[38] P. Cassidy, K. Clarke, and D. Edwards, "Determining the tuning and matching requirements of rf coils using electromagnetic simulation and electric circuit analysis," *Concepts in Magnetic Resonance Part B: Magnetic Resonance Engineering*, vol. 25B, no. 1, pp. 27–41, 2005.

[39] "Coil tuning/matching." Publisher: AD Elster, ELSTER LLC. Available from: `http://mri-q.com/coil-tuningmatching.html#`, Accessed: 2021-03-02.

[40] P. K. Mandal, "Magnetic Resonance Spectroscopy (MRS) and Its Application in Alzheimer's Disease," *Concepts in Magnetic Resonance Part A*, vol. 30A, pp. 40–64, 2007.

[41] K. Richter, V. Mathes, M. Fronius, M. Althaus, A. Hecker, G. Krasteva-Christ, W. Padberg, A. J. Hone, J. M. McIntosh, A. Zakrzewicz, and V. Grau, "Phosphocholine – an agonist of metabotropic but not of ionotropic functions of alpha 9-containing nicotinic acetylcholine receptors," *Sci Rep*, vol. 6, 2016.

[42] A. Lehmann, H. Hagberg, I. Jacobson, and A. Hamberger, "Effects of status epilepticus on extracellular amino acids in the hippocampus," *Brain res*, vol. 359, pp. 147–151, 1985.

[43] O. Gonen, A. Mohebbi, R. Stoyanova, and T. R. Brown, "In vivo phosphorus polarization transfer and decoupling from protons in three-dimensional localized nuclear magnetic resonance spectroscopy of human brain," *Magn Reson Med*, vol. 37, pp. 301–306, 1997.

[44] L. Valkovič, W. T. Clarke, A. I. Schmid, B. Raman, J. Ellis, H. Watkins, M. D. Robson, S. Neubauer, and C. T. Rodgers, "Measuring inorganic phosphate and intracellular ph in the healthy and hypertrophic cardiomyopathy hearts by in vivo 7T 31P-cardiovascular magnetic resonance spectroscopy," *Journal of Cardiovascular Magnetic Resonance*, vol. 21, 2019.

[45] M. Schepers, A. Tiane, D. Paes, S. Sanchez, B. Rombaut, E. Piccart, B. P. F. Rutten, B. Brône, N. Hellings, J. Prickaerts, and T. Vanmierlo, "Targeting Phosphodiesterases—Towards a Tailor-Made Approach in Multiple Sclerosis Treatment," *Front Immunol*, vol. 10, 2019.

[46] C. Andrade, M. Otaduy, K. Valente, D. Maia, E. Park, R. Valério, M. Tsunemi, and C. Leite, "Phosphorus magnetic resonance spectroscopy in malformations of cortical development," *Epilepsia*, vol. 52, pp. 2276–84, 2011.

[47] W. J. M. van der Kemp, B. L. Stehouwer, J. H. Runge, J. P. Wijnen, A. J. Nederveen, P. R. Luijten, and D. W. J. Klomp, "Glycerophosphocholine and Glycerophosphoethanolamine Are Not the Main Sources of the In Vivo 31P MRS Phosphodiester Signals from Healthy Fibroglandular Breast Tissue at 7T," *Front Oncol*, vol. 6, p. 29, 2016.

[48] R. B. Moon and J. H. Richards, "Determination of intracellular ph by 31p magnetic resonance," *Journal of Biological Chemistry*, vol. 248, no. 20, pp. 7276–7278, 1973.

[49] F.C.Wermter, N. Mitschke, C. Bock, and et al, "Temperature dependence of 1h nmr chemical shifts and its influence on estimated metabolite concentrations," *Magn Reson Mater Phy*, vol. 30, pp. 579–590, 2017.

[50] A. Wong and C. Lucas-Torres, "High-resolution magic-angle spinning (hr-mas) nmr spectroscopy," in *NMR-based Metabolomics* (H. C. Keun, ed.), ch. 5, pp. 133–150, The Royal Society of Chemistry, 2018.

[51] G. S. Payne, H. Troy, S. J. Vaidya, J. R. Griffiths, M. O. Leach, and Y.-L. Chung, "Evaluation of 31p high-resolution magic angle spinning of intact tissue samples," *NMR in Biomedicine*, vol. 19, no. 5, pp. 593–598, 2006.

[52] A. Sodickson and D. Cory, "Shimming a high-resolution mas probe," *J Magn Reson*, vol. 128, no. 1, pp. 87–91, 1997.

[53] A. Sodickson and D. Cory, "Shimming a high-resolution mas probe," *Journal of Magnetic Resonance*, vol. 128, no. 1, pp. 87–91, 1997.

[54] M. Piotto, K. Elbayed, J.-M. Wieruszeski, and G. Lippens, "Practical aspects of shimming a high resolution magic angle spinning probe," *Journal of Magnetic Resonance*, vol. 173, no. 1, pp. 84–89, 2005.

[55] D. Wishart, C. Bigam, J. Yao, F. Abildgaard, H. Dyson, E. Oldfield, J. Markley, and B. Sykes, "1h, 13c and 15n chemical shift referencing in biomolecular nmr," *J Biomol NMR*, no. 2, pp. 135–40, 1995.

[56] T. Parella, *PULSE PROGRAM CATALOGUE: 1D AND 2D NMR EXPERIMENTS*, vol. 1. Bruker BioSpin GmbH, 2010.

[57] O. Beckonert, H. Keun, T. Ebbels, and *et. al.*, "Metabolic profiling, metabolomic and metabonomic procedures for nmr spectroscopy of urine, plasma, serum and tissue extracts," *Nat Protoc*, vol. 2, pp. 2692–2703, 2007.

[58] R. T. Mckay, "How the 1d-noesy suppresses solvent signal in metabonomics nmr spectroscopy: An examination of the pulse sequence components and evolution," *Concepts in Magnetic Resonance Part A*, vol. 38A, no. 5, pp. 197–220, 2011.

[59] G. Bodenhausen and D. Ruben, "Natural abundance nitrogen-15 nmr by enhanced heteronuclear spectroscopy," *Chemical Physics Letters*, vol. 69, pp. 185–189, 1980.

[60] "2d nmr introduction.." (2020, August 14). Retrieved March 8, 2021, `https://chem.libretexts.org/@go/page/1805`.

[61] T. Parella, "Nmrguide3.5." Publisher: BRUKER Biospin, 1998-2003.

[62] J. S. i Jiménez, "Modern nmr methodologies for the measurement of homo- and heteronuclear coupling constants in small molecules."

[63] "J-coupling (scalar).." (2020, August 22). Retrieved March 8, 2021, from `https://chem.libretexts.org/@go/page/1826`.

[64] E. T. Sahakyan, "Predicting scalar coupling constants using machine learning." (2019, August 5). Available from: `https://medium.com/@liztersahakyan/predicting-scalar-coupling-constants-using-machine-learning-c213af14e862`. Accessed: 2021-03-08.

[65] Y. Lin, Q. Zeng, L. Lin, Z. Chen, and P. Barker, "High-resolution methods for the measurement of scalar coupling constants," *Progress in Nuclear Magnetic Resonance Spectroscopy*, vol. 109, 08 2018.

[66] "MRS parameters." Publisher: AD Elster, ELSTER LLC. Available from: `http://mriquestions.com/choice-of-trteetc.html`, Accessed: 2020-10-19.

[67] L. Y, X. D, O.-I. E, L. JM, C. AP, and et al, "T1 and T2 Metabolite Relaxation Times in Normal Brain at 3T and 7T," *J Mol Imaging Dynam*, vol. S1:002, 2012.

[68] M. Carl, M. Bydder, J. Du, A. Takahashi, and E. Han, "Optimization of RF excitation to maximize signal and T2 contrast of tissues with rapid transverse relaxation," *Magnetic Resonance in Medicine*, vol. 64, no. 2, pp. 481–490, 2010.

[69] J. Graessner, "Bandwidth in MRI?," *MAGNETOM Flash*, vol. 2, pp. 3–8, 2013.

[70] "Nuclear Overhauser Enhancement (NOE)." Publisher: AD Elster, ELSTER LLC. Available from: `http://mriquestions.com/noe.html`, Accessed: 2020-11-01.

[71] R. HJ, "The Nuclear Overhauser Effect." Syllabus for Course 605. University of Wisconsin, Madison, 2014, Available from: http://mriquestions.com/uploads/3/4/5/7/34572113/noe_reich_chapter.pdf.

[72] B. Zeinali-Rafsanjani, R. Faghihi, M. A. Mosleh-Shirazi, S. M. Moghadam, M. Lotfi, R. Jalli, S. Sina, and L. Mina, "Mrs shimming: An important point which should not be ignored," *Journal of biomedical physics and engineering*, vol. 8, no. 3, pp. 261–270, 2018.

[73] "15 - measurement," in *Pipeline Rules of Thumb Handbook (Eighth Edition)* (E. McAllister, ed.), pp. 541–624, Boston: Gulf Professional Publishing, eighth edition ed., 2014.

[74] H. E. Plesser, "Reproducibility vs. replicability: A brief history of a confused terminology," *Frontiers in neuroinformatics*, vol. 11, no. 76, 2018.

[75] Bratinova S, Raffael B, Simoneau C. Guidelines for performance criteria and validation procedures of analytical methods used in controls of food contact materials. EUR 24105 EN. Luxembourg (Luxembourg): Publications Office of the European Union; 2009. JRC53034.

[76] P. Cool and M. Ockendon. Stats Book. Available from: http://countcool.com, Accessed: 2021-06-10.

[77] "Free induction decay." Publisher: AD Elster, ELSTER LLC. Available from: https://www.mriquestions.com/free-induction-decay.html, Accessed: 2020-10-23.

[78] M. Schär, B. Strasser, and U. Dydak, "Csi and sense csi," *eMagRes*, vol. 5, pp. 1291–1306, 2016.

[79] A. Tannús and M. Garwood, "Adiabatic Pulses," *NMR in Biomed*, vol. 10, pp. 423–434, 1997.

[80] D. L. Arnold, P. M. Matthews, and G. K. Radda, "metabolic recovery after exercise and the assessment of mitochondrial function in vivo in human skeletal muscle by means of 31p nmr," *Magnetic Resonance in Medicine*, vol. 1, no. 3, pp. 307–315, 1984.

[81] I. Lanza, S. Bhagra, K. Nair, and J. Port, "Measurement of human skeletal muscle oxidative capacity by 31p-mr spectroscopy: a cross-validation with in vitro measurements," *J Magn Reson Imaging*, vol. 34, no. 5, pp. 1143–50, 2011.

[82] S. Naruse, K. Hirakawa, Y. Horikawa, C. Tanaka, T. Higuchi, S. Ueda, H. Nishikawa, and H. Watari, "Measurements of in vivo 31p nuclear magnetic resonance spectra in neuroectodermal tumors for the evaluation of the effects of chemotherapy," *Cancer Research*, vol. 45, no. 6, pp. 2429–2433, 1985.

[83] S. Smith, P. Martin, J. Davies, R. Edwards, and A. Stevens, "The assessment of treatment response in non-hodgkin's lymphoma by image guided 31p magnetic resonance spectroscopy," *Br J Cancer*, vol. 61, no. 3, pp. 485–90, 1990.

[84] A. Madden, M. O. Leach, D. J. Collins, and G. S. Payne, "The water resonance as an alternative ph reference: Relevance to in vivo 31p nmr localized spectroscopy studies," *Magnetic Resonance in Medicine*, vol. 19, no. 2, pp. 416–421, 1991.

[85] G. D. Najafpour, "Chapter 5 - growth kinetics," in *Biochemical Engineering and Biotechnology* (G. D. Najafpour, ed.), pp. 81–141, Amsterdam: Elsevier, 2007.

[86] B. Soussi, J. Idström, A. Bylund-Fellenius, and T. Scherstén, "Dynamics of skeletal muscle energetics during ischemia and reperfusion assessed by in vivo 31p nmr," *NMR Biomed*, vol. 3, no. 2, pp. 71–77, 1990.

[87] L. Valkovič, M. Chmelík, and M. Krššák, "In-vivo 31p-mrs of skeletal muscle and liver: A way for non-invasive assessment of their metabolism," *Analytical Biochemistry*, vol. 529, pp. 193–215, 2017.

[88] M. J. Kushmerick, T. S. Moerland, and R. W. Wiseman, "Mammalian skeletal muscle fibers distinguished by contents of phosphocreatine, ATP, and Pi.," *Proc. Natl, Acad. Sci*, vol. 89, pp. 7521–25, 1992.

[89] L. Valkovič, M. Chmelík, B. Ukropcová, T. Heckmann, W. Bogner, I. Frollo, H. Tschan, M. Krebs, N. Bachl, J. Ukropec, S. Trattnig, and M. Krššák, "Skeletal muscle alkaline Pi pool is decreased in overweight-to-obese sedentary subjects and relates to mitochondrial capacity and phosphodiester content," *Scientific Reports*, vol. 6, 2016.

[90] J. P. Wijnen, W. J. M. van der Kemp, M. P. Luttje, M. A. Korteweg, P. R. Luijten, and D. W. J. Klomp, "Quantitative 31P Magnetic Resonance Spectroscopy of the Human Breast at 7T," *Magnetic Resonance in Medicine*, vol. 68, pp. 339–348, 2012.

[91] T. G. Demarest, G. T. D. Truong, J. Lovett, J. G. Mohanty, J. A. Mattison, M. P. Mattson, L. Ferrucci, V. A. Bohr, and R. Moaddel, "Assessment of NAD+ metabolism in human cell cultures, erythrocytes, cerebrospinal fluid and primate skeletal muscle," *Analytical Biochemistry*, vol. 572, pp. 1–8, 2019.

[92] "Mr core facility." Publisher: Norwegian University of Science and Technology. Available from: `https://www.ntnu.edu/mh/mr-corefacility`. Accessed: 2021-03-05.

[93] "Nmr spectroscopy." Publisher: Norwegian University of Science and Technology. Available from: `https://www.ntnu.edu/mh/mr-corefacility/nmr-spectroscopy`. Accessed: 2021-03-05.

[94] R. Simões, A. P. Candiota, M. Julia-Sape, and C. Arús, *In Vivo Magnetic Resonance Spectroscopic Imaging and Ex Vivo Quantitative Neuropathology by High Resolution Magic Angle Spinning Proton Magnetic Resonance Spectroscopy*, vol. 77, pp. 329–365. 04 2012.

[95] "MAGNETOM Terra." Available from: `https://www.siemens-healthineers.com/no/magnetic-resonance-imaging/7t-mri-scanner/magnetom-terra`, Accessed: 2020-09-30.

[96] MAGNETOM Terra, System Owner Manual, syngo MR E12, Siemens Healthineers.

[97] K. L. Granlund, E. Staroswiecki, M. T. Alley, B. L. Daniel, and B. A. Hargreaves, "High-resolution, three-dimensional diffusion-weighted breast imaging using dess," *Magnetic Resonance Imaging*, vol. 32, no. 4, pp. 330 – 341, 2014.

[98] "User manual." Publisher: Bruker Corporation. Version: 012. Pages: 272. Available from: `https://www.bruker.com/en/services/software-downloads.html`, Accessed: 2021-03-04.

[99] Y.-S. Jung, J.-S. Hyeon, and G.-S. Hwang, "Software-assisted serum metabolite quantification using nmr," *Analytica Chimica Acta*, vol. 934, pp. 194–202, 2016.

[100] "Support." Publisher: Chenomx Inc. Subtitle: General Technical Questions Available from: `https://www.chenomx.com/support/`, Accessed: 2021-03-04.

[101] R. Simpson, G. A. Devenyi, P. Jezzard, T. J. Hennessy, and J. Near, "Advanced processing and simulation of MRS data using the FID appliance (FID-A)—An open source, MATLAB-based toolkit," *Magnetic Resonance in Medicine*, vol. 77, 2015.

[102] D. Wishart, Y. Djoumbou, A. Marcu, A. Guo, K. Liang, R. Vázquez-Fresno, T. Sajed, D. Johnson, C. Li, N. Karu, Z. Sayeeda, E. Lo, N. Assempour, M. Berjanskii, S. Singhal, D. Arndt, Y. Liang, H. Badran, J. Grant, and A. Scalbert, "Hmdb 4.0: The human metabolome database for 2018," *Nucleic Acids Research*, vol. 46, 11 2017.

[103] A. Nardi-Schreiber, G. Sapir, A. Gamliel, O. Kakhlon, J. Sosna, J. M. Gomori, V. Meiner, A. Lossos, and R. Katz-Brull, "Defective atp breakdown activity related to an entpd1 gene mutation demonstrated using 31p nmr spectroscopy," *Chem. Commun.*, vol. 53, pp. 9121–9124, 2017.

[104] J. Gard, G. Kichura, J. Ackerman, J. Eisenberg, J. Billadello, B. Sobel, and R. Gross, "Quantitative 31p nuclear magnetic resonance analysis of metabolite concentrations in langendorff-perfused rabbit hearts," *Biophysical Journal*, vol. 48, no. 5, pp. 803–813, 1985.

[105] J.-H. Chen, Y. V. Wu, P. DeCarolis, R. O'Connor, C. J. Somberg, and S. Singer, "Resolution of creatine and phosphocreatine 1h signals in isolated human skeletal muscle using hr-mas 1h nmr," *Magnetic Resonance in Medicine*, vol. 59, pp. 1221–1224, 2008.

[106] P. Lundberg. private communication.

[107] R. F. Busse, "Flip angle calculation for consistent contrast in spoiled gradient echo imaging," *Magnetic Resonance in Medicine*, vol. 53, no. 4, pp. 977–980, 2005.

[108] T. E. Ryan, W. M. Southern, M. A. Reynolds, and K. K. McCully, "A cross-validation of near-infrared spectroscopy measurements of skeletal muscle oxidative capacity with phosphorus magnetic resonance spectroscopy," *Journal of Applied Physiology*, vol. 115, no. 12, pp. 1757–1766, 2013. PMID: 24136110.

[109] R. G. Weiss, J. C. Chatham, M. J. Charron, D. Georgakopolous, T. Wallimann, L. Kay, B. Walzel, Y. Wang, D. A. Kass, G. Gerstenblith, and V. Chacko, "An increase in the myocardial pcr/atp ratio in glut4 null mice," *The FASEB Journal*, vol. 16, no. 6, pp. 613–615, 2002.

[110] K. P. Braun, R. M. Dijkhuizen, R. A. de Graaf, K. Nicolay, W. Vandertop, R. H. Gooskens, and K. A. Tulleken, "Cerebral ischemia and white matter edema in experimental hydrocephalus: a combined in vivo mri and mrs study," *Brain Research*, vol. 757, no. 2, pp. 295–298, 1997.

[111] C. M. U. B. t. Valkovič, L., "Skeletal muscle alkaline pi pool is decreased in overweight-to-obese sedentary subjects and relates to mitochondrial capacity and phosphodiester content," *Sci Rep*, vol. 6, 2016.

[112] M. Meyerspeer, T. Scheenen, A. I. Schmid, T. Mandl, E. Unger, and E. Moser, "Semi-laser localized dynamic 31p magnetic resonance spectroscopy in exercising muscle at ultra-high magnetic field," *Magnetic Resonance in Medicine*, vol. 65, no. 5, pp. 1207–1215, 2011.

[113] L. Valkovič, M. Chmelík, and M. Krššák, "In-vivo 31p-mrs of skeletal muscle and liver: A way for non-invasive assessment of their metabolism," *Analytical Biochemistry*, vol. 529, pp. 193–215, 2017.

[114] K. Sahlin, R. Harris, B. Nylind, and *et al*, "Lactate content and ph in muscle samples obtained after dynamic exercise," *Pflugers Arch*, vol. 367, pp. 143–149, 1976.

[115] N. D. Naimon, J. Walczyk, J. S. Babb, and et al., "A low-cost mr compatible ergometer to assess post-exercise phosphocreatine recovery kinetics," *Magn Reson Mater Phy*, vol. 30, pp. 281–289, 2017.

[116] H. B. Rossiter, S. A. Ward, F. A. Howe, J. M. Kowalchuk, J. R. Griffiths, and B. J. Whipp, "Dynamics of intramuscular 31p-mrs pi peak splitting and the slow components of pcr and o2 uptake during exercise," *Journal of Applied Physiology*, vol. 93, no. 6, pp. 2059–2069, 2002. PMID: 12391122.

[117] L. Clos, M. Jofre, J. Ellinger, and et al, "Nmrbot: Python scripts enable high-throughput data collection on current bruker biospin nmr spectrometers," *Metabolomics*, vol. 9, pp. 558–563, 2013.

Appendix A

The '^{31}P metabolites phantom'

In Table A.1 is the target and true masses of the different metabolites used in the main phantom listed. The true masses were used to calculate the true concentrations in the main phantom using the following equation:

$$[\text{Metabolite}] = \frac{\text{True mass} \cdot 1000}{V_{tot} \cdot M} \tag{A.1}$$

where V_{tot} is the total volume of the main phantom, which was 400 g, and M is the molar mass of the metabolite given in g/mol. 1000 is a scaling factor since the concentrations are given in mM.

Table A.1: The target and true masses of the different metabolites used in main phantom.

Metabolite	**Target mass [g]**	**True mass [g]**
ATP	1.217	1.146
PCr	0.337	0.324
PBS	2 tablets	2 tablets
GPC	0.205	0.215
PE	0.056	0.057
PC	0.147	0.150
NAD	0.053	0.051

Figure A.1 and A.2 shows the 1D ^{1}H and 1D ^{31}P spectra of the '^{31}P metabolites phantom' acquired from the HR MAS MRS experiment. Both spectra are viewed using the analysis software TopSpin [117].

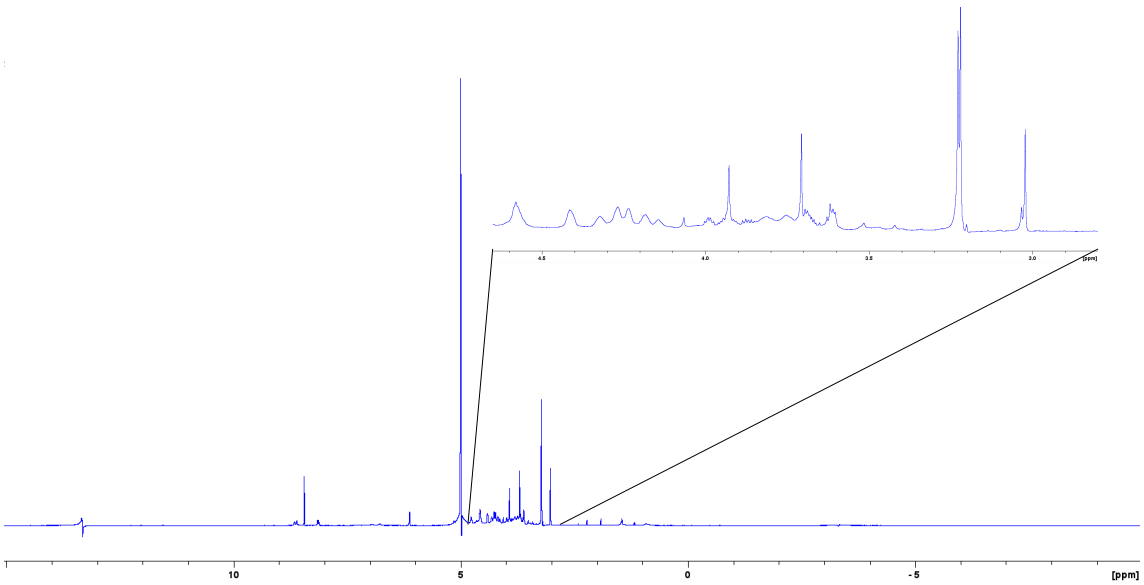

Figure A.1: 1D ^{1}H spectra of the '^{31}P metabolites phantom'. The highlighted part of the spectra shows the part used in the 2D spectra in Figure 4.1a.

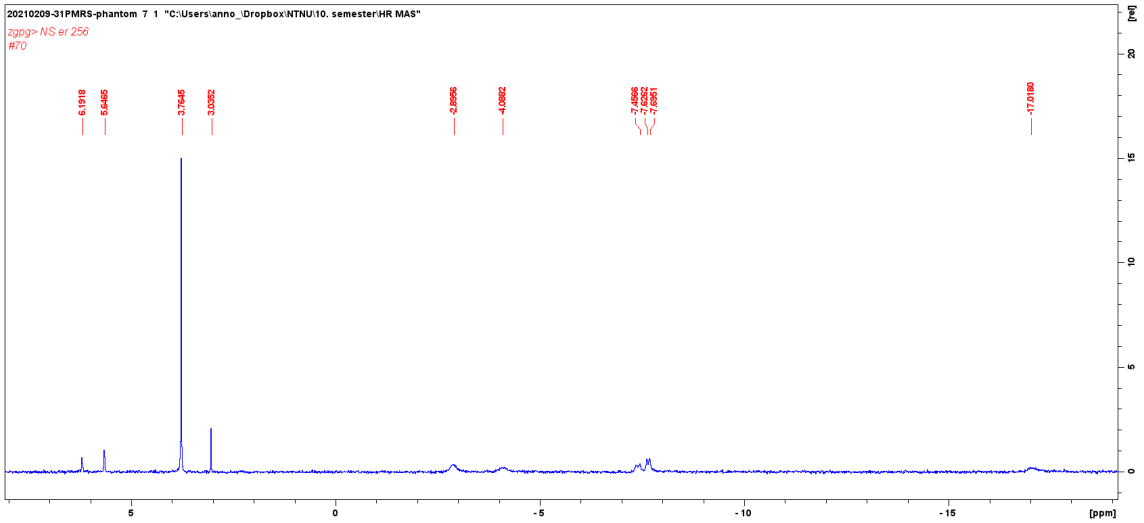

Figure A.2: 1D ^{31}P spectra of the '^{31}P metabolites phantom'. The peaks are marked with ppm values using the software TopSpin.

Appendix B

Protocol optimization

Table B.1 shows the data presented in Figure 4.6 in the Results chapter. The SNR values were calculated using the 'op_getSNR' function from FID-A in MATLAB. The theoretical SNR ratio is equal to the square root of the difference between the number of signal averages. For example, the theoretical signal difference between NSA = 16 and NSA = 128 is: $\sqrt{128/16} = 2.83$.

Table B.1: SNR values for different numbers of NSA used to create a specter. Both the relative ratio and the theoretical ratio is based on NSA = 16 as the reference.

NSA	SNR (PCr)	Calculated ratio	Theoretical ratio
1	203	0.79	0.25
2	195	0.76	0.35
3	211	0.82	0.43
4	198	0.77	0.50
8	215	0.84	0.71
16	257	1.00	1.00
32	335	1.30	1.41
64	477	1.85	2.00
128	636	2.47	2.83
256	831	3.23	4.00

Protocol specifications for some of the protocols that was tried during the protocol optimization:

- Phantom protocol: TR 8000 ms, NSA 16, BIR-4, fa 60°, BW 10000 Hz, VS 2048.
- Siemens protocol: TR 400 ms, NSA 256, Rectangular, fa 90°, BW 10000 Hz, VS 1024.
- Optimal protocol: TR 800 ms, NSA 256, Rectangular, fa 90°, BW 10000 Hz, VS 1024.

Figure B.1 shows the calculated peak area for PCr for every average for the three scans in segment 1 for volunteer 2 and 3. The two spectra for each volunteer were acquired with one week interval.

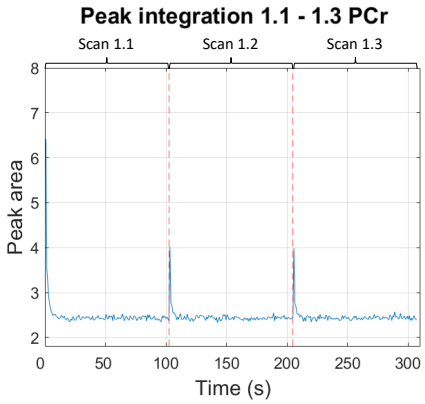

(a) Volunteer 2, week 1

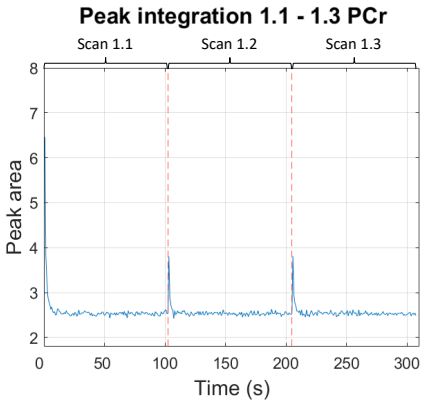

(b) Volunteer 2, week 2

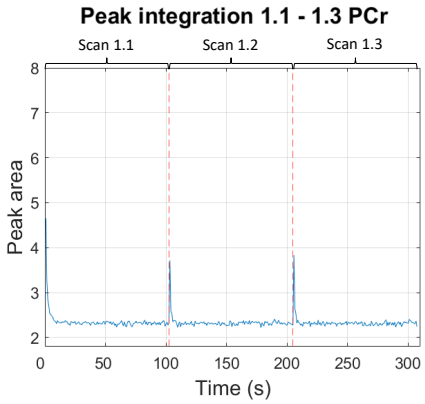

(c) Volunteer 3, week 1

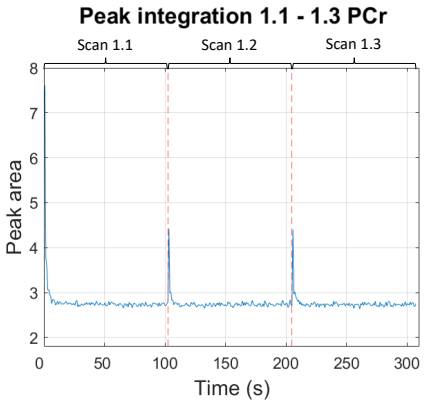

(d) Volunteer 3, week 2

Figure B.1: Calculated peak area of PCr for every average for scan 1.1 to 1.3 in volunteer 2 and 3. The two spectra (a) and (b) were acquired with one week interval.

Appendix C

Repeatability data

Table C.1 shows the mean values and standard deviations for scan 1.1, 1.2 and 1.3 for all volunteers.

Table C.1: Mean value and standard deviation for scan 1.1, 1.2 and 1.3 for all volunteers.

	Volunteer 1		Volunteer 2		Volunteer 3	
Scan	**Week 1**	**Week 2**	**Week 1**	**Week 2**	**Week 1**	**Week 2**
1.1	2.03 ± 0.03	2.21 ± 0.03	2.44 ± 0.04	2.54 ± 0.04	2.33 ± 0.04	2.75 ± 0.04
1.2	2.02 ± 0.03	2.20 ± 0.03	2.44 ± 0.04	2.54 ± 0.04	2.32 ± 0.04	2.73 ± 0.04
1.3	2.01 ± 0.03	2.20 ± 0.03	2.44 ± 0.04	2.53 ± 0.04	2.31 ± 0.04	2.74 ± 0.04

Table C.2 shows the mean values and standard deviations for segment 1, 2 and 3 for all volunteers.

Table C.2: Mean value and standard deviation for segment 1, 2 and 3 for all volunteers.

	Volunteer 1		Volunteer 2		Volunteer 3	
Seg	**Week 1**	**Week 2**	**Week 1**	**Week 2**	**Week 1**	**Week 2**
1	2.02 ± 0.03	2.20 ± 0.03	2.44 ± 0.04	2.54 ± 0.04	2.32 ± 0.04	2.74 ± 0.04
2	2.17 ± 0.03	2.17 ± 0.03	2.70 ± 0.04	2.50 ± 0.04	2.56 ± 0.04	2.72 ± 0.04
3	2.32 ± 0.04	2.30 ± 0.03	2.43 ± 0.04	2.53 ± 0.04	2.40 ± 0.04	2.42 ± 0.04

Figure C.1 shows the measured peak area for PCr after repositioning of the coil for all volunteers. The red dotted line shows when the coil was repositioned. For some of the volunteers the peak area changes between each repositioning of the coil, as seen in Figure C.1a, C.1c and C.1e, while for some of the scans there is only a major change in peak area for one repositioning (Figure C.1b and C.1f), and for volunteer 2 in Figure C.1d is there no major changes between the repositioning of the coil.

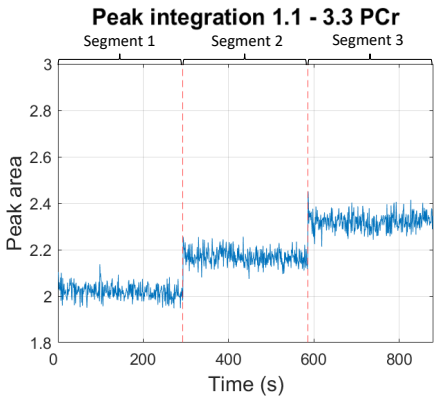

(a) Volunteer 1, week 1

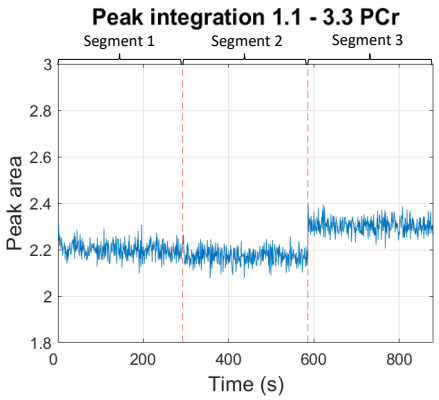

(b) Volunteer 1, week 2

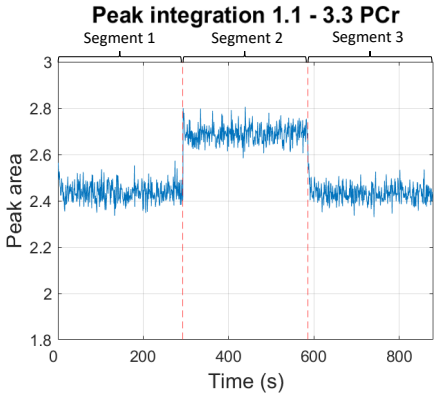

(c) Volunteer 2, week 1

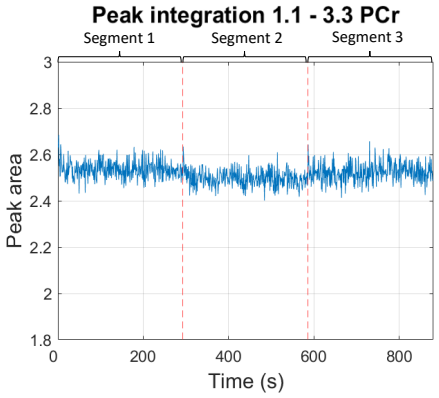

(d) Volunteer 2, week 2

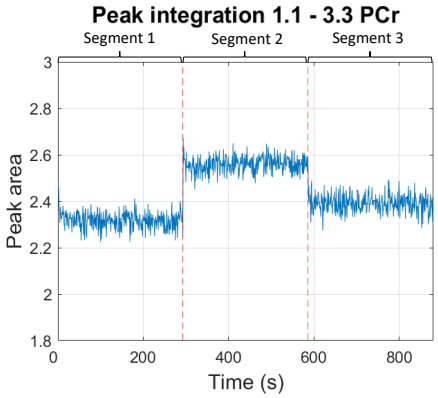

(e) Volunteer 3, week 1

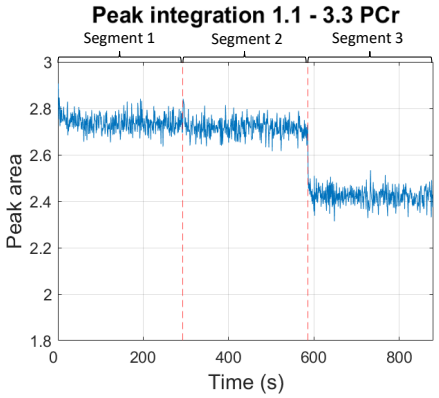

(f) Volunteer 3, week 2

Figure C.1: Integrated peak area for the metabolite PCr for all scans in segment 1, 2 and 3 for all volunteers.

Figure C.2 shows box-plots of measured peak area of Pi for segments 1, 2 and 3 for all volunteers.

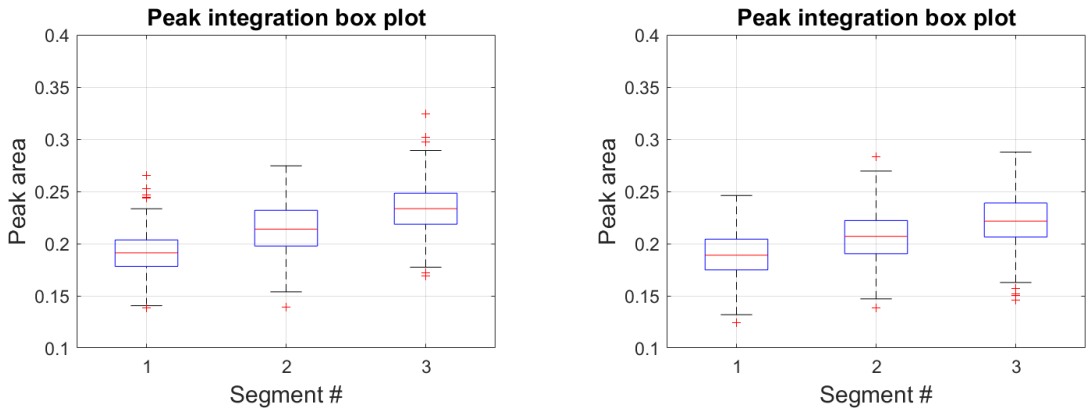

(a) Volunteer 1, week 1

(b) Volunteer 1, week 2

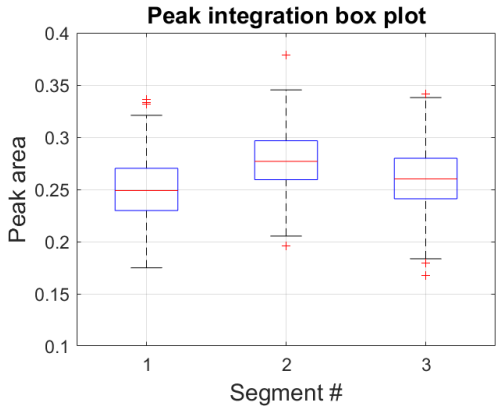

(c) Volunteer 2, week 1

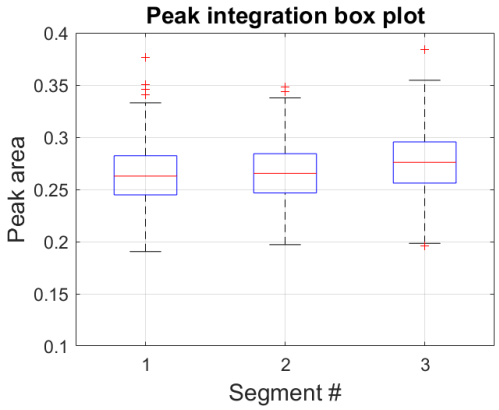

(d) Volunteer 2, week 2

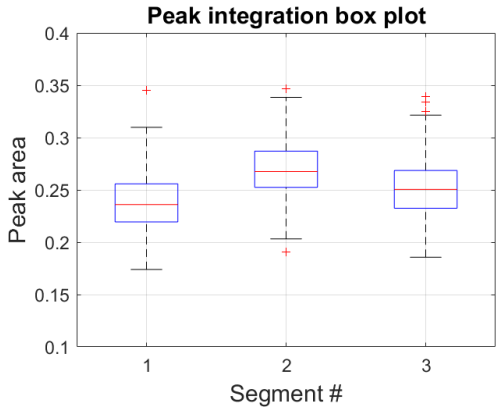

(e) Volunteer 3, week 1

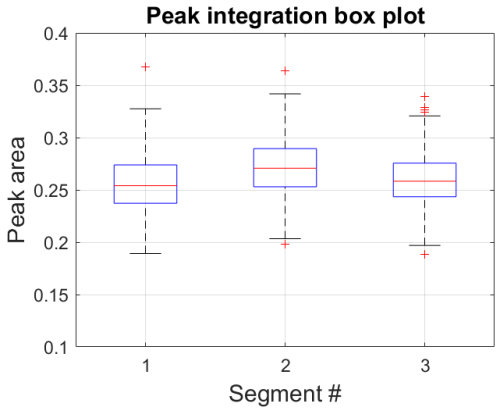

(f) Volunteer 3, week 2

Figure C.2: Box plot of measured peak area for Pi for the three first segments for all volunteers. The red central mark indicates the median, while the top and bottom edges of the box indicate the 75^{th} and 25^{th} percentiles, respectively. The black lines extended from the box represents the data points not considered outliers, while the red + signs marks the data points considered as outliers.

Appendix D

pH measurements

In order to calculate the pH in the calf muscle of the healthy volunteers, the analysis tool SIVIC was used. In SIVIC the ppm values of the metabolites PCr, Pi and α-ATP were registered after the spectra was 0^{th} and 1^{st} order phased. The ppm-values for all scans for every volunteer is presented in Table D.1 for week number one for each volunteer, and in Table D.2 for week number two for each volunteer.

Table D.1: PPM-values for PCr, Pi and α-ATP from scan number one of the healthy volunteers. All ppm-values found with SIVIC.

	Volunteer #1			**Volunteer #2**			**Volunteer #3**		
Scan #	**PCr**	**Pi**	**a-ATP**	**PCr**	**Pi**	**a-ATP**	**PCr**	**Pi**	**a-ATP**
1.1	9.577	4.674	-2.842	9.583	4.710	-2.832	9.654	4.797	-2.758
1.2	9.582	4.677	-2.845	9.575	4.716	-2.837	9.655	4.797	-2.752
1.3	9.573	4.679	-2.841	9.582	4.712	-2.844	9.652	4.798	-2.751
2.1	9.584	4.702	-2.833	9.667	4.797	-2.745	9.586	4.713	-2.830
2.2	9.583	4.711	-2.838	9.668	4.797	-2.734	9.580	4.713	-2.833
2.3	9.587	4.702	-2.831	9.661	4.798	-2.743	9.578	4.712	-2.833
3.1	9.498	4.625	-2.905	9.580	4.716	-2.932	9.585	4.717	-2.834
3.2	9.503	4.625	-2.906	9.578	4.715	-2.838	9.580	4.716	-2.838
3.3	9.490	4.635	-2.912	9.578	4.716	-2.839	9.586	4.717	-2.838
4.1	9.577	4.796	-2.766	9.599	4.785	-2.753	9.666	4.877	-2.678
4.2	9.580	4.797	-2.748	9.585	4.782	-2.750	9.667	4.879	-2.672
4.3	9.590	4.797	-2.744	9.586	4.779	-2.763	9.667	4.877	-2.675
5.1	9.500	4.635	-2.906	9.575	4.714	-2.828	9.654	4.795	-2.758
5.2	9.499	4.635	-2.915	9.589	4.713	-2.836	9.655	4.795	-2.761
5.3	9.502	4.635	-2.911	9.584	4.716	-2.836	9.663	4.794	-2.758
5.4	9.500	4.635	-2.912	9.581	4.716	-2.834	9.668	4.797	-2.758
5.5	9.501	4.635	-2.903	9.579	4.713	-2.824	9.661	4.793	-2.756

Table D.2: PPM-values for PCr, Pi and α-ATP from scan number two of the healthy volunteers. All ppm-values found with SIVIC.

	Volunteer #1			**Volunteer #2**			**Volunteer #3**		
Scan #	**PCr**	**Pi**	**a-ATP**	**PCr**	**Pi**	**a-ATP**	**PCr**	**Pi**	**a-ATP**
1.1	9.498	4.633	-2.911	9.504	4.636	-2.912	9.577	4.717	-2.832
1.2	9.499	4.633	-2.921	9.503	4.633	-2.921	9.578	4.716	-2.833
1.3	9.499	4.633	-2.916	9.498	4.633	-2.910	9.583	4.717	-2.839
2.1	9.666	4.797	-2.756	9.494	4.636	-2.909	9.588	4.714	-2.838
2.2	9.671	4.797	-2.756	9.504	4.636	-2.912	9.584	4.714	-2.844
2.3	9.669	4.797	-2.755	9.505	4.635	-2.918	9.587	4.717	-2.838
3.1	9.574	4.713	-2.840	9.740	4.877	-2.682	9.586	4.713	-2.841
3.2	9.578	4.716	-2.840	9.741	4.877	-2.682	9.579	4.709	-2.840
3.3	9.583	4.711	-2.845	9.720	4.877	-2.682	9.587	4.713	-2.835
4.1	9.687	4.879	-2.651	9.752	4.952	-2.595	9.594	4.797	-2.750
4.2	9.674	4.879	-2.682	9.746	4.955	-2.601	9.593	4.796	-2.752
4.3	9.645	4.878	-2.679	9.752	4.959	-2.595	9.586	4.797	-2.759
5.1	9.580	4.710	-2.831	9.750	4.877	-2.676	9.586	4.715	-2.830
5.2	9.578	4.720	-2.834	9.728	4.877	-2.810	9.587	4.716	-2.836
5.3	9.583	4.715	-2.834	9.752	4.879	-2.668	9.583	4.717	-2.837
5.4	9.571	4.720	-2.832	9.728	4.879	-2.678	9.581	4.717	-2.835
5.5	9.585	4.716	-2.835	9.734	4.877	-2.671	9.585	4.713	-2.836

Appendix E

FWHM measurements

The FWHM is a measurement of how broad a peak in the spectra was at half maximum. Table E.1 shows the average measured FWHM value for the three scans completing the first segment for the volunteers. The measured FWHM value hardly varied between the three scans completing the first segment for each volunteer. A large variation was observed between each week of scanning for each volunteer where the coil was placed differently on the muscle. The phasing of the spectra also varied between the different weeks of scanning and for the volunteers, which directly affected the measured value of FWHM.

Table E.1: The measured FWHM mean + standard deviation for PCr for each of the three scans completing the first segment for all volunteers. All numbers in Hz and measured with the analysis software FID-A.

	Volunteer 1		**Volunteer 2**		**Volunteer 3**	
Scan	**Week 1**	**Week 2**	**Week 1**	**Week 2**	**Week 1**	**Week 2**
1.1	21.6 ± 0.5	19.6 ± 0.4	22.2 ± 0.6	19.4 ± 0.5	27.2 ± 0.7	19.2 ± 0.3
1.2	21.8 ± 0.5	19.6 ± 0.3	22.2 ± 0.6	19.4 ± 0.5	27.3 ± 0.8	19.2 ± 0.4
1.3	21.9 ± 0.6	19.5 ± 0.4	22.1 ± 0.5	19.5 ± 0.5	27.1 ± 0.7	19.2 ± 0.3

The measured average FWHM value for PCr for all volunteers are presented in Table E.2 for the three first segments with standard deviation. There were some variations in the average FWHM value between the segments for each volunteer, especially for the second week for volunteer 1 and 2, and for the first week for volunteer 3. The standard deviation varied from 0.2 Hz to 0.7 Hz for the different segments. There was a clear change in the measured FWHM for segment 4 compared to the other two segments. For four of the six measurements made for this segment the measured FWHM decreased (volunteer 1 and 3), while it increased for two of those (volunteer 2).

Table E.2: The measured FWHM mean + standard deviation for PCr for all segments for all volunteers. All numbers in Hz and measured with the analysis software FID-A.

	Volunteer 1		**Volunteer 2**		**Volunteer 3**	
Segment	**Week 1**	**Week 2**	**Week 1**	**Week 2**	**Week 1**	**Week 2**
1 (1.1-1.3)	21.7 ± 0.4	19.5 ± 0.4	22.1 ± 0.4	19.4 ± 0.3	27.2 ± 0.5	19.2 ± 0.3
2 (2.1-2.3)	19.5 ± 0.5	24.3 ± 0.7	21.0 ± 0.4	27.6 ± 0.6	20.5 ± 0.2	20.3 ± 0.3
3 (3.1-3.3)	17.3 ± 0.5	22.0 ± 0.3	24.1 ± 0.4	23.8 ± 0.3	22.9 ± 0.3	19.3 ± 0.3
4	13.9 ± 0.3	16.1 ± 0.8	26.0 ± 0.5	24.1 ± 0.5	14.2 ± 0.3	13.8 ± 0.2
5	17.3 ± 0.3	21.4 ± 0.4	24.1 ± 0.3	26.4 ± 0.4	21.3 ± 0.3	18.6 ± 0.3

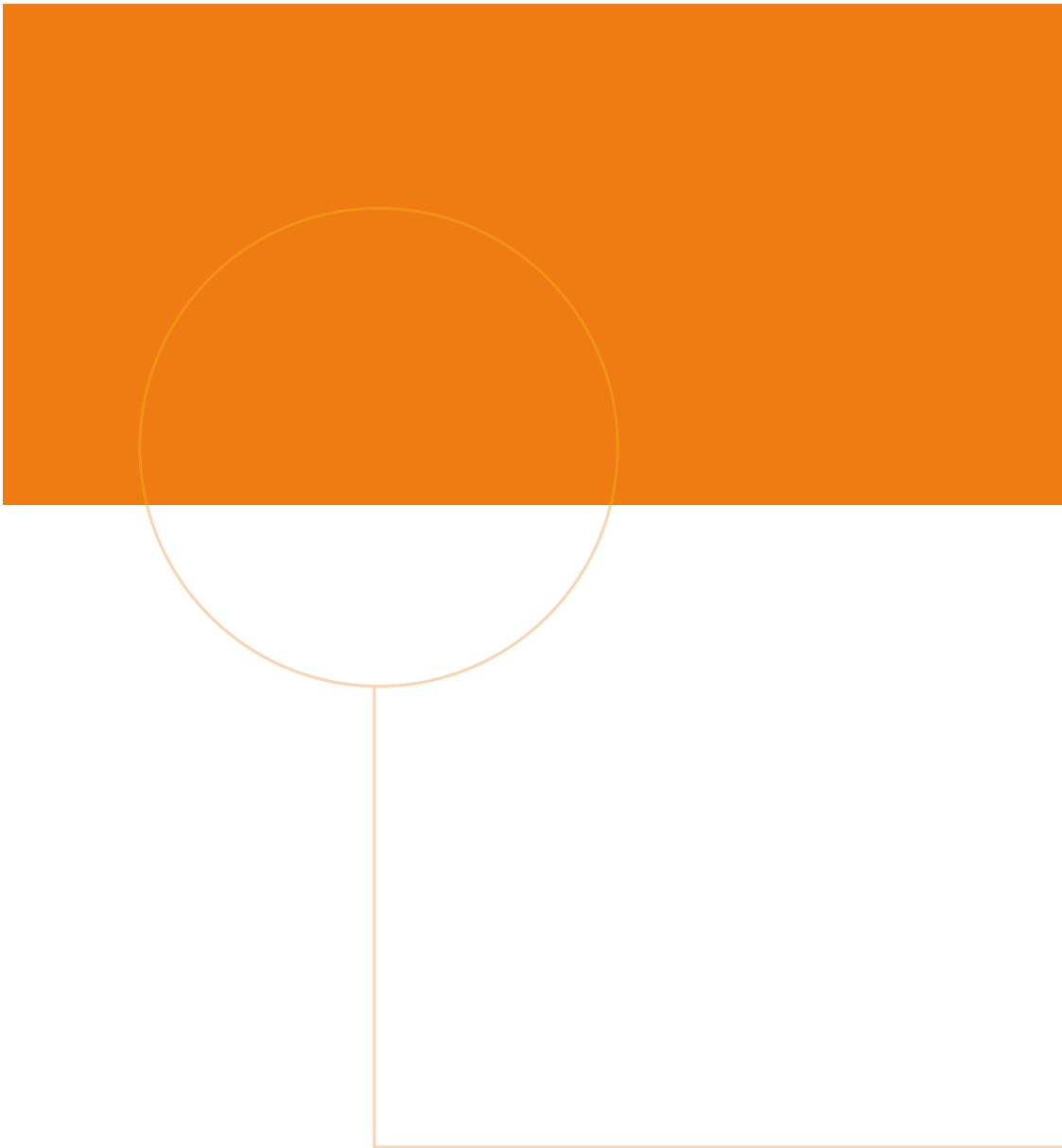

NTNU

Norwegian University of
Science and Technology